Surface reactivity of soft minerals at the atomic scale

Bahareh Zareeipolgardani

▶ **To cite this version:**

THÈSE DE DOCTORAT DE L'UNIVERSITÉ DE LYON
opérée au sein de
l'Université Claude Bernard Lyon 1

École Doctorale ED52
Physique et Astrophysique de Lyon

Spécialité de doctorat : Physique

Soutenue publiquement le 14/02/2019, par :
Bahareh Zareeipolgardani

Surface reactivity of soft minerals at the atomic scale

Devant le jury composé de :

Churakov Sergey, Professeur, University of Bern	Rapporteur
Zuddas Pierpaolo, Professeur, Pierre and Marie Curie University	Rapporteur
Barentin Catherine, Professeur, Université Claude Bernard Lyon 1	Examinateur
Dysthe Dag Kristian, Professeur, University of Oslo	Examinateur
Lespiat Rémi, Responsable industriel, Saint-Gobain	Examinateur
Müller Pierre, Professeur, Aix-Marseille University	Examinateur
Pierre-Louis Olivier, Directeur de Recherche, CNRS	Examinateur
Colombani Jean, Professeur, Université Claude Bernard Lyon 1	Directeur de thèse

THESIS SUBMITTED TO THE UNIVERSITY OF LYON
Université Claude Bernard Lyon 1

For the degree Doctor of Philosophy
Department of Physics

Presented by:
Bahareh Zareeipolgardani
14/02/2019

Surface reactivity of soft minerals at the atomic scale

The jury members:

Churakov Sergey, Professeur, University of Bern	Reviewer
Zuddas Pierpaolo, Professeur, Pierre and Marie Curie University	Reviewer
Barentin Catherine, Professeur, Université Claude Bernard Lyon 1	Examiner
Dysthe Dag Kristian, Professeur, University of Oslo	Examiner
Lespiat Rémi, Responsable industriel, Saint-Gobain	Examiner
Müller Pierre, Professeur, Aix-Marseille University	Examiner
Pierre-Louis Olivier, Directeur de Recherche, CNRS	Examiner
Colombani Jean, Professeur, Université Claude Bernard Lyon 1	PhD supervisor

Abstract

Identifying reaction mechanisms of minerals is fundamental to understand diagenesis, i.e, sedimentary rock formation, construction material, like cement or gypsum, hardening, and biomineralization. The macroscopic reaction rates of minerals are generally deduced from solution chemistry measurements. Beside the measurement of macroscopic reaction rates, the study of the reactivity of minerals includes now the investigation of the atomic mechanisms involved in the reactions. This has been made possible for two decades by the use of tools resolving nanometric objects, such as vertical scanning interferometry (VSI) and atomic force microscopy (AFM). Gypsum and calcite are among soft minerals. They are extremely widespread mineral that can be found naturally in sedimentary rocks. They are also used in many industrial fields.

Gypsum ($CaSO_4, 2\,H_2O$) is an evaporate mineral. Gypsum uses include: manufacture of wallboards, plaster of Paris, soil conditioning, and hardening retarder in Portland cement. Varieties of gypsum known as "satin spar" and "alabaster" are used for a variety of ornamental purposes; however, their low hardness limits their durability. Calcite, the most stable crystalline form of $CaCO_3$, is moreover important as a bio-mineral and a major constituent of host rock in carbonate reservoirs, which host drinking water and natural oil and gas. When biological organisms grow their shells, they control the crystal morphology, size, orientation and even the crystal phase of precipitated calcium carbonate. This results in materials with physical and chemical properties that differ significantly from those of inorganically precipitated calcite. Gaining more insight into the surface reactivity of calcite and the effect of surface impurities will bring us one step closer to being able to synthesize biomimetic material, which mimic the properties of biogenic calcite.

In this thesis, I had three main focus points. In the first part I studied the effect of stress on the dissolution mechanisms. I investigated to deduce the dissolution rate from the atomic kinetics. The second and the most extensive was the study of the influence of stress on the calcite growth and probing the role of an organic additive on the dynamics of calcite growth while applying stress. In the third part I emphasised on quantitative topographic measurements of dissolving calcite crystal over a relatively large and fixed view at vast range of pH. I considered the influence of an organic additive on the dissolution and surface reaction kinetics at this larger scale. Both macroscopic and microscopic dissolution rates can also be deduced from the dynamics of molecular events (etch pit growth, atomic step migration), but they hardly ever agree, even qualitatively, and the elaboration of a general theory linking the kinetics at the two scales is still in progress.

I presented here microscopic dissolution rates of gypsum, measured by atomic force microscopy (AFM), in quantitative agreement with macroscopic rates. This agreement has been obtained in taking care to neutralize the bias induced by the force applied by the AFM tip on the surface, and to identify clearly the driving molecular mechanism. The force applied by the AFM tip on the surface has been seen to increase the solubility of the mineral, thereby introducing a bias, so I have always worked with a constant and low applied force. This result shows that the determination, among the topographic changes during the dissolution of a mineral, of the dominant one, and the measurement of its dynamics, may permit deducing from AFM experiments a reliable macroscopic dissolution rate.

iv

The transformation of loose grains into a cohesive solid requires the crystallites to grow eventually constrained by the surrounding grains. Whereas never measured, this confinement and the associated stress is expected to influence noticeably the growth, and the final properties of the material. We report here on atomic force microscopy measurements of atomic step velocity during calcite growth, with a varying stress applied by the tip to the surface. The stress has a double influence: it both slows down the growth, and modifies the material crystalline phase. Furthermore, the addition of a small quantity of oligopeptide in the growth solution is shown to have no significant influence on the kinetics, but to completely cancel the phase change under stress. Our results emphasize the previously unknown role of stress on growth mechanisms and parallely identify a new possible role of organic molecules in tuning the morphology of bio-mineralized material.

I used vertical scanning interferometer for surface height maps of a dissolving calcite crystal, which were produced periodically and repetitively at regular time interval. These reaction-measurement cycles were accomplished without changing the crystal surface position relatively to the instrument optical axis at every fixed pH. By this constituted record of reactions, I was able to understand the relationship between changes in the overall dissolution rate of the surface with the pH and the changes of the morphology of the surface itself, particularly the relationship between (a) large etch pits related to screw dislocations; (b) shallow etch pits probably related to point defects; (c) Mega steps, and surface normal retreat and step wave formation. I observed that different surface mechanisms control dissolution at different pH. Furthermore the addition of a peptide during the dissolution has shown that the inhibition of dissolution by this organic molecule depends on the pH, where the rate of inhibition is linked to the predominant mechanism acting on dissolution.

Keywords: AFM, VSI, calcite, gypsum, dissolution, growth, atomic step, biomineralization.

Résumé

Il est indispensable pour comprendre la diagenèse, i.e., la formation des roches sédimentaires, le durcissement des matériaux de construction hydrauliques comme le ciment ou le plâtre, ou la biominéralisation, d'identifier les mécanismes élémentaires de la cristallisation minérale. Le taux de réaction macroscopique des minéraux est généralement déduit de mesures de chimie des solutions. A côté de ces mesures macroscopiques, l'étude de la réactivité des minéraux inclut maintenant l'analyse des mécanismes atomiques à l'origine des réactions chimiques. Cela a été rendu possible depuis deux décennies par l'apparition d'outils capables d'observer des surfaces avec une résolution nanométrique, tels que la microscopie à force atomique et l'interférométrie à balayage vertical.

Le gypse et la calcite font partie des minéraux dits mous. Ce sont des minéraux extrêmement répandus, que l'on peut trouver autant dans la nature sous forme de roches sédimentaires que dans le monde industriel. Le gypse ($CaSO_4, 2\,H_2O$) est une évaporite dont les applications incluent la fabrication des plaques de plâtre, l'ajout au ciment Portland comme retardateur, l'élaboration du plâtre de Paris et l'amendement des sols. La sélénite ou l'albâtre sont des variétés de gypse utilisés comme matériaux pour l'ornement, mais leur faible dureté limite leur durabilité. La calcite, forme la plus stable de $CaCO_3$, est un des principaux biominéraux, et un des constituants majeurs des roches des réservoirs carbonatés, stockant naturellement de l'eau, du pétrole ou du gaz naturel. Quand les organismes biologiques font croître leur coquille, ils contrôlent la morphologie, la taille, l'orientation et même la phase des cristaux de carbonates de calcium qui la constituent. Cela conduit à des biomatériaux présentant des propriétés physiques et chimiques qui diffèrent significativement de ceux de la calcite inorganique. Une connaissance plus approfondie des mécanismes sous-jacents à la réactivité de surface de la calcite et de l'effet des impuretés sur celle-ci permettra de nous rapprocher de la possibilité de synthétiser des minéraux biomimétiques, aux propriétés comparables à celles de la calcite biogénique.

Dans ce contexte, ma thèse s'est développée dans trois directions. Dans la première, j'ai étudié l'influence d'une contrainte mécanique sur les mécanismes de dissolution. Mon objectif dans cette partie a été de tâcher de déduire le taux de dissolution macroscopique à partir de la cinétique des mécanismes atomiques. La seconde partie de la thèse, la plus conséquente, a consisté à étudier l'influence d'une contrainte mécanique sur la croissance de la calcite, et à sonder le rôle d'un additif organique lors de cette croissance sous contrainte. Dans la troisième partie, je me suis penchée sur la dissolution de cristaux de calcite à l'aide de mesures topographiques quantitatives sur des aires relativement étendues de la surface des cristaux, dans une large gamme de pH. J'ai en particulier étudié l'influence d'un additif organique sur la dissolution et la cinétique de réaction à grande échelle.

Les taux de dissolution macroscopique et microscopique, c'est-à-dire déduits de la dynamique d'évènements moléculaires (croissance de piqûre d'attaque, migration de marche atomique), ne sont presque jamais en accord, même qualitativement, et l'élaboration d'une théorie générale liant la cinétique du phénomène aux deux échelles est encore en cours. Je présente ici des taux de dissolution microscopique du gypse, mesurés par microscopie par force atomique (AFM), en accord quantitatif avec les taux de dissolution macroscopiques. Cet accord inédit a été obtenu en prenant soin de neutraliser le biais induit par le fait que la pointe AFM applique

une force sur la surface qu'elle sonde, et en identifiant avec soin les mécanismes moléculaires majeurs à l'œuvre lors de la dissolution. Nous avons constaté que la force appliquée par la pointe sur la surface augmentait localement la solubilité du minéral, à l'origine d'un biais dans la mesure, ce qui nous a conduits à travailler systématiquement à basse force appliquée. Ce résultat montre que la détermination, parmi les changements topographiques ayant cours pendant la dissolution du minéral, du changement dominant, et la mesure de la cinétique de celui-ci, peut permettre de déduire d'expériences AFM une mesure fiable du taux de dissolution macroscopique.

La transformation de grains indépendants en un matériau cohésif nécessite que les cristallites croissent, en fin de prise du matériau, contraintes par les grains environnants. Bien que cela n'ait jamais été mesuré, on s'attend à ce que ce confinement et la contrainte associée à celui-ci, influencent notablement la croissance, et partant les propriétés finales du matériau. Nous rendons compte ici de mesures par AFM de vitesses de marches atomiques pendant la croissance de la calcite, acquises pour différentes contraintes appliquées par la pointe de l'AFM. Nous avons constaté que cette contrainte a une double influence, d'une part elle ralentit la croissance, et d'autre part elle modifie la phase cristalline du matériau. De plus, l'ajout d'une petite quantité d'oligopeptide dans la solution de croissance, si elle n'a pas d'influence sur la cinétique, annule complètement ce changement de phase sous contrainte. Nos résultats mettent en valeur le rôle jusque-là inconnu d'une contrainte sur les mécanismes de croissance, et identifient un nouveau rôle possible des molécules organiques dans la sélection de la morphologie des matériaux biominéralisés.

J'ai utilisé l'interférométrie à balayage vertical pour cartographier la surface d'un cristal de calcite pendant sa dissolution, par des mesures périodiques répétées. Ces cycles de réaction-mesures ont été réalisés en replaçant systématiquement la surface de l'échantillon à la même position par rapport à l'axe optique de l'instrument. Ces mesures ont été réalisées à différents pH dans la gamme pH3 – pH10. Grâce à cette acquisition régulière, j'ai pu comprendre la relation entre les changements de taux de dissolution d'ensemble aux différents pH et les changements de la morphologie de la surface elle-même, particulièrement la relation entre (a) des piqures d'attaque profondes, autour de dislocations émergentes, (b) des piqures d'attaque peu profondes, autour de défauts ponctuels, et (c) des méga-marches, et la vitesse de retrait normale à la surface, et l'apparition « d'ondes » de marches atomiques. J'ai observé que la contribution de ces différents mécanismes variait avec le pH. De plus, l'addition de peptide pendant la dissolution a permis de montrer que le taux d'inhibition de la dissolution par cette molécule organique dépend du pH, et dépend du mécanisme atomique dominant la dissolution.

Mots-clés : AFM, VSI, calcite, gypse, croissance, dissolution, marche atomique, biominéralisation.

Acknowledgements

The risk of forgetting someone when writing such a paragraph is always pending. I hope the list of the people to thank will be exhaustive.

I wish I could someday finally be able to give back to Prof. Jean Colombani for the things he managed to teach me, although I know this task is impossible. So many hours he spent for discussing with me, explaining and listening to me. He put me along the path of an extremely interesting research subject, from which I hope he got back some satisfaction.

I would like to express my deepest gratitude to Dr. Agnès Piednoir for her excellent guidance, caring, patience, and providing me with an excellent atmosphere. I thank all the member of liquids and interfaces group, who have contributed to make the group an inspiring and fun place to work.

I would also like to thank my committee members, Prof. Catherine Barentin, Prof. Sergey Churakov, Prof. Dag Kristian Dysthe, Dr. Rémi Lespiat, Prof. Pierre Müller, Prof.Olivier Pierre-Louis and Prof. Pierpaolo Zuddas for serving as my committee members. I also want to thank them for letting my defense, being an enjoyable moment, and for their brilliant comments and suggestions.

I would like to thank Tanja laine Clausen, who as a good friend was always willing to help and give her best suggestions.

I thank all the people at National IOR Centre of Norway and university of Stavanger for their hospitality and nice scientific cooperation.

In addition, I would especially like to thank Laura Bruno and Florent Songoro aids in experimental settings.

Finally my family, my friends have all stood at me. I would not have made it without your encouragement and patience.

Contents

List of Figures

List of Tables

List of Abbreviations

GCC	Ground Calcium Carbonate
PCCs	Precipitated Calcium Carbonates
SI	Saturation Index
AFM	Atomic Force Microscopy
STM	Scanning Tunnelling Microscopy
VSI	Vertical Scanning Interferometry
SEM-EDX	Scanning Electron Microscopy Energy Dispersive X-Ray Analyzer
TST	Transition State Theory
SFM	Scanning Force Microscopy
ICP-MS	Inductively Coupled Plasma Mass Spectroscopy

Chapter 1

Introduction

The work presented in this thesis was part of the European Union's Horizon 2020 research and innovation program under the Marie Sklodowska-Curie grant agreement No 642976. This European project is an Initial Training Network (ITN) called "Nano-tailoring organo-mineral materials - Controlling strength and healing with organic molecules in mineral interfaces", the acronym of which is "NanoHeal".

This project is built up by cooperation of academic and industrial research labs with a wide range of disciplines and expertise. In this framework 15 PhD students are trained on different topics with the unique goal of the Nanoheal project. They focus on the interactions between a model mineral system —calcium carbonate— and simple organic molecules, to study mechanical properties of mineral materials, their durability, nano-confinened growth mechanisms and healing properties, spanning from atomic to macroscopic lengthscales. The final goal of this project was to understand the fundamental processes underlying mineral-fluid interactions and improve the strength and durability of natural sedimentary rocks inside reservoirs, construction materials and bio-materials.

1.1   Background

The reactivity of mineral-fluid interface was primarily studied for geological reservoirs because the thermodynamic reactions on mineral surfaces determine their stability and destiny in a certain environment. But it has nowadays prominent implications for society, biology and industry.

Mineral interactions in aqueous solutions play a central role in elemental cycling at every lengthscale ranging from local soil weathering to global-scale denudation of continents. First and notable, aquifers reside on bedrocks and groundwater flows through pores of rocks and soils. Partitioning of pollutant to mineral surfaces, precipitation and incorporated impurities are factors for predicting toxic mobility and environmental fate of pollutant, heavy metals and pesticides in environmental system.

Concrete is the largest volume manufactured solid on the earth [42]. It is mostly made of limestone. The most common cement is Ordinary Portland Cement, that goes through chemical reaction, polymerization and crystallization during mixing with water. This production contributes to the emission of 60% of fossil CO_2. A multitude of low CO_2 concrete with different chemistries an mechanical properties has been proposed. For instance the tensile strength of concrete is the most important in the faced challenges. The limited ductility of the hardened cement paste as well poses important issues of lack of tightness in deep oil well cementing for zonal isolation and plug and abandonment. Recent important failures resulted in impressive blow-outs and oil spills [116].

A substantial part of world's known largest oil reservoir is hosted by carbonated rocks [48]. These reservoirs are prone to creep, compaction and subsidence during oil production. During the injection of water or CO_2 to enhance oil recovery, the compaction causes well damage and leakage. As these reservoirs are economically interesting large scale storage CO_2 option, the risk of further compaction resulting from CO_2 injection needs to be assessed. The CO_2 storage in carbonate reservoir thus requires a very high control of long term strength of the reservoir rock. Numerous living organisms produce organic molecules which can direct the nucleation, growth, and morphology of biominerals [81, 43].

These composite materials contain an organic matrix and nano- or micro-scale amorphous or crystalline minerals. Biomineral composite materials include bone, dentine, enamel, statoliths, otoliths, mollusk and crustacean shells, coccolith scales, eggshells, sponge silica skeletons, algal, radiolarian and diatom silica micro-shells, and a variety of transition metal minerals produced by different bacteria.

These biotic materials have stronger and more resilient structures and textures than the same minerals formed in the absence of the organisms. Although made of the same minerals, biotic apatite, aragonite, and calcite are quite different from their abiotic counterparts. Recent investigation show that chalk collected as drill cores in the North Sea basin were biomineralized by cocolithophores during the Maastrichian era (70-65 Ma) and have remained intact until now [49].

In all these examples and also during the sedimentary rock formation and diagenesis, fluid-driven mineral reactions take place in nm- to μm-wide confined spaces. Fundamentally, this process depends on molecular-scale interactions of the species comprising the aqueous matrix and the mineral surface.

Dissolution and precipitation phenomena lead to cohesion between grains and make cement from them. Consequently the reactive mineral contacts at grain boundaries and asperities often control macroscopic mechanical strength of rocks and building materials [110]. It is not clear yet what is the relative importance of dissolution, precipitation and interfacial forces in determining the strength of individual solid-solid contacts. At solid–solid contact, stress is generally existing, due to the simultaneous growth of multiple grains in a constrained space. In geological setting and in burial condition in the earth mantle, down to several km depth in the subsurface, lithostatic pressure of up to a few GPa adds to this stress

During cementation, the mineral surfaces come to within a few nanometers of each others, separated by a nanoconfined water film. This nm-thick water films persists even at high overburden pressures. The properties of this film fluid can significantly differ from bulk fluid ones. The pressure of a stress at the grain contact may have dramatic consequences. Indeed, it constitutes a mechanical stimulus that can trigger chemical reactions, as dissolution (called "pressure solution") or precipitation [44].

In the case of material cementation, this dissolution or crystallization by stress takes place in the nanofilm of water, existing between the growing grains. This constrained environment limits advection and slows down diffusion [113, 94]. As the actual contact surface area between grains is generally much smaller than the apparent one, much higher stresses should build up. Recent investigations showed that the nano-confined situation of mineral interfaces changes nucleation and growth at adjacent solid surfaces [26].

Understanding minerals response to stress is key important to get a better interpretation of different observed properties of rocks and materials. This understanding applies fundamentally to control and predict physico-chemical behaviors of minerals either in dissolution or growth procedure. This consideration would

also give us a closer concept of the thermodynamic reactions on mineral surface and determination of their stability and fate in a specified environment.

Gypsum ($CaSO_4, 2H_2O$) and calcite ($CaCO_3$) are the most common soft minerals, abundant in sedimentary rocks and geological setting with vast implications in material science. In this PhD project, the focus is on the study of water interaction with single crystal of gypsum and calcite. These minerals were chosen due to their existence and application and moreover i) dissolution and growth rates are measurable in laboratory times, ii) dissolution and growth proceed through a well-defined mechanism, and iii) they exhibit a perfect cleavage.

Knowledge of water-gypsum interactions is important in many fields of inquiry, including geochemistry, crustal deformation, soil science, in trapping large oil and gas accumulations, and in environmental and material science. Understanding of gypsum behaviour in contact with aqueous solutions is also relevant for predicting the evolution of the wide areas of gypsum karsts existing worldwide, their instability and potential collapse [54]. The presence of calcium and sulfate ions in water influences the dissolution of other minerals containing toxic metals as well [59] and consequently affects the quality of drinking water [99]. As gypsum is one of the main inorganic scale deposits in hydrocarbon reservoirs [101], understanding its behaviour is required in the oil and gas industry. It can significantly affect oil recovery. A better understanding of gypsum dissolution would also provide insights into the mechanism of the strong enhancement of creep of plaster boards in humid environments [14]. This behaviour is also related to the dissolution of gypsum in the inter-crystalline water of the plaster.

Gypsum dissolution plays a critical role in the hydration of Portland cement. Gypsum is added to suppress the rapid hydration reaction of calcium aluminate during cement setting. Immediately upon wetting of the cement, the dissolution of gypsum releases calcium and sulfate ions into solution that react with aluminate and hydroxyl ions forming ettringite ($Ca_6Al_2(SO_4)_3(OH)_{12}26H_2O$) needles, which subsequently precipitate on calcium aluminate grains, retarding their hydration [16].

Calcite is the most common polymorph of calcium carbonate and the thermodynamically most stable at standard conditions (room temperature and atmospheric pressure). Calcite is one of the most common minerals in the earth's crust, and the main component of limestone. Due to its ubiquitousness, surface reactions on calcite play an important role in geochemical and environmental systems. The reactivity of its surface makes calcite a potentially important sink for heavy metals, metalloids and other contaminants in aquifers [27] and soil [135], in travertine [66], lacustrine, or marine sediments [106]. It also functions as a reservoir that buffers aqueous and atmospheric levels of CO_2. The buffering effect of bicarbonate has a major influence on the chemical behaviour of soils and sediments.

Moreover calcite has many applications in industrial processes, such as paper and cement production. It plays a noticeable role in geochemical engineering projects like nuclear wastes [5], CO_2 storage and oil product. The calcite is also used as a process chemical (mainly filling material).

One of the most important processes involving calcite in an industrial context is the production of burnt lime CaO, which is named after the production process in which natural limestone is burned at temperatures between 900 °C and 1300 °C releasing large quantities of CO_2 into the atmosphere. Burnt lime is after H_2SO_4 the second most produced chemical worldwide. It is the raw material for the production of slaked or hydrated lime ($Ca(OH)_2$), which can react with CO_2 to form calcite. This process is also applied for the manufacture of **p**recipitated **c**alcium **c**arbonates (**PCCs**). These compounds, and to some extent natural limestone powder, **g**round

calcium carbonate (**GCC**), are mostly used as filling material in paper, but also in cement, synthetics, plastics, paints and varnish. To a lesser extent PCCs are used in pharmaceuticals and edibles.

Many different experimental techniques have been developed to quantify overall dissolution rates. For example, bulk solution chemistry can be used to determine rates by measurement of element flux within a system. However, this technique does not provide detailed information about the reaction mechanism at the crystal surface. Since two decades, several precise technological advances like **a**tomic **f**orce **m**icroscopy (**AFM**) and **v**ertical **s**canning **i**nterferometry (**VSI**) have been used to characterize mineral dissolution and growth rates in aqueous solution, measuring the surface elevation and topography changing at micro- and nanoscale. By using these methods we are able to perform direct monitoring of localized changes at the surface. These techniques provide fundamental insight into the reaction mechanisms of crystal-solution interaction and their relationship to thermodynamic descriptions of the bulk system. Our ultimate prospect in this research is an integrated study of dissolution and precipitation on calcite and gypsum conducted over multiple spatial and temporal scales. Establishing this crosslink would be a significant step forward.

1.2 Gypsum

1.2.1 Gypsum properties

Gypsum is a soft sulphate mineral composed of calcium sulphate dihydrate, with the chemical formula ($Ca\,SO_4, 2\,H_2O$). Gypsum is an evaporate mineral most commonly found in layered sedimentary deposits in association with halite, anhydrite, sulphur, calcite, and dolomite. Gypsum uses include: manufacture of wallboard, plaster of Paris, soil conditioning, and a hardening retarder in Portland cement. Varieties of gypsum known as "satin spar" and "alabaster" are used for a variety of ornamental purposes; however, their low hardness limits their durability.

Gypsum crystal system is monoclinic in prismatic class. The crystal habit is massive and flat. It elongates generally in prismatic crystals (figure 1.1). The solubility of gypsum in pure water at 20°C is 2.531 g/L, or 14.7 mM/L. It is roughly 140 times lower than the solubility of common halite (360 g/L) but three orders of magnitude greater than the solubility of $CaCO_3$ (1.5 mg/L) [57].

FIGURE 1.1: Elongated prismatic gypsum crystals used in this project
from Mazan (Vaucluse) in France.

1.2.2 Gypsum crystal dissolution

The atomic structure of gypsum constructs as repeating units of Ca and SO_4 layers perpendicular to the *b*-axis with each individual unit consisting of a plane of Ca sandwiched by two planes of SO_4 such that every SO_4 group is tetrahedrally bound by four Ca atoms. The H_2O molecules are positioned in between these Ca–SO_4 units to link adjacent SO_4 planes through weak hydrogen bonding. This atomic structure allows the perfect {010} cleavage of gypsum. In the various studies it was shown that the growth and dissolution events on the {010} surface is a layer-by-layer process [47]. Gypsum (010) planes are composed of divalent cations and anions and two slices of $Ca\,SO_4$ with an overall height of ~ 7.6Å (figure 1.2).
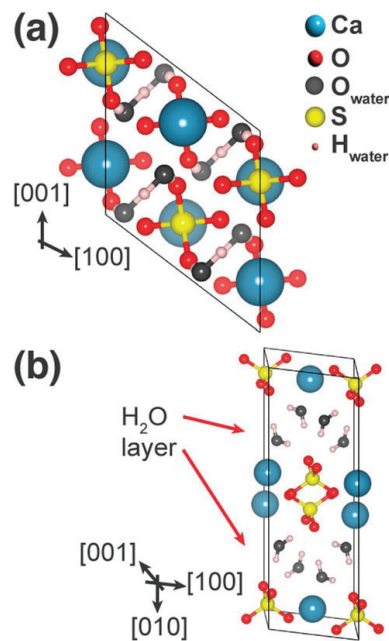
FIGURE 1.2: a) Atomic structure of the (010) surface of gypsum and b) the unit cell with the inter spaced H_2O layer shown.

Dissolution on the gypsum cleavage surface starts with the formation of monomolecular holes, then hole growth and forming rhombic etch pits less than a minute after the input of undersaturated solutions, irrespective of saturation state. The constrained atomic structure of the (010) plane reveals that the crystallographic directions of the steps enclosing any stable etch pits formed on {100} are [100] and [001] steps (figure 1.3). Based on the reported data and also on our observation, the step velocity is highly anisotropic with the [100] moving much faster than the [001] at any saturation conditions. Beside these straight steps, we observed an extensive occurrence of high-speed steps that usually did not have well defined orientations, with concave and convex shape, but were in the general direction of [u0w] [33]. These steps are called rough steps (see 1.4). Rough steps can sweep the etch pits through the surface and continuously erode the surface. Their source has not been detected yet. There are hypotheses like that these steps are initiated by dissolution at the corners and edges of the samples, or generated by the merger of etch pits. The reason for their high dissolution rate is unclear, but may be attributed to the lower step stability in these directions. It was suggested that any [u0w] step should have stability close to that of [010] and hence dissolves faster than [001] and [100]. The majority of the observed pits had a depth that ranged from ~ 0.7 to ~ 5 nm (a few monolayers),

and pits deeper than 10 nm were in general not a common occurrence although they were observed from time to time.
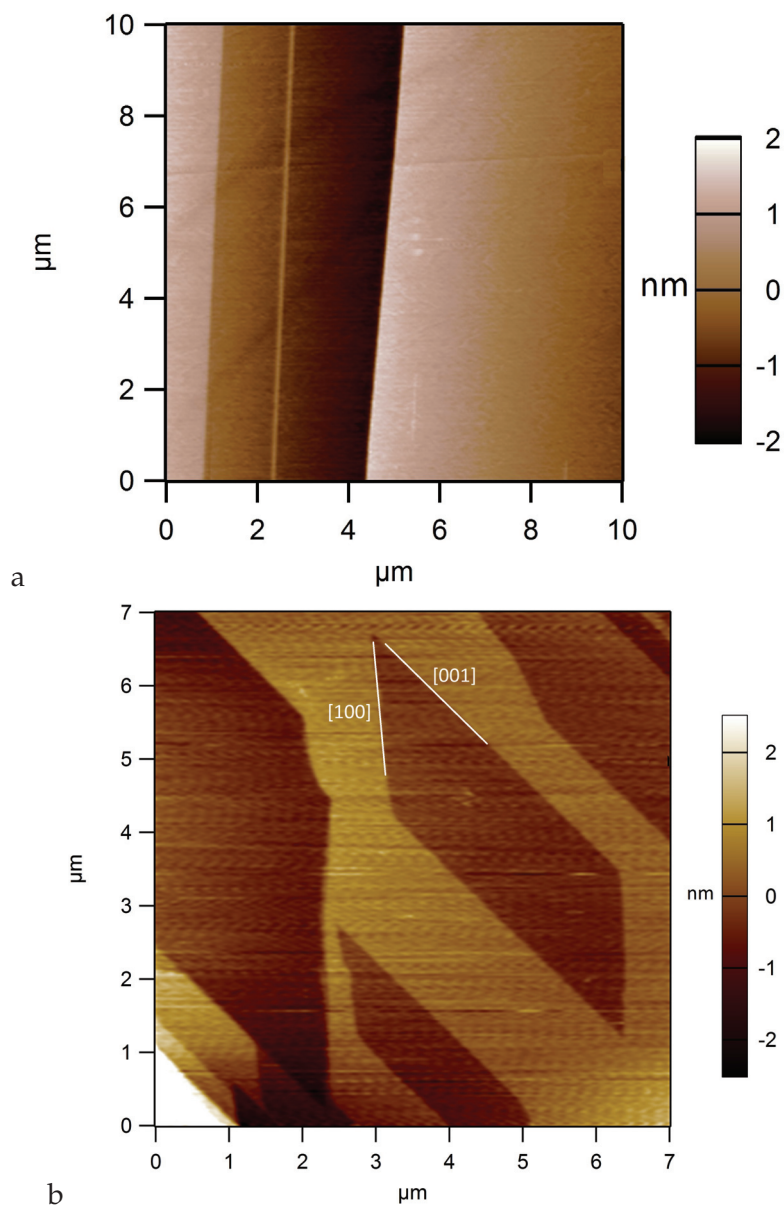
FIGURE 1.3: a) AFM image of the (010) face of a gypsum single crystal, (b) Etch pits formed on gypsum (010) experiencing dissolution in a flowing calcium sulfate aqueous solution with saturation index 90%

However, in most cases new pits would continue and elongate due to anisotropy of step velocities, nucleate and grow, and then merge with the neighbouring pits. So they become larger pits that also move through the surface (figure 1.5). Step movement, inducing perpendicular digging and lateral spreading of the etch pits, control the pit size. To sum up, the lack of deep pits on gypsum surface is a result of the faster lateral dissolution of the less stable steps in the [u0w] directions.
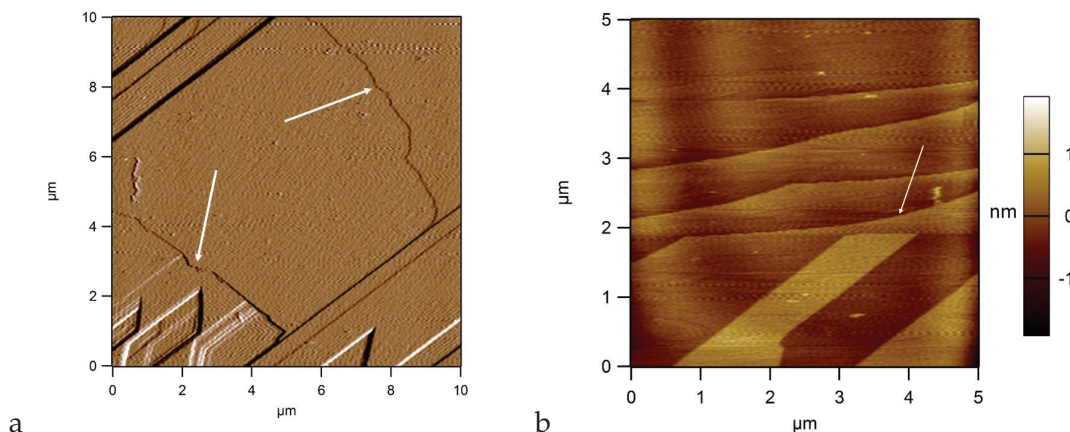
FIGURE 1.4: a)Deflection and b) topography AFM image showing fast-moving rough steps (arrows).

1.3 Calcite

1.3.1 Calcite properties

The structure of the $R\bar{3}C$ calcite is in the hexagonal unit cell. If the c-axis of the calcite unit cell is oriented vertically, calcium cations form horizontal layers separated by planar CO_3 groups (figure1.6 C). The calcite surface is simply a termination of the bulk structure. The covalent CO_3 group has short $C-O$ bond distances because of electron-sharing. Ca and C atoms are orthogonally arranged and sit in the {10$\bar{1}$4} plane, linked by one fully bonded O from each CO_3 group. On the 10$\bar{1}$4 plane of bulk calcite, coplanar Ca and C are separated by 3.2 Å. In this termination, the trigonal planar CO_3 groups are tipped at about 44° such that an underbonded O atom from each group protrudes about 0.8 Å normal to the plane [114]. The CO_3 groups and the octahedral O coordination around Ca alternate in orientation along step edges so each alternating site has its own distinct geometry [115]. Carbonate along step edge is marked as Ac1 and Ac2 on the acute corner and Ob1 and Ob2, at the obtuse corner. At the Ac2, Ob1 and Ob2 carbonate sites, all oxygen atoms are fixed in the calcite structure with two O bound to one Ca and a third O bound to two Ca atoms. The Ac1 group, every second CO_3^{2-} on acute steps, has one O atom from the calcite structure free. Hence, the ion that attaches at the Ac1 group can more easily adapt its orientation than for the Ac2, Ob1, and Ob2 sites. This would influence attachment rates for the Ac1 groups (figure 1.6 b). It is likely that the ions can attach more easily at the Ac1 site but they are also more exposed to attack by Brownian motion of the water molecules and pairing with other ions. Likewise, Ca^{2+} can attach and also detach more easily from the acute steps [130].

For this research the rhombohedral Iceland spar calcite crystal from chihuahua in Mexico were used. Inductively coupled plasma atomic emission spectroscopy (ICP-AES) analysis and scanning electron microscopy energy dispersive X-Ray (SEM-EDX) analysis were done to detect the impurities of the calcite. Based on the obtained results the calcite was 99% pure and the impurities were mostly Mg and Na. These results are presented on appendix A.2.
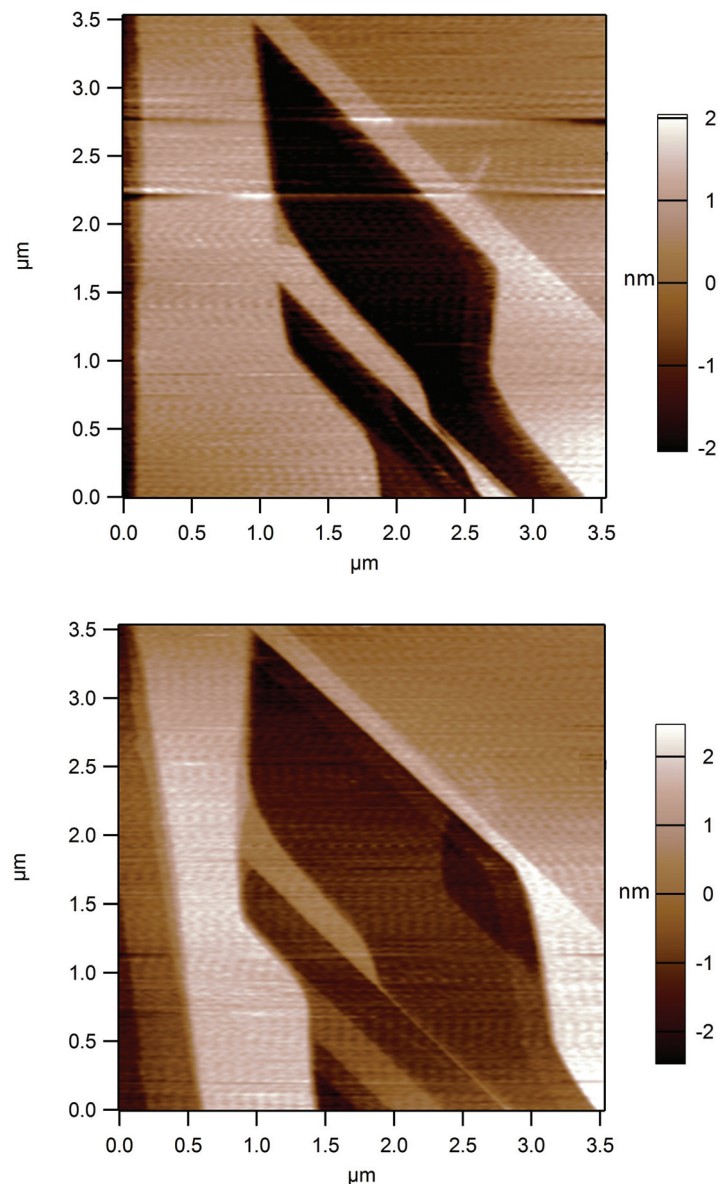
FIGURE 1.5: AFM image of (010) face of gypsum showing a merger of etch pits and travelling etch pits through the gypsum surface during dissolution with saturation index 90% and time interval 1024 seconds between 2 images.

1.3.2   Speciation of the calcite-water interface

The interaction of water and mineral surfaces leads to a variety of surface processes containing adsorption of ions and molecules, growth and dissolution. Due to the widespread existence of calcite in nature and its application in industry, this reactivity has attracted many people since 1960. In 1990 the first spectroscopic study of water adsorption on calcite was performed by Stipp and Hochella (1991) [61]. They suggested that water is strongly associated with calcite. Since then the first model of carbonate minerals by Van Cappellen et al. (1993) [121] built upon the results obtained by Stipp and Hochella in 1991 and on existing surface speciation models for metal oxides and hydroxides. This model assumed hydroxylated calcium sites as the primary hydration site, in parallel to metal oxide surface.
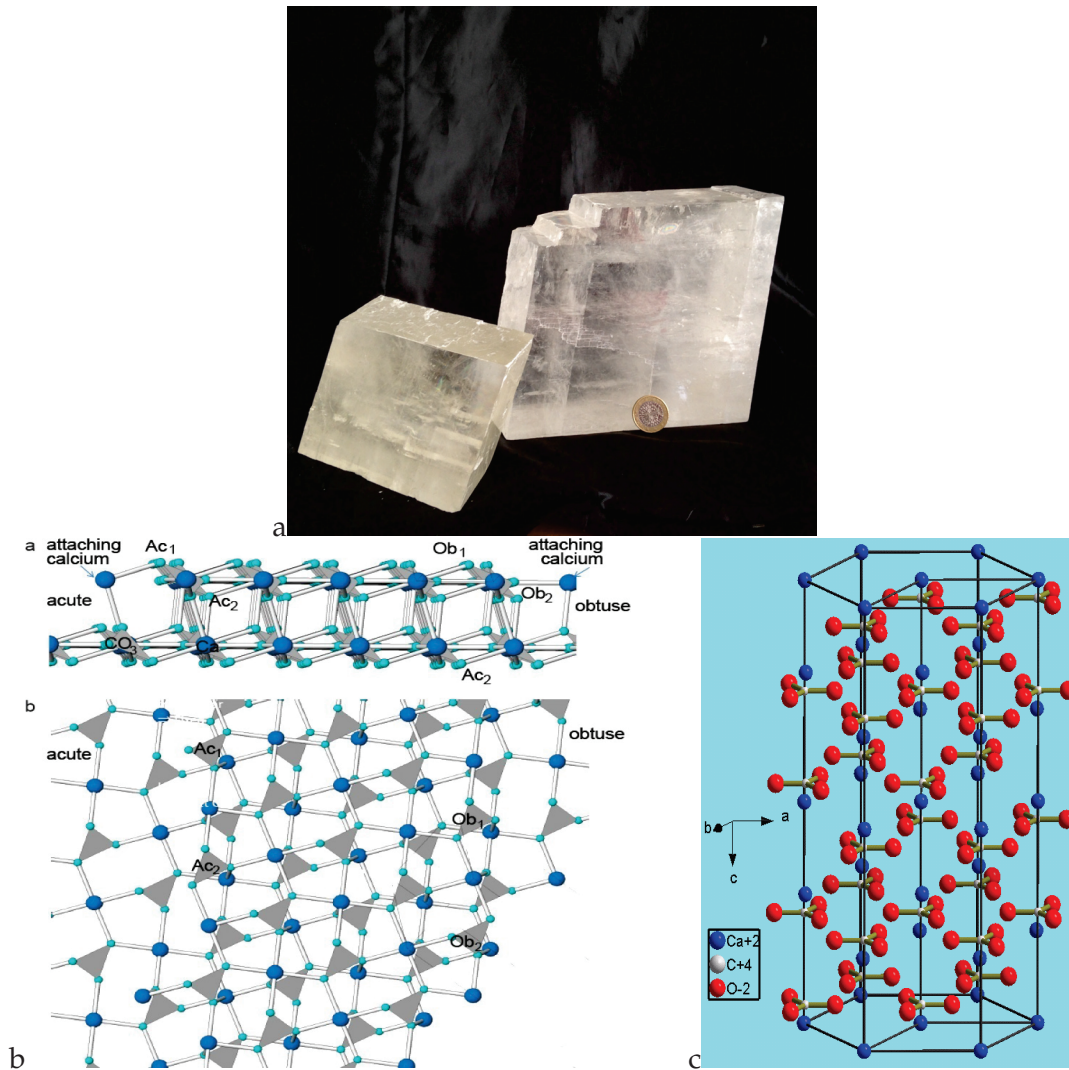
FIGURE 1.6: a) The rhombohedral Iceland spar calcite crystal from Chihuahua, Mexico, b) View of an acute step, Ac (left) and an obtuse step, Ob (right). Gray represents CO_3; bright blue, oxygen; dark blue,Ca^{2+} (generated by the software Atoms) , c) Crystal structure of calcite.

This resulted in the following surface reactions:

Surface reaction	$\log K$ (25°, 1 atm, $I = 0$ M)	
$\equiv CO_3H^0 \rightleftharpoons\ \equiv CO_3^- + H^+$	-4.9	(1)
$\equiv CO_3H^0 + Me^{+2} \rightleftharpoons\ \equiv CO_3Me^+ + H^+$	-2.8	(2)
$\equiv MeOH_2{}^+ \rightleftharpoons\ \equiv MeOH^0 + H^+$	-12.2	(3)
$\equiv MeOH^0 \rightleftharpoons\ \equiv MeO^- + H^+$	-17	(4)
$\equiv MeOH^{0+} CO_2 \rightleftharpoons\ \equiv MeHCO_3{}^0$	6	(5)
$\equiv MeOH^{0+} CO_2 \rightleftharpoons\ \equiv MeCO_3{}^- + H^+$	-2.6	(6)
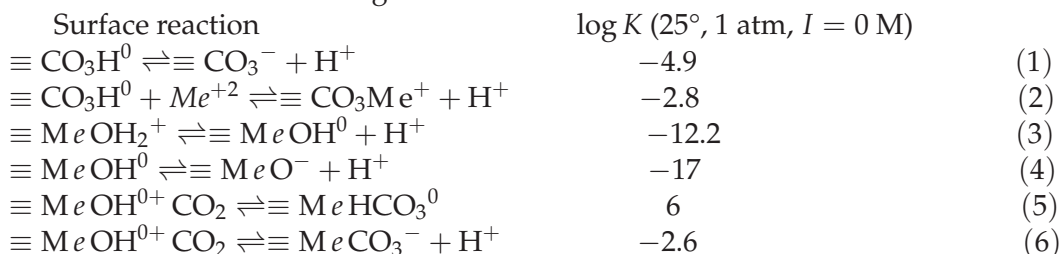
The equilibrium constants for the six reactions were estimated so that the model resulted in a pH at the point of zero charge of 8.2 for calcite at ambient condition and atmospheric P_{CO_2}. The surface complexation model allows an interpretation of the dissolution kinetics of carbonate minerals based on surface speciation. The observed enhancement of the dissolution rate of calcite by protons and carbonic acid correlates with the protonation of carbonate surface sites and carbonation of surface calcium sites, respectively. The protonation and carbonation reactions promote the release

to solution of surface lattice cations through the formation of more reactive surface species. Thus the calcite dissolution and growth depends on many parameters like P_{CO_2}, pH, temperature and alkalinity.

The speciation of the calcite at equilibrium also varies with the pH. The most pH dependence of speciation predominant pH-dependent species are H_2CO_3, HCO_3^- and CO_3^{2-} (figure 1.7). The reactions are the following:

$CaCO_3 + 2H^+ \rightleftharpoons Ca^{2+} + H_2CO_3^0$ Calcite equilibrium at low pH ≤ 6

$CaCO_3 + CO_2(g) + H_2O \rightleftharpoons Ca^{2+} + 2\,HCO_3^-$ Calcite equilibrium neutral pH ≈ 8

$Ca^{2+} + CO_2(g) + 2\,HO^- \rightleftharpoons CaCO_3 + H_2O$ Calcite equilibrium at high pH ≥ 10
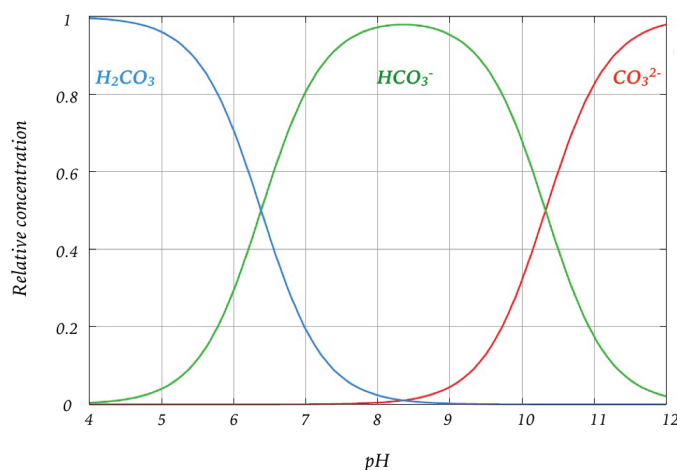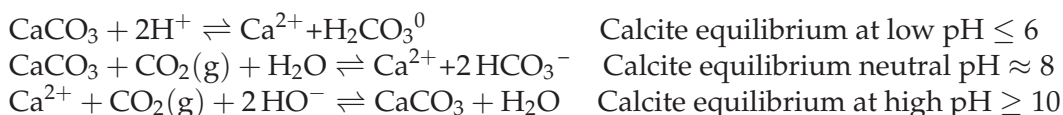
FIGURE 1.7: The activity of H_2CO_3, bicarbonate and carbonate ions as a function of pH, for a total concentration of 0.1 M. This is an example of Bjerrum plot.

Addition of other components like salts, acids and bases to the carbonate system, in addition to the above-mentioned parameters, interacts with carbonate speciations and results in pH-effects, complexation and change in solubility of calcite and CO_2. Because the ionic strength is increased by additional ionic species the predominant carbonate species are shifted. This effect explains the strong decrease in the solubility of CO_2 as the electrolyte content of a solution is increased. This is due to the strong increase in the activity coefficient of $CO_{2(aq)}$ as the ionic strength is increased.

1.3.3 Calcite crystal dissolution

Dissolution rates of calcite far from equilibrium were observed to depend on surface preparation and on surface morphology resulting from defects outcropping at the crystal surface. The high dissolution rate for mechanically polished surfaces is attributed to enhanced dissolution at cracks and dislocation loops produced in the grinding process [75].

The dissolution of the calcite (104) cleavage surface at nanoscale, at far from equilibrium conditions begins with the formation of monomolecular holes [68]. Dissolution then proceeds with the "growth" of the hole into an etch pit, facilitated by anisotropic retreat of crystallographically-oriented monomolecular steps [52, 45, 114]. A step retreat on the crystal surface is the result of kink formation and kink propagation represented by the removal of lattice components along monomolecular step edges. These kink sites are self-replicating, that is, the removal of a kink atom turns the adjacent atom into a kink atom. Repeated removal of kink atoms

accounts for the spatial motion of steps across the crystal surface [39]. As etch pits grow in size and depth, they coalesce with and annihilate neighboring etch pits. If dissolution continues at undersaturated conditions the crystal will experience retreat normal to the surface [73, 64].

Dissolution studies in many cases have focused on etch pit development and coalescence to explain the rate of overall dissolution.Different from this view of dissolution, based on the theoretical models that have emphasized the concept of the dissolution process, dissolution occurs as trains of monomolecular "stepwaves" propagating from the upper bounding edges of etch pits [79]. Etch pit is a source for the formation of monolayer stepwaves. As etch pits coalesce, stepwaves increase in length and can travel throughout the crystal surface and control the overall dissolution. A typical rhombic etch pit and the retreat of steps is shown in figure 1.8.
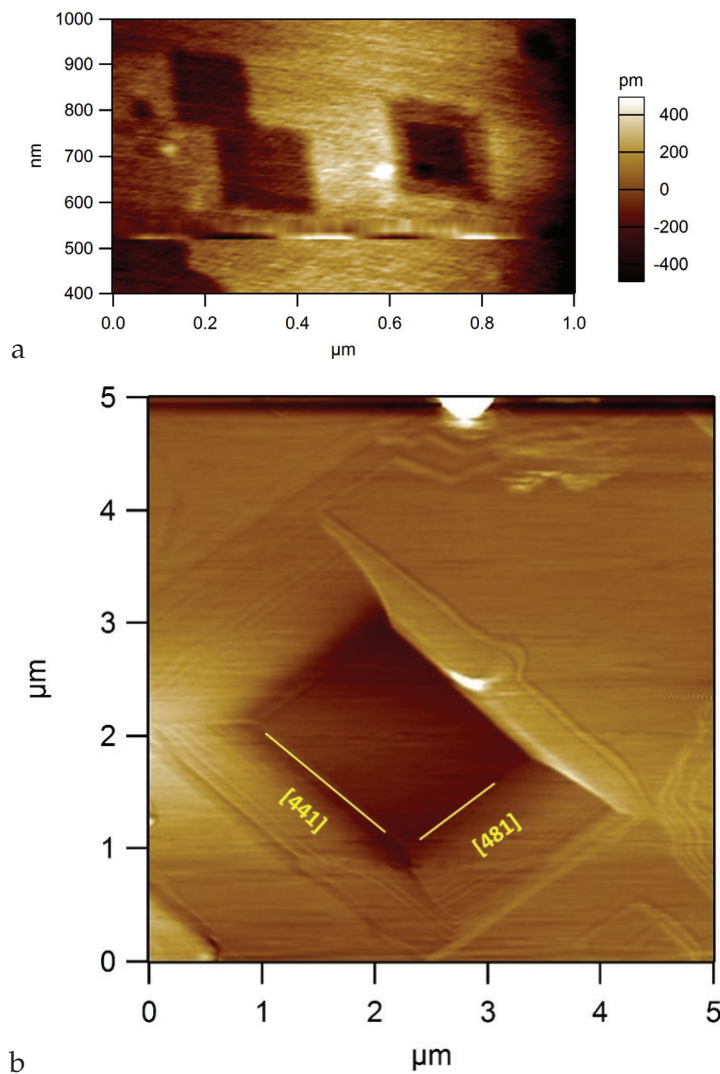
FIGURE 1.8: Atomic force microscopy images of typical rhombohedral etch pits with four step edges, two of them aligned along the [441] and two of them aligned along the [481] orientation.

The shape of the pit is reminiscent of the rhombohedral lattice with the obtuse angle of $102°$ and acute angle of $78°$. The height of step is mostly one atomic layer ≈ 0.3 nm, the steps being along either the [481] or [441] direction. Step velocities can be classified as slow V_s for $[441]^-$ and $[481]^-$ and fast V_f for $[441]^+$ and $[481]^+$. For

one type of step, the step-edge atoms on the upper terrace overhang and an acute angle is formed, while at the opposite side of the pit, an obtuse step is formed. Such a difference in structure causes two dissolution step velocities, a fast velocity V_f for the obtuse steps (in sum), and a slow velocity V_s for the acute steps (in sum). The two obtuse steps due to similarity in geometry and chemistry show the same behaviour and usually they are added and called V_f. Respectively the same tendency are observed for two acute steps and they are displayed as V_s. Thus, the dissolution is anisotropic. The ratio of the two velocities V_f / V_s remains as a constant having a value of approximately 2.3 [68].

Since 1990, a major research on the dissolution at nanoscale has been focused on the relationship between step velocity, spacing, geometry, and observables related to solution properties like pH, dissolved lattice ions, impurity components, supporting electrolytes, ionic strength, etc. However the dissolution of the calcite surface at microscale has revealed a significant complexity in step movement and morphology. This complexity implies that the general morphology of the surface is a sensitive reflector, not only of its interactions with the surrounding solution, but with itself as well [55].

An image of dissolved surface of calcite with a gold coated portion as a height reference at large scale taken by Vertical Scanning Interferometry is shown in figure 1.9. In figure 1.9a and b the reaction surface after 4 hours of reaction at pH=6 dissolution involves several, well-developed, shallow etch pits (the outcrop of shallow screw dislocations), flat terraces with only few minors etch pits and steps. Figure 1.9c displays the reaction surface after 4 hours of reaction at pH = 4. Here the dissolution is associated with giant, well-developed deep etch pits (the outcrop of deep screw dislocations), flat terraces with only few minors etch pits and mega steps.

Based on reported data and on our observation in this research, dissolution of the cleaved calcite surface is conducted by the combination of deep growing etch pits, shallow growing etch pits, step migration on terrace and overall surface retreat. Dissolution according to the stoichiometry conditions and to the surface morphology (defects and dislocation) is driven predominately by one or a combination of these phenomena.

1.3.4   Calcite crystal growth

Calcite crystal growth occurs when calcite precipitates from supersaturated solution. The crystal growth depends on supersaturation state [85, 118], pH [104, 53], $[Ca^{2+}]/[CO_3{}^{2-}]$ ratio [85, 53, 108] and surface morphology [118, 53, 108]. The supersaturation, in the form of the **S**aturation **I**ndex **SI** of calcite in solution, is defined as :

$$SI = \log\left(\frac{[Ca^{2+}][CO_3{}^{2-}]}{K_{sp,\text{calcite}}}\right) \tag{1.1}$$

$K_{sp,\text{calcite}}$ represent the solubility product of calcite, which is $10^{-8.48}$ at 25°C [97] and $[Ca^{2+}]$ and $[CO_3{}^{2-}]$ the activities of calcium and carbonate ions. The growth rate increases with increasing supersaturation and depends on pH and $[Ca^{2+}]/[CO_3{}^{2-}]$ratio in a nonlinear manner (see figure 1.10).
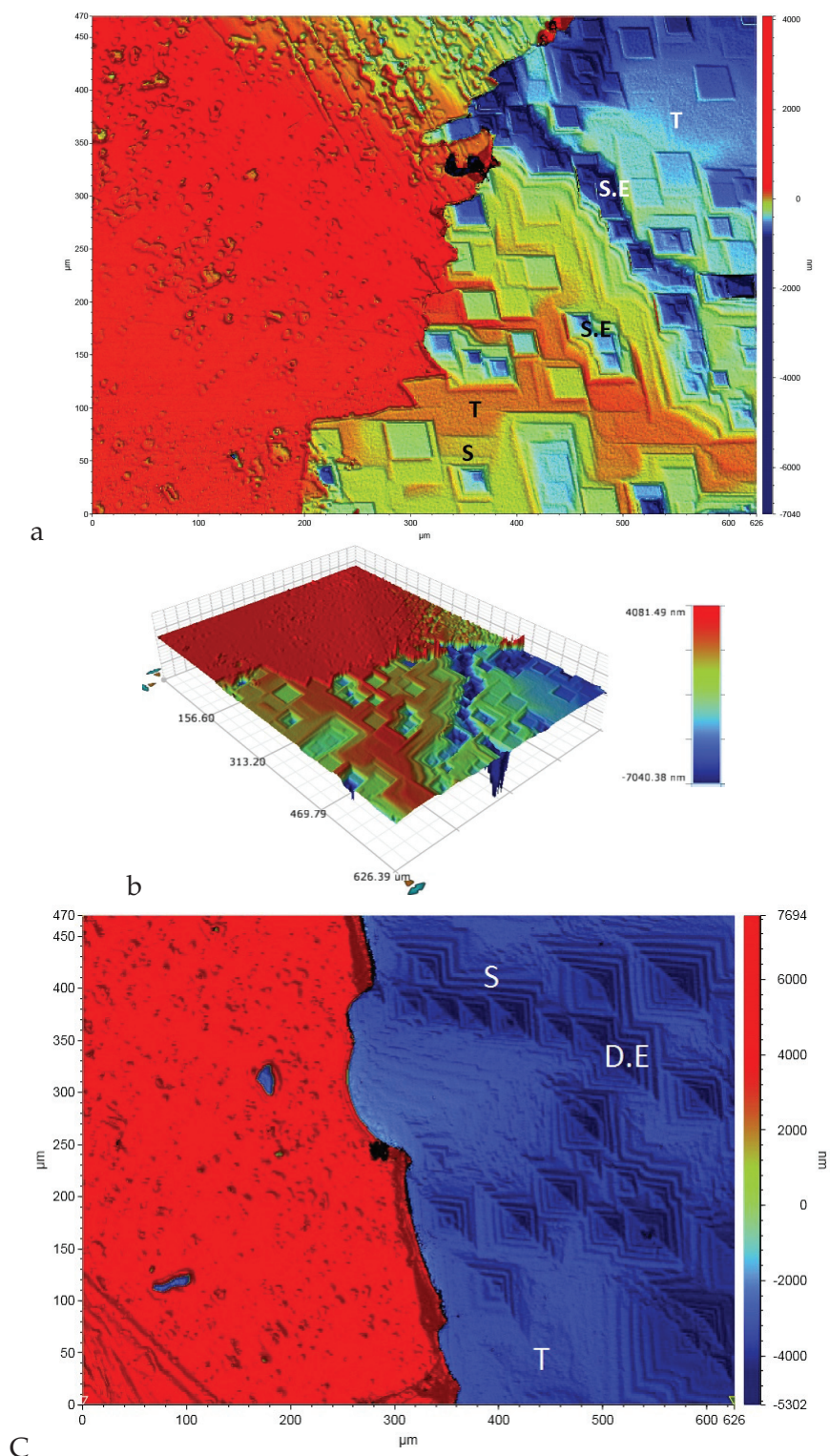
FIGURE 1.9: (a) VSI color map of calcite after 4 hours of reaction at pH=6, with terrace ("T"), shallow etch pit ("S.E"), step ("S"). (b) VSI height color map of image (a) after 4 hours of reaction at pH=6. (c) VSI color map of calcite at pH=4, with terrace ("T"), deep etch pit ("D.E"), step ("S"). The red color region in both images is the gold-masked reference surface.
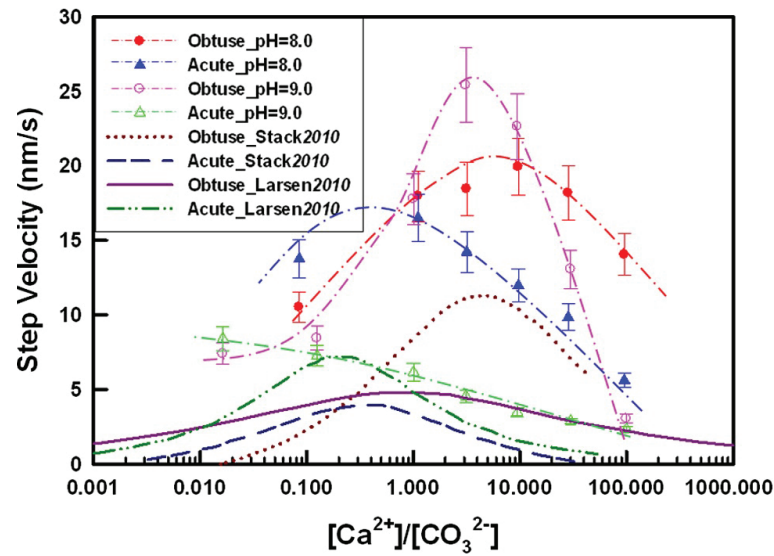
FIGURE 1.10: The dependency of growth rate of calcite growth spiral
on pH, Ca^{2+}/CO_3^{2-} and growth site geometry. Figure adapted from
Hong & Teng [53].

The most stable calcite surface, $\{10\bar{1}4\}$, is anisotropic. As detailed in the previous
section, growth steps exhibit an open (obtuse) or closed (acute) geometry (see figure
1.11). Because of the different geometries of obtuse and acute steps, their growth
are not equivalent and their dependence on solution parameters differ, as shown
in figure 1.10. Growth steps generally have a low kink density in the absence of
impurities and it is believed that kink formation is the rate limiting step in calcite
growth [4].
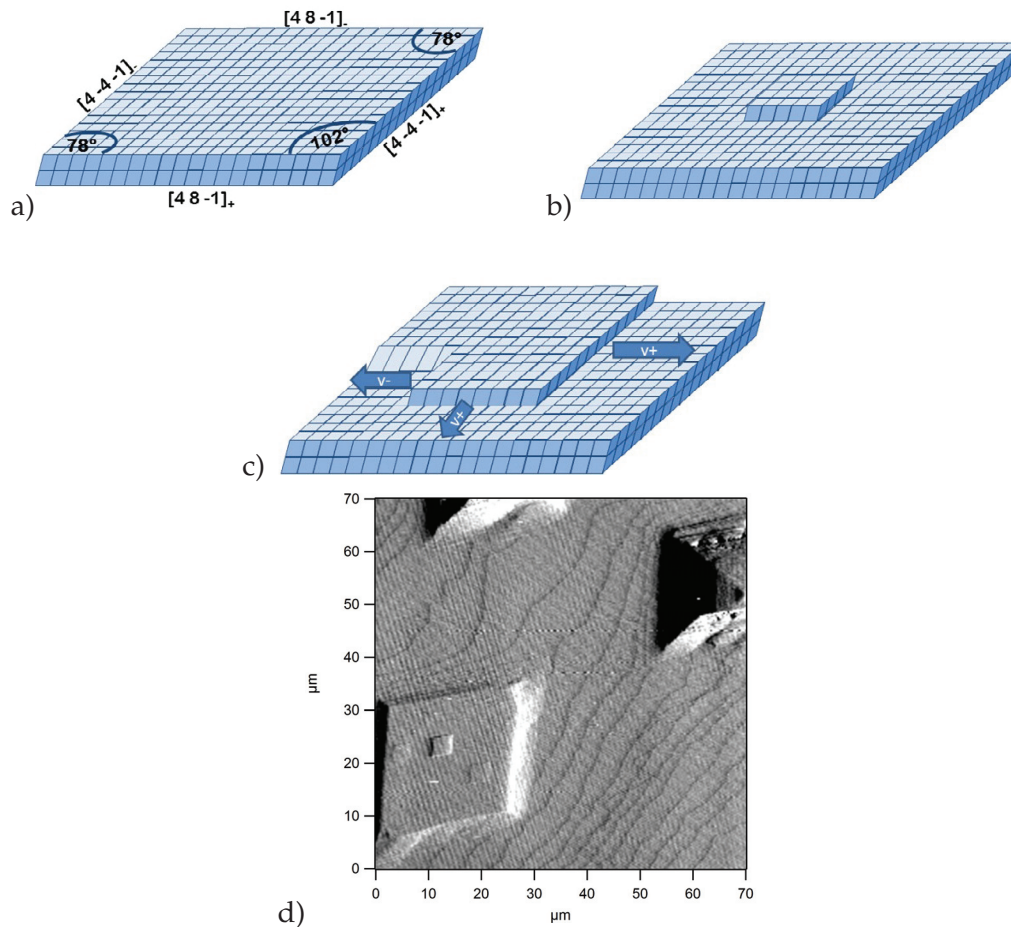
FIGURE 1.11: The 2D growing calcite {10$\bar{1}$4} surface. (a) The anisotropic nature of the surface with acute and obtuse steps. (b) 2D nucleation, where Ca^{2+} and CO_3^{2-} ions are adsorbed from solution to the flat surface, forming a new growth site. (c) Growth from 2D nucleation. (d) Deflection AFM image of a layer growing from new sites of 2D nucleation. Figures a, b and c adjusted from [50]).

There are two common growth mechanisms for the calcite which depend on the supersaturation of the solution: Spiral growth and 2D nucleation. Spiral growth starts when steps grow from one or more screw dislocation (see figure 1.12 c). Once the step reaches the supersaturation-dependent critical length, another step starts growing and a pyramid forms [118]. Spiral growth from single dislocation produces single steps pyramid (figure 1.12 a). Spiral growth from double dislocation (Burgers vector two lattice parameter long) produces double steps pyramid (figure 1.12 d) and spiral growth from triple dislocation produces triple steps pyramid (figure 1.12 e). The density of screw dislocations is independent of supersaturation. It depends on the defect density of the underlying calcite surface. If the supersaturation is high enough, 2D nucleation becomes the dominant growth mechanism [120]. In 2D nucleation, the adsorption of constituent ions occurs spontaneously onto the flat surface (figure 1.11). Because the newly formed surface is flat, new layers are formed at the next 2D nucleation event [50]. Teng et al.(2000) have shown that 2D nucleation becomes dominant at supersaturation above 0.7 [120].

In addition to the solution parameters already discussed, growth rate depends heavily on the presence of impurities [9, 46, 126, 118, 23] and the effects of impurities
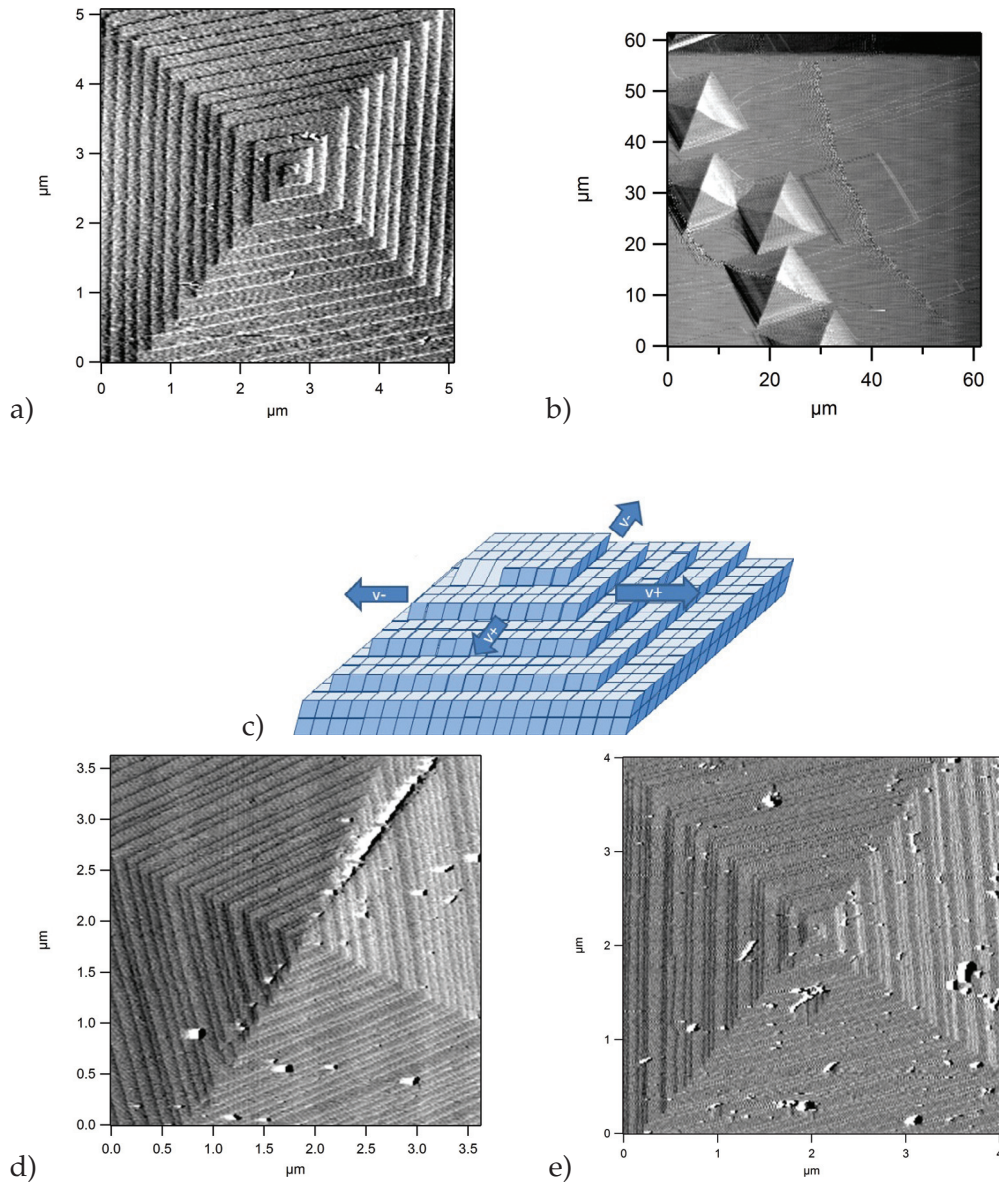
FIGURE 1.12: (a) A close AFM image of pyramid as a result of single
spiral growth and steps resulting from spiral growth. (b) AFM im-
age of groups of pyramid. (c) The spiral growth from a single screw
dislocation on {10$\bar{1}$4} surface. The step length depends on the super-
saturation of growth solution (figure c adjusted from [50]). (d) A close
AFM image of double step pyramid as a result of spiral growth on a
double dislocation. (e) A close AFM image of a triple step pyramid as
a result of spiral growth on a triple dislocation.(the images a,b,d and
e are AFM deflection image)

are direction-specific [126, 118, 23]. Impurities can inhibit calcite growth by blocking
surface sites [7, 127] (see figure 1.13) and by imposing strain in the calcite surface
structure when incorporated into the surface or the bulk of the mineral [23]. Some
organic impurities have been shown to promote calcite growth through dehydration
of calcium ion and calcite growth steps, like amino acid glycine and pentaglycine,
two peptides [40, 31, 86] (see figure 1.13). Because impurities interact with obtuse
and acute steps differently they can stabilize other facets on the calcite surface, there-
fore the morphologies of calcite particles change when they grow in the presence of

impurities [92, 34] (figure 1.13).

Shell forming organisms have been shown to utilize impurities to control crystal shape, size, and even phase, by stabilizing other calcium carbonate polymorphs, with a combination of organic molecules [8, 126, 40], mostly proteins and polysaccharides, and inorganic ions [109].
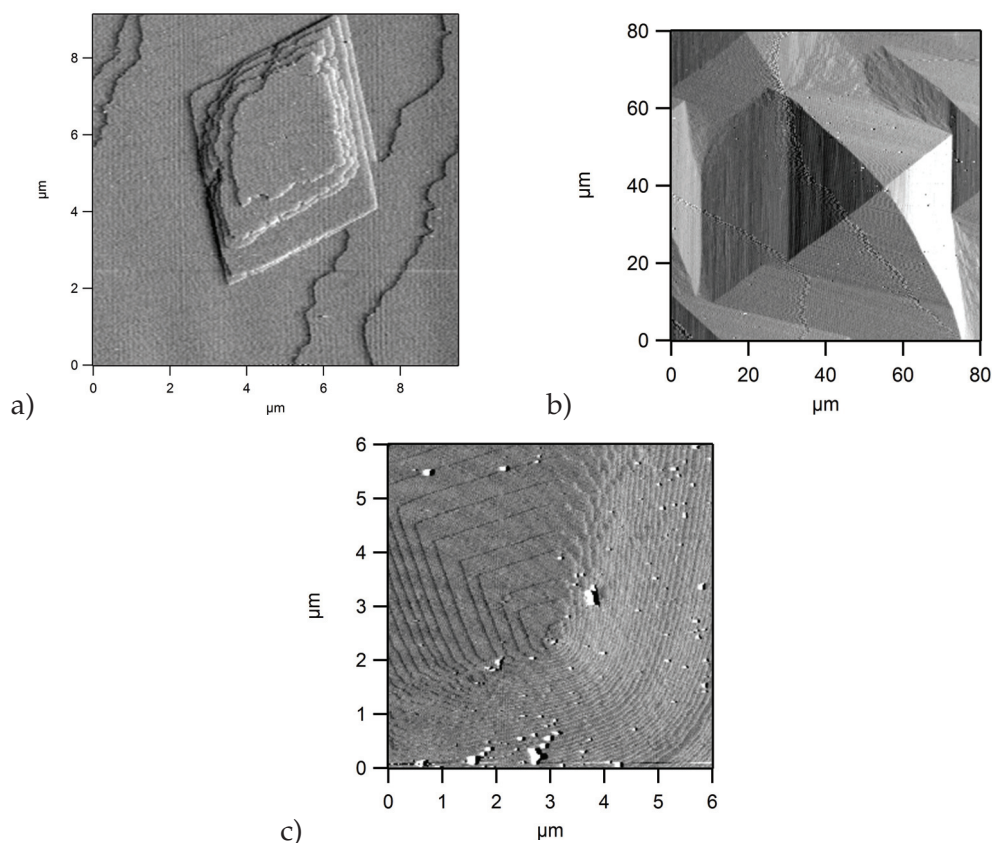
FIGURE 1.13: (a) AFM image of inhibited spiral growth due to unknown impurities. (b) Spiral growth (pyramid) in a growth solution containing 82 μM of pentaglycine without observable changes of morphology of the pyramid. (c) Spiral growth (pyramid) in a growth solution containing 7 mM of hexanoate with rounded obtuse steps (image c was from collaboration with Tanja Lain Clausen from University of Copenhagen)(All the images are AFM deflection image).

1.4 Thesis objectives

The main objective of my PhD research was fundamentally to contribute to understand the process of material hardening, for instance during rock formation, diagenesis, cementation and biomineralisation. This phenomenon proceeds by dissolution and growth in nano-confined condition, generally in presence of considerable stress and impurities.

Recent experimental and modelling studies of confined single crystal precipitation suggest that there is a strong link between confined mineral growth and the presence of stress, that may control the nucleation and growth on the surfaces [67, 25, 41, 26].

One of the challenges of this research was to find reliable cross-links between dissolution/growth rates of mineral from nano to mega scale. Studies about dissolution, nucleation and growth have started more than 50 years. They had focused on the chemical reaction and bulk diffusion and advection. Since two decades, the use of tools resolving nanometric objects, such as vertical scanning interferometry (VSI) and atomic force microscopy (AFM) have changed our view on these phenomena. In this research we used these tools to study how the physical changing of the solid surface at atomic scale surface reactivity, in addition to chemistry effects. The objectives of each of the three different studies presented in this thesis are the following.

In the first study *"dissolution rate from molecular measurements"*, my goal is to identify the atomic scale mechanisms during gypsum cleaved surface dissolution by the AFM, with the final aim to be able to upscale their dynamics. Furthermore in order to understand how aqueous fluids interact with gypsum-bearing rocks loaded either by overburden, or tectonic stresses, I studied the effect of stress on the dissolution mechanisms. Concerning the rate of dissolution I focused to deduce the macroscopic dissolution rate from the atomic kinetics. The main research questions in this study were:

How does an applied stress affect the atomic mechanisms of gypsum dissolution?

Can we compute the macroscopic dissolution rate from the atomic step kinetics?

In the second study "*Influence of stress on calcite growth*", the first objective of this research is to evidence the influence of stress on the calcite growth, in view of a comprehensive understanding, taking into account surface elasticity, diffusion and advection of solution in overburdened conditions. I tried to use a single contact to apply a force on the surface and studied the dynamics of calcite growth at different applied forces. For mimicking the nature, and being inspired by bio-mineralization and how the nature can make brittle materials harder and more flexible, I used pentaglycine as an additive to observe its effect on the kinetics of calcite growth. The main research questions in this study were:

How the surface can adjust nucleation and growth while it is under pressure?

What is the effect of pentaglycine on the dynamics of calcite growth?

What is the influences of pentaglycine and varied applied force on calcite growth?

In the third study "*Microscale influence of pH on calcite dissolution*" I wanted to focus on dissolution and quantify the relevant dissolution mechanisms at the calcite crystal surface over a wide range of length scales. Direct measurements of the three-dimensional calcite crystal surface can provide fundamental insight into the reaction mechanisms of calcite dissolution and their relationship to thermodynamic descriptions of the bulk system. My initial objective was to identified detailed information about the reaction mechanism at the calcite surface at different pH. The most important research questions were:

what is the main surface physical mechanism controlling dissolution at different pH?

How the pH can influence calcite dissolution at nano scale?

What is the influence of glycine at different pH on calcite dissolution?

1.5   Analytical techniques

1.5.1   AFM

Atomic **F**orce **M**icroscopy (**AFM**) was developed when people tried to extend the **S**canning **T**unnelling **M**icroscopy (**STM**) technique to investigate electrically non-conductive materials, like proteins. The idea of AFM was demonstrated for the first time by Binnig and Quate in 1986. They used an ultra-small probe tip at the end of a cantilever. Then in 1987 its setup was developed with a vibrating cantilever technique which used the light-lever mechanism of Wickramasinghe et al [10].

The AFM analysis technique allows for high resolution imaging of surface in air or in a solution . This technique works by moving a cantilever, which uses a micrometric sharp tip to probe the surface features by raster scanning. A ceramic piezoelectric controls the normal tip moving on the surface. It can do it quickly and accurately. The tip is often made of silicon nitride.

A highly dense laser beam is focused onto a reflective spot on the cantilever surface to direct it toward the photodiode so that any changes in the interaction between the tip and sample causes the cantilever to bend and a deflection of the laser beam to be recorded [10] (Figure 1.14). AFM can image the surface topography with atomic resolution and provides thereby the possibility of recording images of surface during growth and dissolution [117, 120].

Additionally to probing the surface AFM is used for the detection of adhesion forces between the tip and the surface of the sample. Several studies have been conducted in this perspective, like [133, 93, 36, 35] for the case of soft materials. AFM cannot provide users with direct information about the chemical composition of the surface.
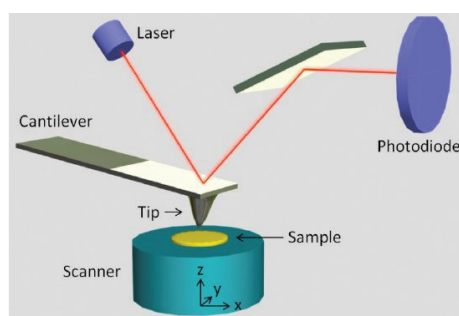
FIGURE 1.14: Schematic illustration of the principle of AFM. The scanner is composed of three piezo components, which control the horizontal (x and y) and vertical (z) movement of the sample.

AFM is usually performed in three operational modes: *Contact mode* where the tip is in contact with the surface and the deflection of the cantilever is kept constant. In this mode the probe is in continuous contact with the sample while it raster scans the surface. The interaction between the tip and the surface can be adhesive or repulsive, which depends on the surface. In contact mode with constant force, the output consists of two images: height (z topography) and deflection or error signal. The

contact mode can be used for delicate samples in liquid, as long as the force can be controlled. *Non-contact mode*, where the tip is oscillated at the resonance frequency close but not to the surface and the amplitude of the oscillation is kept constant. Finally the *tapping mode* where the tip oscillates at its resonance frequency near or just close to the surface.

For my study of gypsum dissolution and calcite growth, I used a commercial atomic force microscope (MFP3D, Asylum Research, Oxford Instruments) in contact mode, equipped with a custom made fluid cell (Figure 1.15) with a peristaltic pump. This allowed me to image gypsum dissolution and calcite growth in the solution flowing over the surface at a constant flow rate of 0.275 mL/min.
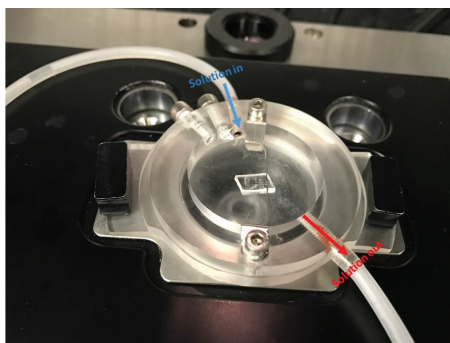
FIGURE 1.15: The custom fluid cell in my AFM experiments. Fresh solution continuously flows over the mounted calcite crystal. The output of the flow is situated at the top of the fluid cell to facilitate removal of any dust at the air solution interface.

1.5.2   VSI

Vertical **S**canning **I**nterferometry (**VSI**) is based on the principle of a Michelson interferometer. Then it has been adapted to microscopy , and called Mirau interferometer. This scanning white light phase shift interferometer is used to quantify the surface dynamics during processes like dissolution and growth, among others. This scanning technique uses Mirau objectives, and the objective plays the role of the interferometer. The objectives 5×, 10× and 50× are used (see Figure 1.16). A main advantage compared to other interferometric techniques, which use an open beam path, is that the system is very compact and does not need an expensive clean lab. However, it is necessary to avoid vibrations as much as possible. For that an anti-vibration air table works successfully.

The technique provides near-atomic scale investigations with a vertical resolution better than 2 nm and a lateral resolution of 0.5 to 1.2 μm (depending on the objective used). Rather "large" vertical scan range of the analytical system is an important prerequisite to study mineral surfaces that have often steps with several μm or even tens of μm height differences. This requirement often limits the application of atomic force microscopy. This method provides a vertical scan range of up to 1 mm, and, therefore, the possibility to study macro-steps on crystal surfaces [73]. An optimal setting is to employ a scan range up to 100 μm with a vertical resolution of about $\sim$ 20 Å. At the same time, the field of view is large compared to that of an atomic force microscope, that is, 1252 × 940 microns (5× objective), 626 × 470 microns (10× objective) or 125 × 94 (50× objective), respectively. This large field of view is critical to be able to study the dynamics of the spatially heterogeneous dissolution (or growth) processes, because the same spot on the surface can be found

more easily, making the comparison of the evolution with time of a given portion of the surface more straightforward. Vertical changes of the surface topography at these mentioned scale can be quantified over a relatively long run duration of experiment.
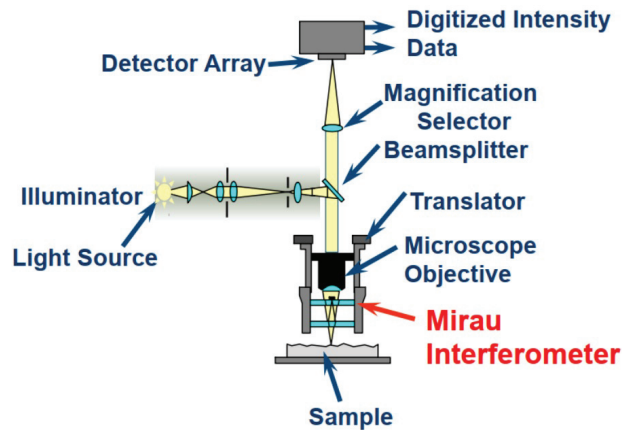
FIGURE 1.16: Adjusted sketch of principle of a VSI [78].

1.5.3 SEM-EDX (Scanning Electron Microscopy Energy Dispersive X-Ray Analyzer)
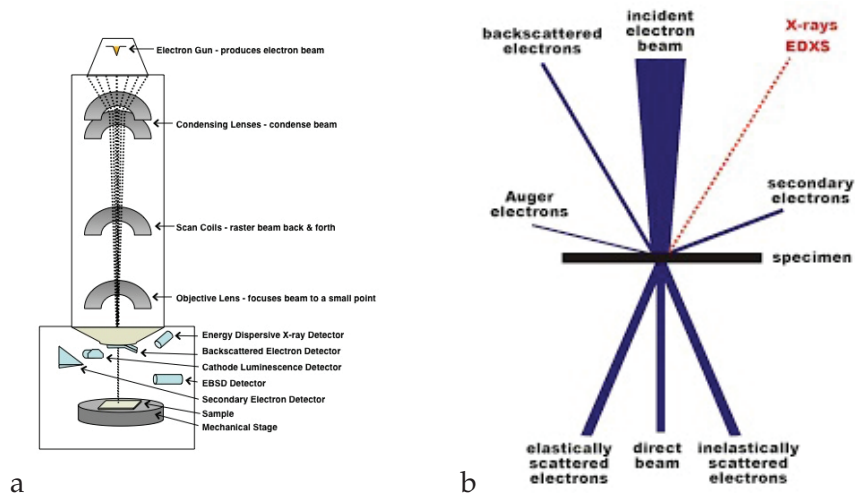
FIGURE 1.17: a) Schematic of scanning electron microscopy. b) Schematic diagram of the type of radiation, scattered electrons and detected electrons in electron microscopy.

Electron microscopy is the imaging of material by illumination with electrons [123]. A beam of incident primary electrons interacts with the sample as shown in figure 1.17. SEM deals with scattered electrons and emitted radiation detected above the surface of the sample. The beam of primary electrons is scanned over the surface in a raster fashion and the intensity of secondary or back scattered electrons is plotted against the position of the beam, resulting in a 2D image of nm resolution. Secondary electrons have undergone elastic scattering, so the kinetic energy of the reflected electrons is unchanged. This results in an image where, in the absence of

charging, the intensity of the detected electrons depends only on the topography of the sample. Back scattered electrons have undergone inelastic scattering. so their kinetic energy is smaller than before their interaction with the sample. Because the electrons have a larger tendency to undergo inelastic scattering when interacting with heavier elements, these tend to be brighter in images recorded from back scattered electrons.

Detailed chemical information can be obtained through the detection of characteristic X-rays, which are emitted when incident electrons cause an atom to emit an electron of its own. After this, two modes of relaxation are possible: X-ray fluorescence or emission of an Auger electron. The probability of X-rays increases with element mass. By analyzing the energy and intensity of the emitted X-rays (Energy dispersive analysis of X-ray spectra, EDX), the composition of the top several hundreds of nm of the sample can be determined. Detection limits are element dependent, but values of around 0.1 % are common [102].

Chapter 2

Dissolution rate from molecular measurements
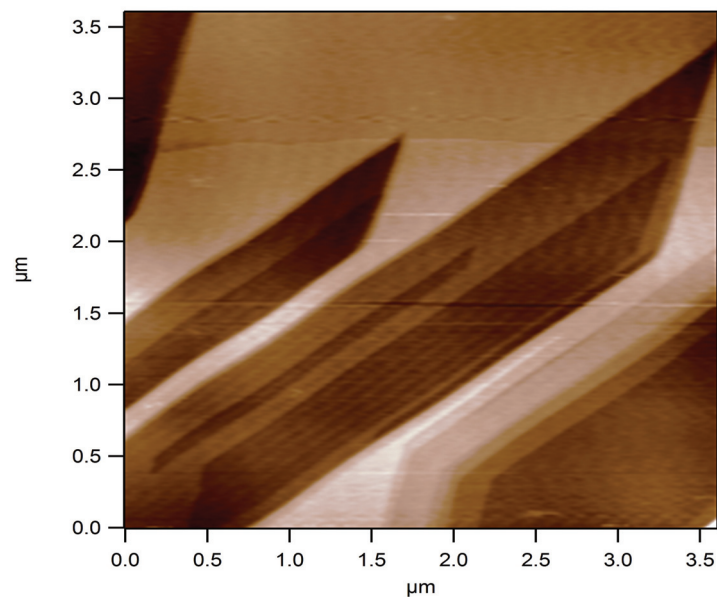
2.1   Preface

Understanding the dissolution behavior of gypsum $CaSO_4, 2H_2O$ in aqueous solutions is of primary importance in many natural and technological processes. The study of the mechanisms and kinetics of water and gypsum interactions may provide insights into the role of gypsum on crustal deformation in numerous geological settings and in trapping large oil and gas accumulations [80, 14]. Since 2 decays AFM is one of the precise used device to observe the evolution of the crystal surface and to deduce the kinetics of dissolution.

The theoretical model that was provided by Lasaga and Lüttge [63] to better understanding of the kinetics of mineral dissolution and to observe the importance of the parameters, like dependence of overall rate dissolution on saturation state of solution. They developed this dissolution theory based on the movement of dissolution step waves stemming from surface defects.

In the first chapter I have introduced the dissolution mechanisms, like etch pit expansion and step motion, on the gypsum cleavage surface at atomic scale. The first aim of this chapter is to better understand in details the mechanism of gypsum dissolution at conditions close to the burial. Therefore this research concerns the influence of pressure on dissolution. In order to understand how aqueous fluids interact with gypsum-bearing rocks loaded either by overburden, or tectonic stresses, it is important to identify the effect of stress on the dissolution mechanisms. To get closer to realistic wet solid-solid contact and imitate real particle interface, i.e., the dissolution behavior of the gypsum surface under the point contact applied force, I used in this experiment AFM tip to apply the force, a configuration close to the actual contact between gypsum grains, occurring at asperities.

In addition gypsum dissolution rates are measurable in laboratory times and the chemical reaction is rather simple. The gypsum has the existence of a surface normal retreat during dissolution [73]. The gypsum rhombohedral etch pits have role of step sequencer source. These two bold properties technically have been made it suitable for investigation at the nanometric scale.

The macroscopic dissolution rate of minerals is generally deduced from solution chemistry experiments. The rate is derived from the increase of the concentration in a liquid where the material dissolves. By using AFM and VSI the microscopic dissolution rate can also be inferred from the dynamics of molecular events, among which the atomic step migration is the dominant ones beside a general vertical retreat of the surface [71]. The obtained results for both hardly ever agree, even qualitatively. In the worst cases, orders of magnitude separate the two. Besides a general theory linking the kinetics at the two scales is still lacking. Keeping this in mind, the second aim of this chapter is to compute a dissolution rate from the kinetics of the molecular mechanisms in quantitative agreement with the macroscopic dissolution rate.

This study demonstrates that, if a dominant mechanism exists, the simple upscaling of the dissolution rate from the atomic level to the macroscopic one, is possible. We should not consider that this upscaling is achievable for every mineral. If several interacting atomic mechanisms are involved, such a simple relationship is excluded, and more complex analyses are required.

2.1.1   Pressure solution

Many geological and material studies have focused on compaction behaviour of sedimentary rocks and material to better predict porosity values [88]. In the early stage they only considered mechanical compaction. Vertical stress and grain size are

the main parameters influencing this compaction. However mechanical compaction does not explain reasonably porosity-depth trends observed in sedimentary basins [20], so the effect of chemical compaction on porosity must be also considered.

The main chemical mechanism during compaction is **pressure solution** creep, which involves local mass transfer by dissolution, diffusion and precipitation processes at the grain scale [20]. This process is considered a key aspect to describe the deformation and compaction of sediments and sedimentary rocks (see sketches in figure 2.1), playing a determining role in processes such as diagenesis, compaction and porosity/permeability evolution in sedimentary basins [30, 111, 100].

The driving mechanism of this chemical compaction is pressure solution, i.e., crystal dissolution in confinement by effect of an external load . Pressure solution takes place at surfaces separated by a thin film of solution from the confining wall (pore surface or other crystal). The dissolution in this process is a consequence of the stress-induced change of the solid chemical potential, that increases locally its solubility. This process is characterized by the three successive processes of dissolution of solid minerals at grain contacts, diffusion of solutes along the grain boundaries and re-precipitation at free surface (see figure 2.1) [84, 111, 2, 134, 58]. Different parameters are involved in pressure solution, including: applied stress, temperature, advective and diffusive fluid transfer, liquid composition.

The experimental studies mostly focused on the effect of the stress on the compaction. They fitted the data according to power law relations between applied load and grain size and strain rate:

$$\dot{S} = P^\alpha d^{-\beta} \tag{2.1}$$

where $\dot{S}$ is the strain rate, d is the grain diameter and P the external stress. Different values for α and β were reported ranging both from 1 to 3 [100, 44, 21].
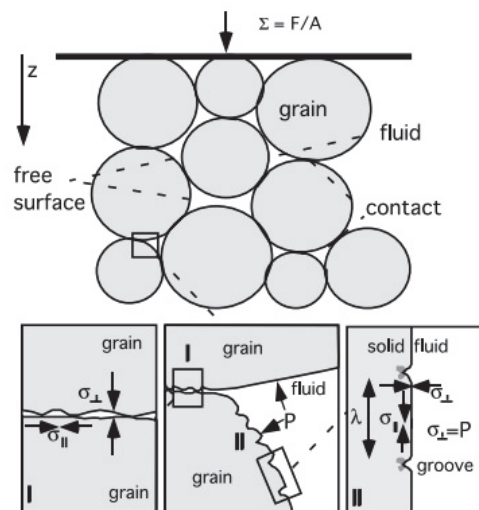
FIGURE 2.1: Schematic image of different reactive sites in an aggregate of grains under compression. The aggregate is compressed by the force F applied on the area A, which results in a stress σ. The coordinate axis z faces downwards. The close-up in the middle shows the two reactive sites. One reactive site is the contact between grains where pressure solution takes place and the other is the contact of grains with the pore fluid. P is the fluid pressure in the pores. The close-up on the left-hand side shows the grain-grain contact [58].Theclose-up on the right side exemplifies the Asaro-Tiller-Grinfeld (ATG) instability.

The contact morphology in pressure solution is important and the strain rate depends on the grain contact, consequently understanding this phenomenon becomes complicated. Several morphologies for this complex contact are observed. The morphologies observed on the grain contact surface after being exposed to pressure solution, are for instance smooth, featuring ridge and plateau structures, with fluid micro-channels and micro-cracks, or dendritic contact regions [24, 19, 44]. Non-hydrostatic stresses near the surface may lead to the Asaro-Tiller-Grinfeld (ATG) instability, destabilizing the surface, controlled by competition of two factors, a compressive mechanical force that favor a roughening of the interface and a stabilizing force due to surface tension. These stresses cause instabilities and various studies have focussed to understand this phenomenon. However in this part of research, I focused to study fundamentally the influence of a force applied in a single contact during the dissolution of gypsum to better understand this chemico-mechanical phenomenon at the atomic scale.

2.1.2   Measuring atomic step movement

For running the experiment, I prepared fresh calcium sulfate aqueous solutions. I dissolved calcium sulfate powder in ultra pure water until saturation, and diluted the solution to the desired concentration. The saturation index Ω is computed as $\Omega = \dfrac{C}{C_{\text{sat}}}$, C being the concentration of Ca^{2+} and SO_4^{2-} Then for every experiments, I freshly cleaved the gypsum surface with a clean scalpel. Then I mounted the sample on the fluid cell (figure 1.15) and it was hold by a spring to prevent its movement during the observation. The room temperature is controlled to be constant at $(22 \pm 1)°C$. A peristaltic pump is used to prevent a changing of the concentration during the measurements due to the dissolution of gypsum in the solution. It pumped through the cell with a flow rate of 0.275 mL/min. The measurements were performed with a MFP-3D Asylum Research AFM (6310 Hollister Avenue, Santa Barbara - California 93117 USA). The AFM is used in contact mode. A silicon nitride tip is used and its characteristics (sensitivity in air, sensitivity in the solution and stiffness) were determined for every used tip to calculate the applied force. Before running the solution, I imaged the surface to observe the crystallographic directions at the surface in air.

As I introduced in the first chapter the gypsum dissolution surface is well-known concerning the etch pits, retreating by monomolecular steps in the crystallographic directions [100] and [001] (figure 1.5). As mentioned by Teng, measuring the step velocities needs accuracy due to AFM electronical drift and lack of stationary reference in the image area because of the continuous changing of the surface by growth and dissolution [119]. I used one of the proposed measurement methods, suggested by Teng, to measure atomic step velocities. In this method, I used the slow-scan-disabled mode of AFM. After I introduced the solution on the gypsum cleaved surface and the an etch pit was created, I put the considered step parallel to the *Y*-axis by adjusting the angle (figure 2.2). At that time I switch on the slow-scan-disabled mode, consequently the AFM tip moves in line parallel to the *X*-axis or more precisely moves along a segment of transverse size equal to the diameter of the tip in line.
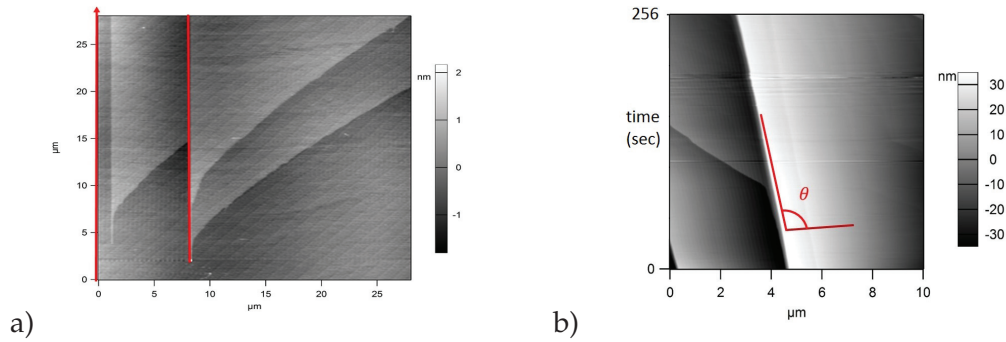
FIGURE 2.2: a) Considered step from an etch pit parallel to the Y axis.
b) Slow-scan-disabled image (kymogram) used to determine the step
velocity from the angle θ.

The step velocity is calculated by the following relation:

$$V_S = \frac{F_B.S_e}{N.\tan\theta} \tag{2.2}$$

with:
-F_B, the frequency (lines/s).
-S_e, the image size or scale (μm^2).
-N, the number of lines in the image.

2.1.3 Influence of saturation index on gypsum dissolution

Dissolution of minerals is an important process for many disciplines. It depend on many factors. These parameters are varied externally or rely on inherent properties of the solid or from the solution. Processes like the structure of the mineral, the surface defects, the adsorbed agents, the reactive surface, pressure, temperature, pH, hydrodynamic conditions, difference in free enthalpy ΔG between solid and liquid, etc. play major roles on this kinetic mechanism. Understanding how these processes act is required for an accurate knowledge of mineral surface reaction rates.

Many studies on the kinetics of mineral-water interaction have done based on dissolution rates measured by volume experiments (reactor, rotating disk, stirred tube, reactor mixed media and channels). In this research, I did not measure directly the retraction rate of the mineral, but I measured it from the evolution of the surface on atomic scale by the AFM. This methods allowed to deduce the dissolution kinetics from the velocities of the atomic steps or the retreat measurement perpendicular to the area. For the majority of mineral, this upscaling generally fails. It has been made possible here thanks to a careful identification of the microscopic mechanisms at play.

In dissolution often the system is far from equilibrium conditions. There is a general agreement that the kinetics of mineral dissolution is dependent on saturation state of the solvent in contact with the mineral. This dependency is very important since it may entail a change of the mechanism of mineral dissolution.

Few studies have been done on gypsum crystal surface during dissolution and atomic steps motion in different saturated indices [33, 93]. The two steps [100] and [001] enclosing the rhomboid etch pit are responsible for its evolution. Due to the complexity and the number of experiments that should be carried out, I have mainly studied the movement of the step [100] which, referring to the literature, has a slower

kinetics [93]. As suggested by Colombani, the overall kinetics of gypsum dissolution is controlled by a mixed mechanism, due to the similarity of the quantity of dissolving and diffusing gypsum in the course of an experiment [18]. Consequently a higher density of steps in one region induces a saturation layer around the surface resulting in a decrease of the driving force of the dissolution and thus a slowing down of the dissolving of the steps. So, I measured the step velocities in areas of the surface with a low density of atomic steps and used the flow-cell in AFM with a constant flow rate. I measured the step [100] velocities at saturation indices $\Omega =$ 75, 80, 85, 90 and 94%, these values presented in percent compared to the saturated solution (100%). Naturally I observed the step [100] moved faster than the step [001] and consequently the etch pit elongated due to this step kinetic anisotropy (figure 2.3).

a)   b)
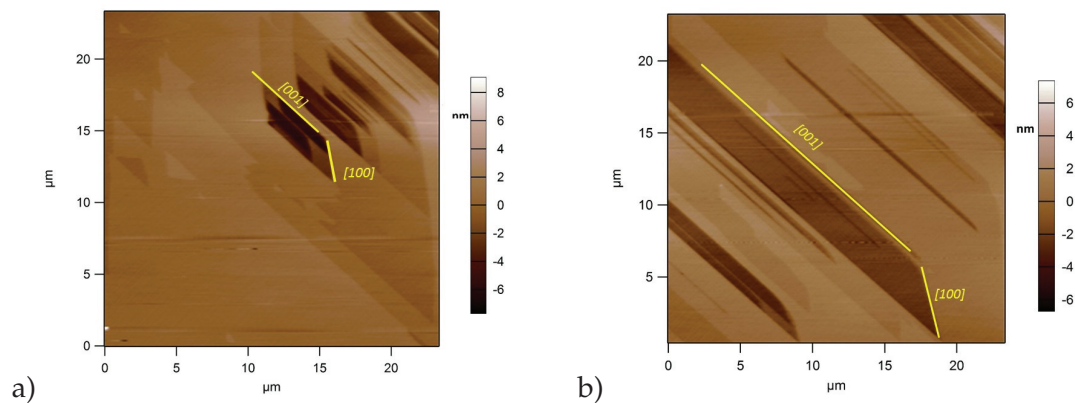
FIGURE 2.3: Evolution of the etch pit and steps [100] and [001] movement on the gypsum surface at saturation index of 90%. From image a to b,the time interval is 1024 seconds.The surface morphology is completely changed. Due to the anisotropy of the step dynamics the etch pit is elongated in the direction of step [001].

The step velocities increase with the decrease of the saturation index in the solution and this decreasing trend is in agreement with the other reported trends [33]. On the other hand I observed a strong disagreement between the values reported in the literature and my obtained results. These data are not in agreement with themselves as well [11, 47, 33, 14]. These discrepancies did not originate from different measurement methods for the step velocities, because I used the same method as Fan and Teng [33] but I also observed a disagreement. So the challenge I faced was to find a reason for the dispersed data shown in figure 2.4.
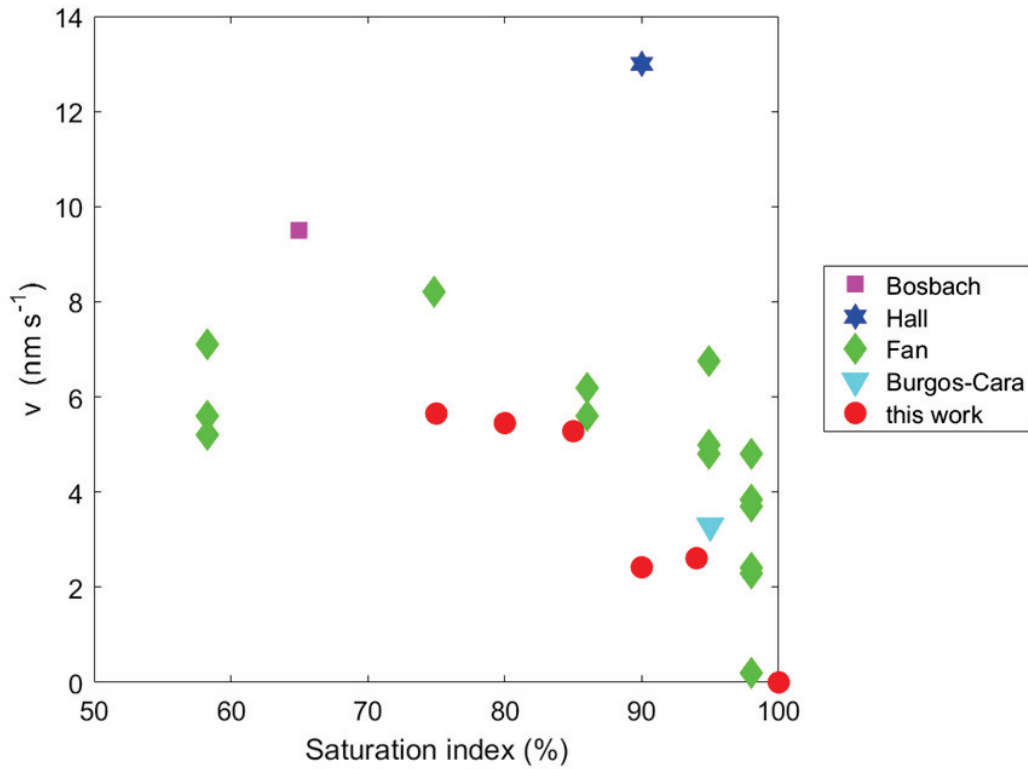
FIGURE 2.4: Evolution with the saturation index of the [100] step velocity on a dissolving gypsum surface in comparison to reported data

If we consider the step propagation mechanism for dissolution, the **Transition State Theory** (**TST**) can help to interpret the obtained results. This model is developed for extrapolating the dissolution rates obtained experimentally close and far from equilibrium. This theory connects the reaction rate $\frac{d\xi}{dt}$ with the difference of free enthalpy between the solid and liquid ΔG according to this relationship:

$$\frac{d\xi}{dt} \approx [1 - exp(\frac{\zeta \Delta G}{RT})] \tag{2.3}$$

with
- R gas constant.
- T the absolute temperature.
- ζ the number of reaction elements, in this study equal to one.

If the gypsum is put far from equilibrium by an undersaturated solution, then the difference in free enthalpy can be expressed as a function of the concentration as below:

$$\Delta G = RT \ln \Omega \tag{2.4}$$

with

$$\Omega = \frac{C}{C_{sat}} \tag{2.5}$$

as introduced earlier.

This leads to the following expression for the reaction advancement:

$$\frac{d\xi}{dt} \approx 1 - \Omega \tag{2.6}$$

Because the matter detachment, or dissolution reaction, originates from the atomic step movement on the crystal surface, the velocity of the steps V must also follow the law described by the TST:

$$V \approx 1 - \Omega \tag{2.7}$$

2.1.4   Influence of force on atomic step movement

In the previous section, due to the scattered results, it was very difficult to show the consistency of the experimental data with equation 2.7, which follows the TST. According to the literature, this dispersion of data could be originated from the variation of the applied force by the AFM tip during the measurements [93]. The force applied by the AFM tip is controlled by three parameters: 1) the stiffness of the cantilever which depends on the material and geometry, 2) the sensitivity of the cantilever and 3) the set point. The set point is a voltage value which is stabilized during scanning with an active feedback loop. It characterizes the strength of interaction between the tip and the surface. The first two parameters are constant but the repulsion force between the tip and crystal surface can be varied by changing the set point. In the following I describe the calculation of force applied by the AFM:

$$\Delta F_{\text{applied}} = \text{set point}[\text{V}] \times \text{sensitivity}[\frac{\text{nm}}{\text{V}}] \times \text{stiffness}[\frac{\text{nN}}{\text{nm}}] \tag{2.8}$$

To know the magnitude of the contact force applied by the tip, first I checked that the set point corresponds to zero volt. The drift of the laser spot on the photodiode is an unavoidable part of the system. For having precise measurements I regularly and several times during the experiments monitored the force by checking the set point. As discussed in section 2.1.2, in the mode *slow scan disabled*, by the obtained space-time image, we are able to compute the step velocity. In this image (space-time), variation in slope means variation in step velocity. To highlight the influence of the force, I increased the applied force by modifying the set point in the middle of an image (see figure 2.5). I observed that the gypsum surface reacted immediately to the changing of the applied force.
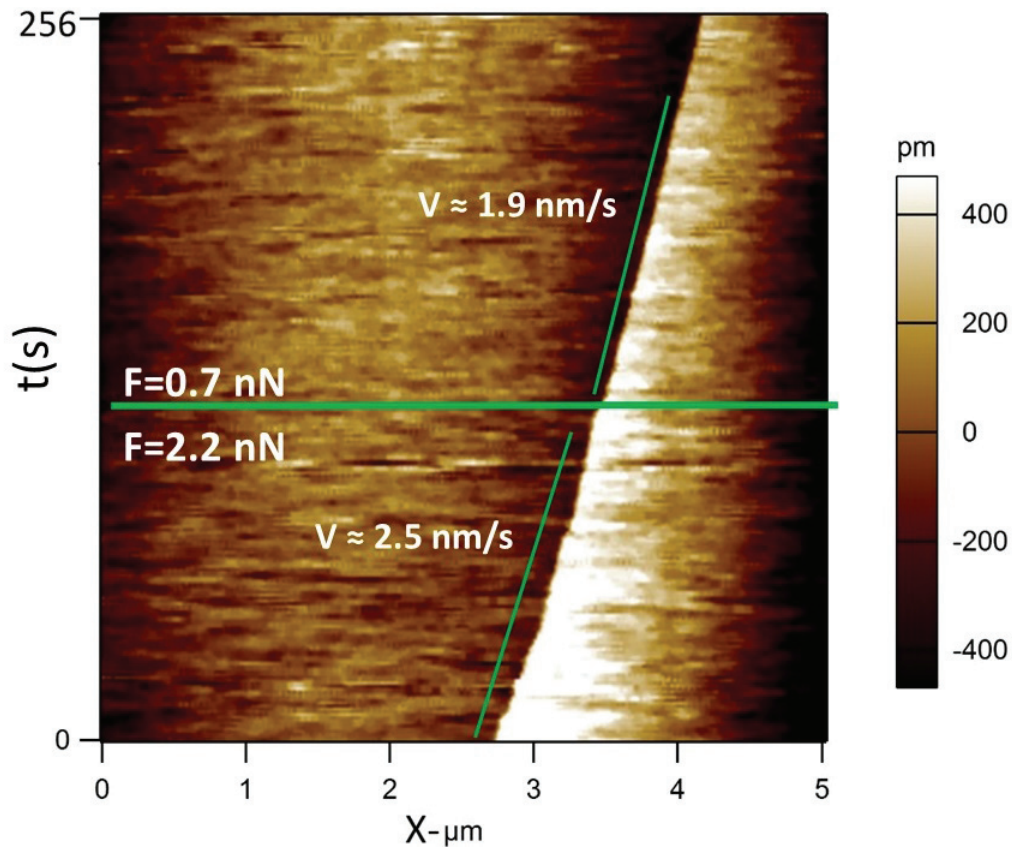
FIGURE 2.5: Spatio-temporal image obtained by AFM of the trace left by the motion of the step [100] versus time. The solution saturation index is 90%. The scan direction is from bottom to top. A different applied force consequently induces a different step velocity.

In reference to this observation, I measured the influence of the applied force by the tip on step [100]. The influence of force on the dissolution of soft minerals like gypsum and calcite was studied by Park et al. and Pachon-Rodriguez et al. [95, 96, 93]. Park et al. studied the wear that was generated by a continuous linear scanning of the AFM tip on the crystal surface. In figure 2.6, reported in the literature [96], is shown the relationship between the length of the track left by the passing tip on the calcite surface and the tip applied force of the **S**canning **F**orce **M**icroscope (**SFM**).
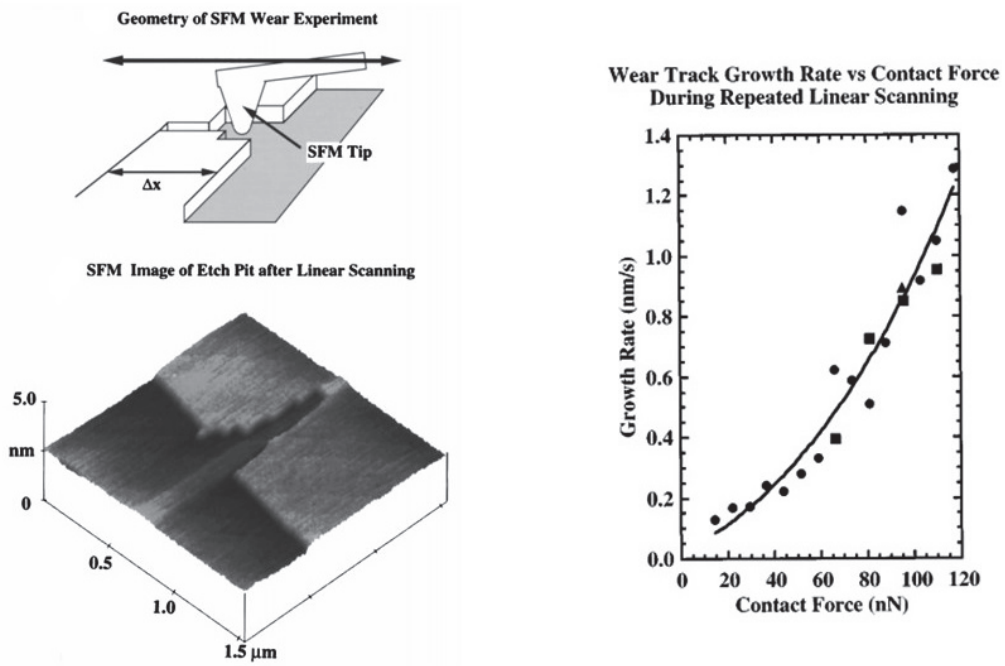
FIGURE 2.6: The wear growth rate of the trace (notch) on the surface of the calcite crystal generated after a linear scanning of the tip of the SFM, as a function of the contact force (figure from [96]).

2.1.5 Theoretical approach of the dissolution under stress

When the AFM tip scanned the crystal surface to make an image, it disturbed the solution around the image area. This local stirring, in addition to the solution flow rate, kept the solution concentration at that region constant. This process suggested that the observed dissolution process by AFM was a process limited by the surface reaction of the crystal and not by the removal of the material, quickly discharged into the liquid. So the evolution of the solid-liquid interface is a consequence of the chemical reaction.

$$Ca\,SO_4, 2\,H_2O \rightleftharpoons Ca^{2+}_{(aq)} + SO_4^{2-}{}_{(aq)} + 2\,H_2O \tag{2.9}$$
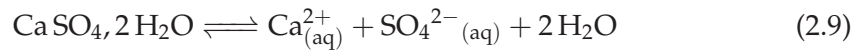
This reaction happens on the mineral surface by atomic detachment. In the pure system, in absence of other salts, to preserve the local electro-neutrality, the two aqueous species must be in the following condition:

$$C_{Ca^{2+}} = C_{SO_4^{2-}} = C \tag{2.10}$$

When the tip probes the surface to record the topography, it creates a local stress in the solid. To estimate this constraint, I considered the Hertzian type contact between AFM tip and crystal surface. In this context, the maximum stress is under the tip. Thus, the pressure P_0 is induced by the tip according to this equation:

$$P_0 = \left(\frac{1}{\pi}\right) \left[\frac{6 F_{\text{tip}} E^2}{((1 - \nu^2)^2 r_{\text{tip}}^2)} \right]^{\frac{1}{3}} \tag{2.11}$$

where
- F_{tip} is the applied force.
- E, ν are Young's modulus and solid Poisson's ratio.
- r_{tip} is the curvature radius of the used tip.

According to the literature, $E = 45$ GPa and $\nu = 0.33$ were used for gypsum. From the experiment $r_{tip} = 10$ nm and $F_{tip} = 10$ nN were considered. By using the equation 2.11, the value of $P_0 = 1.5$ GPa for the normal stress on the surface was obtained.

The applied stress also generated an elastic field around the contact zone. This field influences the chemical potential μ_s of the crystal surface around the contact zone with the tip. It can be written as [103]:

$$\mu_s = \mu_0 + \delta U_e + \delta U_p + \delta U_s \tag{2.12}$$

where
- μ_0 is the chemical potential of the stress-free solid.
- δU_e and δU_p are the contributions related to the elastic and plastic deformation energy respectively.
- δU_s is the parameter related to surface energy.

In this relation, the fluid above the surface is at atmospheric pressure and the normal stress outside the Hertzian contact area is zero. Apart from the atomic step movement, permanent deformations of the solid were not observed. Furthermore during probing and investigation of the surface by the tip, it remained flat. Consequently, the terms of plastic energy and surface energy could be neglected.

The maximum tensile stress at the periphery of the contact zone is described by the following relation:

$$\sigma = (1 - 2\nu)\frac{P_0}{3} \tag{2.13}$$

The molar elastic energy stored by the solid can be written as:

$$\Delta U_e = \frac{\sigma^2 \bar{V}}{2E} \tag{2.14}$$

where $\bar{V}$ is the molar volume of the gypsum. The obtained value of $P_0 = 1.5$ GPa was used in equation 2.13 to determine the stress σ. The stress σ was 170 MPa. The molar volume of gypsum is $\bar{V} = 7.5 \times 10-5 \, \text{m}^3 \, \text{mol}^{-1}$, then the elastic energy $\delta U_e = 24 J mol^{-1}$.

Now the expression of the chemical potential in the constraint condition is known, it was included in the law of the TST dissolution rate. First, the mechanical contribution was introduced in the expression of the difference of free enthalpy between the solid and liquid. The obtained relation is:

$$\Delta G = RT \ln \Omega \tag{2.15}$$

The term of elastic energy δU_e is derived from the molar elastic energy ΔU_e stored during passing the tip.

Consequently, the atomic step velocity can be written with the relation below:

$$v = v_{\lim}[1 - \Omega \exp(-\frac{\alpha^* \sigma^2 \bar{V}}{2ERT})] \tag{2.16}$$

with

- α^* a geometric parameter depending on the shape of the elastic deformation field around the contact zone.

- v_{lim} the maximum atomic step velocity that is intrinsic to the solid-liquid interaction.

By using relation 3.2, we found a strong agreement between the experimental results and the theory (see figure 3 in the paper presented in section 2.2.)

Consequently, considering that the influence of the tip on the solid is related to the contribution of the elastic strain to its chemical potential led to a good fitting of the experimental data, thus it validated the hypothesis of dissolution under local constraint.

2.1.6 Measuring dissolution rate at nanoscale

For many years studies claimed that gypsum dissolution was done by propagation of a well defined system (etch pit) [131, 124] but these measurements hardly showed agreement between macroscopic and nanoscale dissolution rates. In this research I focused to understand the main physical properties of the surface that control dissolution. I introduced in the first chapter, in section 1.2, that I observed another type of steps, called [u0w], which were also reported by Fan and Teng in 2000 [33]. This type of steps were found in the direction close to the step [100] direction (see figure 1.4). I had decided to measure their velocities although due to their high velocity it needed more care. For measuring the step velocities I used the same method as reported in section 2.1.2 but as it moves very fast and sweep the surface I had to adapt the methodology. For adjusting this step parallel to the Y axis first, I put a considered [100] step parallel to the Y axis, as the rough steps were approximately in the same orientation of as steps [100]. As soon as they appeared I checked their parallelism and then I switched on the *slow-scan-disabled mode*. In all rough steps measurement the scan rate was 3 Hz. I computed velocities for rough, [100] and [001] steps, then by knowing the density of steps I was able to calculate the dissolution rate by using the following relation [122].

$$R = \frac{vnh}{\bar{V}} \tag{2.17}$$

with

- n the number of steps at the surface.
- v the step velocity.
- h the height of a step.
- $\bar{V}$ the molar volume of gypsum.

The obtained results showed microscopic dissolution rates of gypsum in quantitative agreement with macroscopic rates. This agreement has been obtained in taking care of two features. First, the force applied by the AFM tip on the surface has been seen to increase the solubility of the mineral, thereby introducing a bias, so I have always worked with a constant and low applied force. Secondly I have clearly identified the driving molecular mechanism, namely the migrations of rough steps, which have often been neglected in former studies. This result shows that a careful analysis of the topographic changes during the dissolution of a mineral may permit to deduce a reliable macroscopic dissolution rate.

## 2.2 Gypsum dissolution rate from atomic step kinetics

An article detailing these results and published in the *Journal of Physical Chemistry C* is presented below.

Gypsum Dissolution Rate from Atomic Step Kinetics

Bahareh Zareeipolgardani, Agnès Piednoir, and Jean Colombani*

Institut Lumière Matière, Université de Lyon, Université Claude Bernard Lyon 1, CNRS UMR 5586, Campus de la Doua, F-69622 Villeurbanne cedex, France

ABSTRACT: The macroscopic dissolution rate of minerals is generally deduced from solution chemistry measurements. A microscopic dissolution rate can also be deduced from the dynamics of molecular events (etch pit growth, atomic step migration, etc.). Both hardly ever agree, even qualitatively, and the elaboration of a general theory linking the kinetics at the two scales is still in progress. We present here microscopic dissolution rates of gypsum, measured by atomic force microscopy (AFM), in quantitative agreement with macroscopic rates. This agreement has been obtained in taking care to neutralize the bias induced by the force applied by the AFM tip on the surface, and to identify clearly the driving molecular mechanism. This result shows that the determination, among the topographic changes during the dissolution of a mineral, of the dominant one, and the measurement of its dynamics, may permit deducing from AFM experiments a reliable macroscopic dissolution rate.
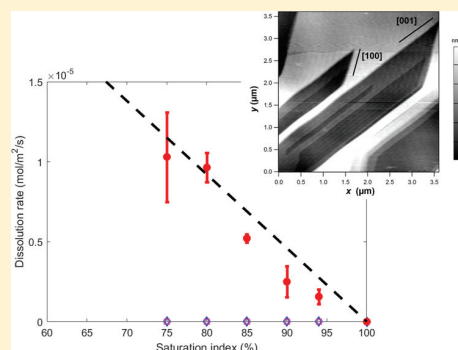
INTRODUCTION

Besides the measurement of macroscopic reaction rates, the study of the reactivity of minerals includes the investigation of the atomic mechanisms involved in the reaction. This has been made possible for two decades by the use of tools resolving nanometric objects, such as vertical scanning interferometry (VSI) and atomic force microscopy (AFM). In the case of the study of dissolution, these techniques enable ex situ as much as in situ observations, and they have brought recently a rather clear view of this phenomenon. For instance, it is now well accepted that the dissolution kinetics of minerals is driven both by the deepening and broadening of etch pits and by the general vertical retreat of the surface.[1] Etch pits are now viewed as contributing to dissolution, not in providing new reactive surface area, but as being a source of moving atomic steps.[2] The way the undersaturation influences dissolution has also received a satisfactory explanation: dissolution in close-to-equilibrium conditions is driven by existing steps, far-from-equilibrium conditions by the nucleation of etch pits on the plane surface, and intermediate conditions by the nucleation of etch pits on defects.[3,4]

If calcite has received the most interest in dissolution studies, we are here concerned with the case of gypsum. In the field, the dissolution of gypsum leads to the formation of karst,[5] is a major source of calcium ion release in drinking water,[6] and has a significant influence on soil quality and plant growth.[7] In the domain of mineral materials, gypsum constitutes a minor component of Portland cement, and experiences dissolution during its setting. But it is also the only component of gypsum plaster (or stucco, or alabaster), and its dissolution under stress is responsible for the moist creep of this material.[8]

The main objective of this study is to bridge quantitatively the gap between the atomic and macroscopic dissolution

kinetics. Indeed, agreement between measured dissolution rates at these two scales is hardly ever obtained.[9] Even studies measuring the microscopic (with AFM) and macroscopic (with a flow cell) dissolution rates in one well-defined system do not get similar values.[10,11] This lack of consistency stems from (i) the fact that the understanding of the molecular mechanisms underlying dissolution is quite recent, as explained above, (ii) the difficulty of getting reliable macroscopic dissolution rates (see ref 12 for the case of calcite), and (iii) the fact that the elaboration of a general theory showing how the atomic mechanisms combine into an overall rate is still under way.[13,14]

The macroscopic rate derives from the combination of various sources of matter removal (broadening and coalescence of pits created at point defects, at dislocations, at grain boundaries, etc.) interacting in a complex manner.[15] But even if the resulting spectrum of microscopic dissolution rates is large, due to the variety of dynamics of these molecular mechanisms, one of them may dominate and drive mainly the overall rate. In this case the upscaling of the dissolution rate is straightforward, easily deduced from the kinetics of the dominant mechanism.

In the case of gypsum, this upscaling had not yet given values compatible with experimental macroscopic ones because only events that had a minor contribution to the rate (migration of straight steps, etch pit spreading) had been investigated. We show here that the overall rates computed from the kinetics of the dominant microscopic mechanism (rough step migration) agree quantitatively with experimental macroscopic ones.

■ EXPERIMENTAL SECTION

All experiments have been performed with fresh cleaved surfaces of natural transparent gypsum ($CaSO_4 \cdot 2H_2O$), from the quarry of Mazan (Vaucluse, France). This mineral displays a perfect (010) cleavage plane due to the weak H-bonding between the water molecules.[16] The undersaturated solutions have been prepared in dissolving calcium sulfate in water up to saturation, and then adding ultrapure water (resistivity ≥0.18 MΩ·m) until the desired saturation index is obtained. The saturation index has been computed as $\Omega = c/c_{sat}$, where c is the concentration of dissolved calcium sulfate, and $c_{sat} = 15$ mmol/kg is its value at equilibrium.[17]

A commercial atomic force microscope (MFP3D, Asylum Research, Oxford Instruments) has been used for the imaging of gypsum surfaces. In this apparatus, a silicon nitride tip is stuck at the free extremity of a cantilever. When approached close to the surface, the interaction force between the surface and the tip induces a bending of the cantilever, detected by a quadrant detector receiving a laser beam reflected by the cantilever. In the contact mode, used here, a feedback loop modifies the vertical position of the tip in order to keep constant the repulsive force. Then a portion of the surface is scanned line by line, which provides a two-dimensional map of the surface height.

The image in Figure 1a is topographic, i.e., shows directly the height of the surface in the (x, y) plane. But to gain clarity, the presented image in Figure 1b shows at each point the error signal, i.e., the difference between the vertical deflection and the set point, proportional to the desired force, which is equivalent to the derivative of the height with the position. This signal emphasizes the relief of the surface. The images have a 256 × 256 resolution and are collected in about 4.5 min with a 1 line/s frequency.

The dissolution has been studied in situ, thanks to a homemade fluid cell, in which the undersaturated solution is flowing past the mineral surface, with a 0.275 mL/min flow rate, during the AFM measurements. The continuous flow leads to the establishment of a steady concentration field above the surface. Despite being stationary, the concentration distribution in the flow cell is highly nonuniform and strongly dependent on its geometry.[18] The way this geometry influences the concentration field and, accordingly, the step velocity, is still quite controversial. Finite element method modeling has shown that the flow rate, cell geometry, and heterogeneity of the surface can strongly influence the gypsum step velocity measured locally with the AFM.[19] But measurements with microelectrodes at different heights from a gypsum dissolving surface for a 1.5 mL/min flow rate show the quasi-absence of a concentration gradient between the surface and the bulk liquid.[20]

To reduce as much as possible the dispersion of the results and gain accuracy in comparison with already existing results, the measurement of the force applied by the tip on the surface was calibrated (zero value and sensitivity) between each image, in order to compensate possible drifts and to guarantee the reproducibility of the applied pressure and the rightness of its measured value.

The velocity of steps has been measured in aligning one monomolecular step with the y scanning direction, and disabling the scan in this directions. Then a kymogram was obtained, with the step migration leaving a track in the (x, t) plane (t is time) and the velocity being the slope of the track.[21]
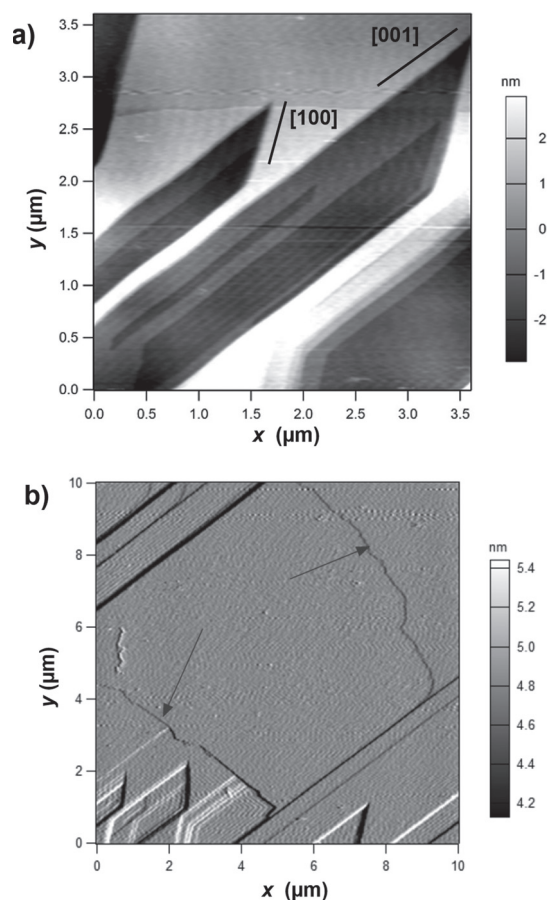
Figure 1. AFM images of the dissolving cleavage surface of a gypsum single crystal in a flowing solution of saturation index 87%. (a) Topographic image exhibiting typical rhomboidal etch pits. (b) Error signal image showing two fast-moving rough steps (arrows).

■ RESULTS AND DISCUSSION

Surface Topography. In a flowing saturated solution, the gypsum cleavage surface appears at rest, with atomic steps moving at velocities lower than 0.03 nm/s. As soon as the imposed concentration departs from its equilibrium value, coherent motions are observed at the crystal surface, which can be classified in two types, as first observed by Fan and Teng.[21]

First, rhomboidal etch pits growing in depth and width are continuously observed at the surface. We have not tried to estimate whether they nucleate at structural defects[22] and whether their nucleation stops close to the saturation.[21] They are enclosed by straight steps, the displacement of which is responsible for the etch pit growth (see Figure 1a). The shape of the pit is reminiscent of the monoclinic Bravais lattice of gypsum, with the obtuse angle of 118° of the monoclinic cell inducing an equivalent angle of the rhomboids. Two facing edges of the pit are longer, because the neighboring edges propagate faster, and vice versa, these fast steps are shorter because the longer ones go slower. The fast steps have been identified as the [100] direction of the lattice, and the slow ones as the [001] direction.[21] The chemical origin of the kinetic anisotropy between [001] and [100] has been analyzed in detail and derives from the difference of molecular stacking in the two steps.[21] It should be noted that fast steps are sometimes wrongly identified as [101], whereas these steps are generally

not present at a gypsum cleavage surface.[21] We observe that some angles of etch pits are sometimes slightly rounded, as in other experiments.[23]

Second, the surface is regularly swept by very fast and rough steps (see two examples in Figure 1b). These steps have an unidentified and changing direction. Scanning progressively all lattice directions of the (010) plane, they have been denoted $[u0w]$.[21] These steps do not belong to any etch pits, and Fan and Teng have suggested that they are generated at the edges of the sample.[21] Although this should be partly true, molecular simulations of dissolving calcium carbonate, where similar rough steps run on the surface, have shown that they may result also from the merging of neighboring pits.[13] These steps are most probably as unstable as would be $[010]$ steps.[21] Their very high velocity is a consequence of the large density of kink sites, which are highly reactive, due to their smaller number of bonds with the surface, compared to atoms in straight steps. These rough steps erode and often completely annihilate existing etch pits. For this reason, the pits have generally no time to grow and pits deeper than a few nanometers are hardly ever observed, whatever the undersaturation.

These topographic transformations of the surface are the molecular consequences of the disequilibrium between the solid and liquid induced by the undersaturation. Therefore, the kinetics of these modifications should, in some form, be linked to the distance from equilibrium. Figure 2 shows the change of the $[100]$ step velocity v with the saturation index Ω, measured in this work, and reported in the literature.
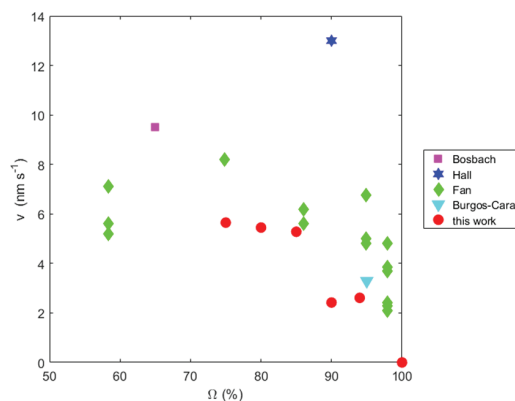
Figure 2. Evolution with the saturation index of the $[100]$ step velocity on a dissolving gypsum surface. The results of Bosbach and Rammensee (pink square),[22] Hall and Cullen (blue star),[23] Fan and Teng (green diamonds),[21] and Burgos-Cara et al. (light blue triangle)[20] have been added to ours (red circles).

We have to mention that we have omitted to include the value measured by Peruffo et al., because it was 2 orders of magnitude larger than the others ($v = 330$ nm/s).[24] This discrepancy may probably be explained by the fact that these measurements have been carried out during the first seconds of contact of the surface with the solution. Being freshly cleaved and unreacted, the gypsum surface is likely to be, in these experiments, highly energetic and therefore much more reactive than in the other long-term experiments.

If we note an enhancement of the step speed when getting away from the saturation, the exact dependence of v on Ω would be difficult to draw from the results in Figure 2. Fan and Teng have suggested, based on their results, that this evolution

is compatible with a law deduced from the transition state theory.[21]

At first order, we have considered here that, for our close-to-equilibrium conditions, all measurements converge to a rough proportionality between the step velocity and the distance from saturation, with a dispersion compatible with the difficulty of the experiments (see Influence of Applied Force). Therefore, the atomic mechanism at the basis of dissolution seems to follow, close to saturation, a first-order evolution with Ω, as has been observed for its macroscopic counterpart, the dissolution rate R:[25]

$$v = v_{\text{lim}}(1 - \Omega) \tag{1}$$

with v_{lim} the step velocity at infinite dilution. Farther from equilibrium, it is likely that the dependency of v with Ω is no more linear.[21]

Influence of Applied Force. As we aim at a quantitative agreement between atomic and macroscopic dissolution rates, we need to avoid all experimental biases as much as possible. We had shown in a previous work that one of the main instrumental sources of uncertainty in AFM dissolution measurements was the modification of the equilibrium between the solid and liquid by the stress σ applied by the tip on the surface.[26] Indeed, the force pressing the surface induces an elastic strain of the solid, which thereby stores the elastic energy:

$$\Delta U_{\text{e}} = \frac{\alpha \sigma^2 \overline{V}}{2E} \tag{2}$$

with α a geometric factor depending on the shape of the elastic strain field around the tip−surface contact, E the Young's modulus of the solid, and $\overline{V}$ its molar volume.

This elastic energy constitutes a second source of distance from equilibrium, adding to the undersaturation of the liquid. In other words, the external stress promotes dissolution, a phenomenon broadly reported in geology.[27] In the case of the dissolution of gypsum, we had demonstrated that the kinetics of the slow steps was thereby modified by the passage of the tip, their dynamics appearing to be driven by a combination of the chemical (eq 1) and mechanical (eq 2) stimuli, both contributing to the Gibbs free energy of the system:[26]

$$v = v_{\text{lim}}\left[1 - \Omega \exp\left(-\frac{\alpha \sigma^2 \overline{V}}{2ERT}\right)\right] \tag{3}$$

To further attest to this disturbing influence of the AFM tip on the surface behavior, we present in Figure 3 the change of the velocity of the fast steps with the force applied by the tip, for a given undersaturation (90%). We see here clearly two distinct regimes. We have ascribed the low-force behavior to the above-described pressure solution influence. To use eq 3, we have modeled the impinging of the surface by the tip with a Hertzian contact. In this case, the maximum tensile stress (at the contact periphery) is $\sigma = ((1 - 2\nu)/\pi)(2FE^2/(9(1 - \nu^2)^2 r^2))$, with ν the Poisson's ratio of the solid, r the size of the contact ($r \sim 40$ nm), and F the force applied by the tip. Using this expression of σ, we have fitted the low-force experimental results in Figure 3 with eq 3. The agreement between the experiment and the model is satisfactory. The value of α brought by the fit is 130, which gives an order of magnitude of the number of molecules, the elastic state of which is modified by the tip.
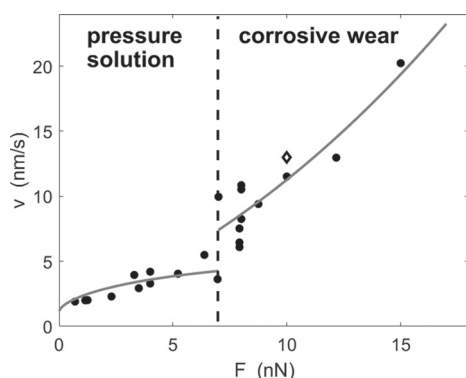
Figure 3. Step velocity in the [100] direction as a function of the force applied by the AFM tip on a gypsum surface for a 90% saturation index of the flowing solution. The open diamond-shaped dot is the datum from Hall and Cullen.[23] The low-force dots are fitted with eq 3, and the high-force ones are fitted with eq 4.

The high-force regime shows a completely different behavior and can be ascribed to an atomic wear phenomenon. Following the analysis of nanotribological experiments on calcite in aqueous solution, we consider that the force applied by the tip is high enough to detach ions along the tip–step contact, which means that the tip scratches the step via a mechanical promotion of the kink nucleation.[28] As this mechanically favored kink nucleation is thermally activated, the step wear is expected to exhibit an Arrhenius exponential evolution with the force:[28]

$$v = v_0 \exp\left(\frac{V_a \sigma}{RT}\right)$$
(4)

with v_0 a preexponential factor and V_a an activation volume. The fit of the experimental data at high force with this equation is shown in Figure 3. The agreement is satisfactory and leads to confirmation that the increase of velocity in this regime is due to a corrosive wear phenomenon in the case of gypsum, as was the case for calcite.[28] The best-fit value of the activation volume is $V_a \sim 100$ cm^3·mol^{-1}. The molar volume of monoclinic gypsum being 74 cm^3·mol^{-1}, this fitted value tends to show that the tip promotes the removal of one or two unit cells.

The existence of this wear regime enables understanding of the unexpectedly high value measured by Hall and Cullen, shown in Figure 2. These authors are the only ones mentioning the force they apply on the surface with the tip: $F = 10$ nN. This value lies clearly in the corrosive wear domain, and the velocity they measure ($v \sim 13$ nm/s) is consistent with the one we measure with this applied force, as can be checked in Figure 3. Hence their experiment investigates tribologically enhanced dissolution, not spontaneous dissolution, and their result is therefore outside the range of expected values of step velocity during dissolution (see Figure 2).

The force for which the transition between pressure solution and corrosive wear of the fast steps occurs, $F_f \sim 7$ nN, is very close to the equivalent value for the slow steps, $F_s \sim 10$ nN.[26] It should therefore stem from the same molecular quantity, most probably the binding force of the structural water of the gypsum molecule with the surface.

We can infer from this investigation of the bias induced by the AFM tip on the dissolution process that, to get reliable and reproducible values of the step velocities, particular care will have to be taken subsequently (i) to choose a small applied force, at least smaller than 7 nN, and (ii) to keep the value of the force similar for all velocity measurements. These two conditions have been always fulfilled thereafter in performing all experiments with a 1.2 ± 0.7 nN force.

Dissolution Rate from the Step Velocity. The heterogeneity of the molecular mechanisms at the basis of dissolution, and the resulting diversity of the local dissolution rates, has been recently acknowledged.[15] In the case of calcite marble, the local rates measured in a plane surface span from 0.03×10^{-6} to 0.7×10^{-6} mol m^{-2} s^{-1}, originating from dislocation-driven etch pit growth, vacancy-driven etch pit broadening, etch pit coalescence, etc.[14] The experimental values of macroscopic rate found in the literature, measured in very diverse samples (single crystals, polycrystals, powders, etc.), range from 0.3×10^{-6} to 5×10^{-6} mol m^{-2} s^{-1} in far-from-equilibrium conditions.[12] We note that the orders of magnitude of the rates do not agree. This discrepancy may originate from the shape of the samples, with grains being likely to be more reactive than plane surfaces, due to higher step and kink density, so to show larger rates. This tiny overlap of the rates of both scales emphasizes the fact that developments in the statistical analysis of the basic mechanisms and their interaction are still needed to recover a unified view of the dissolution of calcite.[29]

Two main strategies exist for accessing the microscopic dissolution rates. The first one uses VSI and measures directly the microscopic rate from the matter loss deduced from the local vertical retreat of the surface. The link between a local rate and its corresponding atomic mechanism is made from the interpretation of the topographic changes. The advantage of this technique is that it provides a map of the microscopic rates (the integration of which gives the overall value); the drawback is that measurements are carried out ex situ (outside the solution). Our study concerns the second one, which uses AFM and attempts to compute microscopic rates from the measured kinetics of atomic events (step velocity, pit spreading, etc.). The advantage of this method is that the measurements are performed in situ (during dissolution); the drawback is that the computation of the overall rate from the kinetics of microscopic events is not straightforward.

In the case of gypsum, we have noticed from the AFM measurements that etch pits do not seem to play a leading role. Indeed they never get deep or very wide. This absence of noticeable growth is not a consequence of a large density of pits, which would lead the pits to coalesce before having time to grow. This limited growth is a consequence of the sweeping of the surface by the rough steps, which regularly make the pits disappear. From this overall assessment of the dissolution processes, we can make the assumption that the phenomenon is driven by the rough atomic step motion.

We have observed that the migration of three families of steps contributes to the release of matter from solid to liquid, the ultimate measure of which is the dissolution rate. To quantitatively estimate the total quantity of matter liberated from the solid by step migration, two quantities are required: the velocity of the steps v and their number density n at the surface. The resulting dissolution rate R is[30]

$$R = \frac{vnh}{\overline{V}}$$
(5)

with h the height of a step ($h = 0.75$ nm) and $\overline{V}$ the molar volume of gypsum ($\overline{V} = 74$ cm^3·mol^{-1}).

The values of v and n for five values of the saturation index have been collected in Table 1. From them and eq 5, the

Table 1. Velocity and Number Density of the Slow [001], Fast [100], and Rough [u0w] Steps during the Dissolution of the Cleavage Plane (010) of Gypsum in Flowing Aqueous Solutions of Calcium Sulfate of Saturation Index Ω

Ω (%)	$v[001]$ (nm/s)	$n[001]$ (μm^{-1})	$v[100]$ (nm/s)	$n[100]$ (μm^{-1})	$v[u0w]$ (nm/s)	$n[u0w]$ (μm^{-1})
75	1.18	0.48	5.64	0.11	1900	0.54
80	0.88	0.44	5.45	0.11	2230	0.43
85	0.56	0.24	5.28	0.10	757	0.68
90	0.60	0.10	2.42	0.08	494	0.50
94	0.58	0.10	2.62	0.07	391	0.39

dissolution rate resulting from the migration of all three steps has been drawn in Figure 4 for the five saturation indices. At
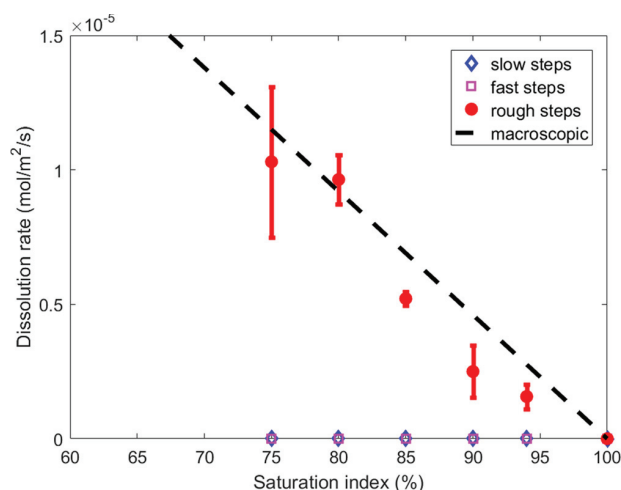

Figure 4. Dissolution rates resulting from fast, slow, and rough step motions at the surface of a gypsum single crystal for various saturation indices of the flowing solution. The dashed line is the macroscopic pure dissolution rate of gypsum, compatible with all published experimental values.[25]

first glance, we see that the contributions from the fast and slow steps are completely negligible, with their velocity being much too small to be comparable with the one of the highly unstable rough steps. Accordingly, the displacement of the [u0w] steps is the only contributor to the dissolution rate.

To compare these values inferred from atomic events with the macroscopic dissolution rates, we have added in Figure 4 the evolution of the macroscopic experimental R with the undersaturation. This $R(\Omega)$ line stems from an analysis of almost all published experimental data of gypsum dissolution (mostly coming from solution chemistry techniques). In these experiments, the solution is always flowing and thereby the measured dissolution rate contains also a contribution from convection, varying with the stirring rate, dissolving particle size, etc. This results in highly dispersed and inconsistent values. Once the blurring influence of hydrodynamics has been removed, one well-defined dissolution rate constant can be drawn from all the experiments.[25] This rate constant has been validated by an original measurement using holographic interferometry in a nonflowing solution, thereby free from any hydrodynamic contribution.[31] Consequently the $R(\Omega)$ line

in Figure 4 represents (i) pure dissolution rate values, (ii) compatible with all the published values of R.

Figure 4 shows that the agreement between the atomic and macroscopic dissolution rate is extremely good. We stress on the fact that both measurements are completely independent; no adjustment has been performed. The fact that both agree quantitatively is a proof that the dissolution of gypsum is completely driven by one well-defined atomic mechanism, namely the migration of [u0w] steps.

This particular analysis, dedicated to gypsum, is the first one showing a perfect agreement between measurements performed at the two extreme scales of dissolution. It shows that a thorough examination of the molecular contributions to the overall dissolution permits bridging the gap quantitatively between the nanometric and macroscopic values. Obviously, this examination has to be completed for every different mineral, and may sometimes be less direct than in the case of gypsum, but it emphasizes the predictive power of AFM experiments.

CONCLUSION

Dissolution rates deduced from atomic step velocity or etch pit growth are hardly ever consistent with rates measured macroscopically. We measure here with atomic force microscopy dissolution rates deduced from atomic motions at the surface of gypsum in complete agreement with macroscopic rates. This consistency can be obtained provided that the bias induced by the promotion of dissolution by the stress applied by the tip is taken into account, and that all atomic mechanisms occurring during dissolution are identified and the driving one ascertained.

In showing that a coherence can be reached between usually incompatible scales of dissolution, we do not mean that the deduction of macroscopic rates from atomic mechanisms is straightforward. In other minerals, such as carbonates or alumino-silicates, it is possible that no unique driving molecular process exists, and that the interaction between several ones has to be understood and modeled, for instance etch pit merging rate and vertical surface retreat. In this case, a concept like the dissolution rate spectrum reveals itself to be necessary and provides a satisfactory description of the heterogeneity of the surface reactivity, i.e., of the spatial distribution of atomic mechanisms.[15] It has also recently been shown that the access to the rate spectrum of one particular polycrystalline material with VSI enables identification of the main defects acting as source of etch pits during dissolution, which in turn can be used to calibrate a kinetic Monte Carlo simulation code, thus improving its predictive power.[14]

But we have shown here that, if AFM does not give direct access to dissolution rates, unlike VSI, it enables a crucial real-time observation of the atomic processes of the phenomenon.

AUTHOR INFORMATION

Corresponding Author
*E-mail: Jean.Colombani@univ-lyon1.fr.
ORCID
Jean Colombani: 0000-0001-8588-2628

Notes

The authors declare no competing financial interest.

REFERENCES

(1) Lüttge, A.; Winkler, U.; Lasaga, A. Interferometric study of the dolomite dissolution: a new conceptual model for mineral dissolution. *Geochim. Cosmochim. Acta* **2003**, *67*, 1099.

(2) Lasaga, A.; Lüttge, A. Variation of crystal dissolution rate based on a dissolution stepwave model. *Science* **2001**, *291*, 2400.

(3) Teng, H. Controls by saturation state on etch pit formation during calcite dissolution. *Geochim. Cosmochim. Acta* **2004**, *68*, 253−262.

(4) Arvidson, R.; Lüttge, A. Mineral dissolution kinetics as a function of distance from equilibrium - New experimental results. *Chem. Geol.* **2010**, *269*, 79.

(5) Jeschke, A.; Vosbeck, K.; Dreybrodt, W. Surface controlled dissolution rates of gypsum in aqueous solutions exhibit nonlinear dissolution kinetics. *Geochim. Cosmochim. Acta* **2001**, *65*, 27.

(6) Raines, M.; Dewers, T. Mixed transport/reaction control of gypsum dissolution kinetics in aqueous solutions and initiation of gypsum karst. *Chem. Geol.* **1997**, *140*, 29.

(7) Herrero, J.; Artieda, O.; Hudnall, W. Gypsum, a tricky material. *Soil Sci. Soc. Am. J.* **2009**, *73*, 1757−1763.

(8) Pachon-Rodriguez, E.; Guillon, E.; Houvenaghel, G.; Colombani, J. Wet creep of hardened hydraulic cements - Example of gypsum plaster and implication for hydrated Portland cement. *Cem. Concr. Res.* **2014**, *63*, 67−74.

(9) Wolthers, M. How minerals dissolve. *Science* **2015**, *349*, 1288.

(10) Shiraki, R.; Rock, P.; Casey, W. Dissolution kinetics of calcite in 0.1 M NaCl solution at room temperature: an atomic force microscopic (AFM) study. *Aquat. Geochem.* **2000**, *6*, 87−108.

(11) Duckworth, O.; Martin, S. Dissolution rates and pit morphologies of rhombohedral carbonate minerals. *Am. Mineral.* **2004**, *89*, 554−563.

(12) Colombani, J. The alkaline dissolution rate of calcite. *J. Phys. Chem. Lett.* **2016**, *7*, 2376−2380.

(13) Kurganskaya, I.; Lüttge, A. Kinetic Monte Carlo approach to study carbonate dissolution. *J. Phys. Chem. C* **2016**, *120*, 6482−6492.

(14) Fischer, C.; Lüttge, A. Beyond the conventional understanding of water-rock reactivity. *Earth Planet. Sci. Lett.* **2017**, *457*, 100−105.

(15) Fischer, C.; Arvidson, R.; Lüttge, A. How Predictable are Dissolution Rates of Crystalline Material? *Geochim. Cosmochim. Acta* **2012**, *98*, 177−185.

(16) Shindo, H.; Kaise, M.; Kondoh, H.; Nishihara, C.; Hayakawa, H.; Ono, S.; Nozoye, H. Structure of cleaved surfaces of gypsum studied with atomic force microscopy. *J. Chem. Soc., Chem. Commun.* **1991**, *16*, 1097.

(17) Pachon-Rodriguez, E.; Colombani, J. Pure dissolution kinetics of anhydrite and gypsum in inhibiting aqueous salt solutions. *AIChE J.* **2013**, *59*, 1622.

(18) Gasperino, D.; Yeckel, A.; Olmsted, B.; Ward, M.; Derby, J. Mass transfer limitations at Crystallizing interfaces in an atomic force microscopy fluid cell: A finite element analysis. *Langmuir* **2006**, *22*, 6578−6586.

(19) Peruffo, M.; Mbogoro, M.; Adobes-Vidal, M.; Unwin, P. Importance of mass transport and spatially heterogeneous flux processes for in situ atomic force microscopy measurements of crystal growth and dissolution kinetics. *J. Phys. Chem. C* **2016**, *120*, 12100−12112.

(20) Burgos-Cara, A.; Putnis, C.; Rodriguez-Navarro, C.; Ruiz-Agudo, E. Hydration effects on gypsum dissolution revealed by in situ nanoscale atomic force microscopy observations. *Geochim. Cosmochim. Acta* **2016**, *179*, 110−122.

(21) Fan, C.; Teng, H. Surface behavior of gypsum during dissolution. *Chem. Geol.* **2007**, *245*, 242.

(22) Bosbach, D.; Rammensee, W. In situ investigation of growth and dissolution on the (010) surface of gypsum by Scanning Force Microscopy. *Geochim. Cosmochim. Acta* **1994**, *58*, 843.

(23) Hall, C.; Cullen, D. Scanning Force Microscopy of gypsum dissolution and crystal growth. *AIChE J.* **1996**, *42*, 232.

(24) Peruffo, M.; Mbogoro, M.; Edwards, M.; Unwin, P. Holistic approach to dissolution kinetics: linking direction-specific microscopic fluxes, local mass transport effects and global macroscopic rates from gypsum etch pit analysis. *Phys. Chem. Chem. Phys.* **2013**, *15*, 1956−1965.

(25) Colombani, J. Measurement of the pure dissolution rate constant of a mineral in water. *Geochim. Cosmochim. Acta* **2008**, *72*, 5634.

(26) Pachon-Rodriguez, E.; Piednoir, A.; Colombani, J. Pressure solution at the molecular scale. *Phys. Rev. Lett.* **2011**, *107*, 146102.

(27) Gratier, J.; Dysthe, D.; Renard, F. The role of pressure solution creep in the ductility of the earth's upper crust. *Adv. Geophys.* **2013**, *54*, 47−179.

(28) Park, N.; Kim, M.; Langford, S.; Dickinson, J. Atomic layer wear of single-crystal calcite in aqueous solution scanning force microscopy. *J. Appl. Phys.* **1996**, *80*, 2680.

(29) Morse, J.; Arvidson, R. The dissolution kinetics of major sedimentary carbonate minerals. *Earth-Sci. Rev.* **2002**, *58*, 51−84.

(30) Vinson, M.; Lüttge, A. Multiple length-scale kinetics: an integrated study of calcite dissolution rates and strontium inhibition. *Am. J. Sci.* **2005**, *305*, 119−146.

(31) Colombani, J.; Bert, J. Holographic interferometry study of the dissolution and diffusion of gypsum in water. *Geochim. Cosmochim. Acta* **2007**, *71*, 1913.

Chapter 3

Influence of stress on calcite growth
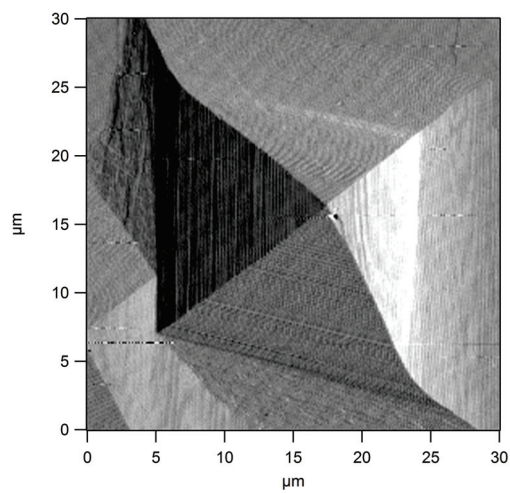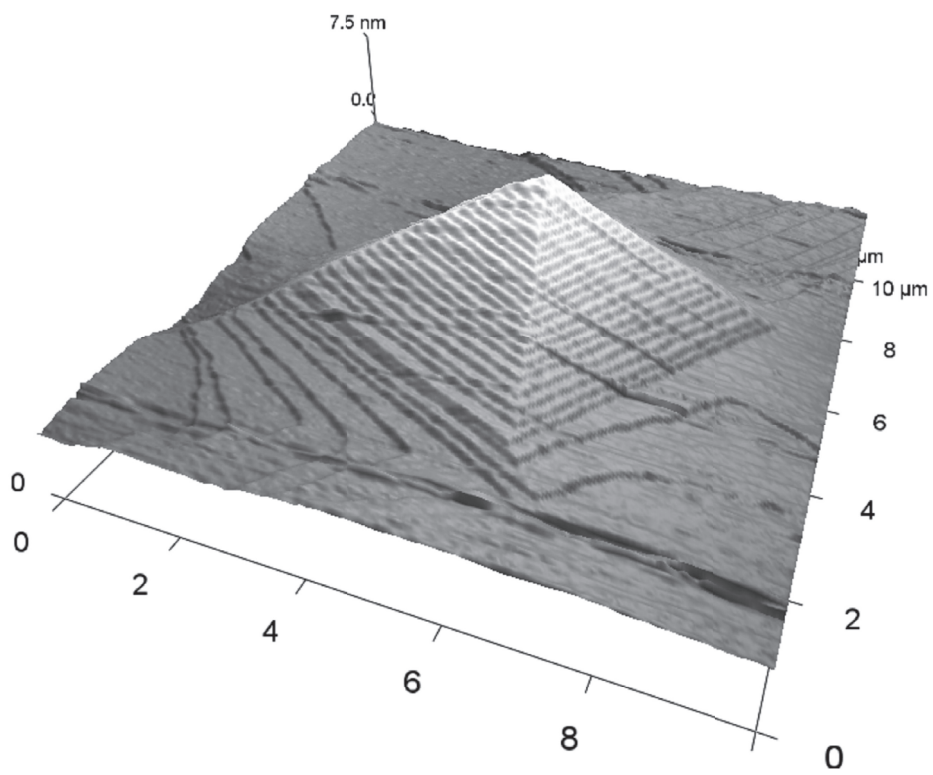
3.1 Preface

In this part of my thesis, I have focused on the calcite surface growth and the effects of normal stress on the calcite surface while it growing at atomic scale.

After the completion of the first project described in the first chapter, I wanted to explore calcite growth under varied normal applied stresses. Although numerous studies deal with calcite growth in aqueous systems, a great deal of relationships between growth rates and thermodynamic driving force for calcite growth in stoichiometric solutions exists [132]. Most attempts to model calcite surface growth and dissolution are based on detachment and attachment rates of $\{Ca^{2+}\}$ and $\{CO_3^{2-}\}$ ions [118, 132], surface speciation models [126, 98, 89] or the adsorption of calcium-carbonate ion pairs [4]. However we are not yet able to completely explain the differences in growth rate that are observed on the structurally distinct sites on calcite surface at non stoichiometric situation.

Furthermore, growth often proceeds in constrained conditions, when growing grains enter into contact for instance, or when crystallization occurs in buried sediments. But the way confinement and stress affect growth has only begun recently to draw attention. Understanding this phenomenon is a key important for clear explanations of cement setting, rock formation, and calcite diagenesis processes.

Several approaches exist to investigate the calcite growth kinetics, both macroscopic (solution based) [62] and microscopic (surface based) [118, 120] and there are comprehensive studies on calcite growth at varying Ca^{2+}/CO_3^{2-} ratios and pH and on the effect of various impurities [23, 120, 7, 53, 108]. The modeling of these data has proven difficult. Most of the existing kinetic growth models that take into account the anisotropic nature of calcite surface have only been used in modelling calcite growth in the absence of impurities [118, 132, 4]. Impurity species significantly influence the dissolution and growth of calcite crystals, both by blocking reactive sites, if adsorbed, and by inducing lattice strain, thus changing the surface free energy, if incorporated into the crystal surface or bulk [23, 91, 90, 7, 62].

Biomineralization is the process by which the biologically mediated activities of organisms lead to mineral nucleation and growth. This process has been divided into two fundamentally different types based on the degree of biological control [70]. In biologically controlled mineralization, morphologically complex structures nucleate and grow in concert with a genetically programmed macromolecular matrix of proteins, polysaccharides, and lipids. The resulting mineral microarchitectures fulfill specific physiological functions [51]. In opposition, biologically induced mineralization occurs as a result of interactions between the biological activities of an organism and its surrounding physical environment to produce secondary mineral precipitation. These minerals lack known biological function [112]. In this type of biomineralization, biological systems exert little direct control over mineral formation although biological surfaces may be important in the induction of processes [51]. However, the application of molecular genetic techniques to study biomolecules, e.g., molluscan shell proteins [1, 3], begins to reveal the structure and functions of the macromolecules involved in the bio-mineralization process. Bio-minerals such as bones, teeth and seashells are characterized by properties optimized for their functions. Despite being formed from brittle minerals and flexible polymers, nature demonstrates that it is possible to generate materials with strengths and toughnesses appropriate for structural applications [128]. Studies in bio-mineralization over the 40 years have shown that the interaction between organic molecules and Ca^{2+} and CO_3^{2-} ions and the forming $CaCO_3$ nuclei and crystal surfaces are complex. Even though it becomes even more complicated if we consider stress during

bio-mineralization. My aim was to explore a simple amino acid (pentaglycine) as impurity during calcite growth because it resembles the proteins found in biominerals [86].

3.1.1 Material

In the analysis of calcite growth in the presence and absence of pentaglycine I have relied on the methods described by Teng and colleagues [118, 120] for the analysis of spiral growth (pyramid) on calcite surfaces with AFM. I described it in details in a previous chapter. Images were obtained on an Asylum MFP-3D atomic force microscopec (see section 1.5.1). As discussed in the previous chapter and also shown in previous studies, the tip-surface interaction can influence crystal dissolution [95, 93]. For this work also I used the AFM tip to apply a force on the surface during the topography probing, to observe the influence of the force on the surface.

For this research I applied two different force regimes: 1) Low force regime with force constants of (30 ± 5) nN/V with tips from Nanosensors; by using this type of tip I was able to apply force to maximum 200 nN; 2) High force regime with force constant 90 ± 10 nN/V with tips from Nanosensors; by using this type of tip I was able to apply force to maximum 800 nN. I calibrated the force between tip and sample daily by using the relation 2.8.

At the beginning of each experiment, a calcite rod of section measuring roughly 0.5×1 cm^2 (Iceland spar purchased from Treasure Mountain mining), was cleaved in air by gently scratching a scalpel along the $\{10\bar{1}4\}$ cleavage plane to achieve a 1 to 2 mm high calcite crystal with a fresh surface. The fresh surface was cleaned of any dust by blowing with a jet of pure nitrogen and the crystal was mounted in a custom made flow cell (see figure 1.15). The surface of the crystal was imaged in air to assure that the surface looked flat and fresh (see figure 3.1), before introduction of a growth solution of desired supersaturation index in the flow cell.
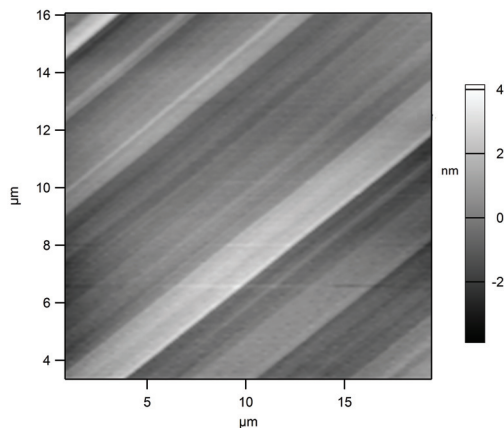
FIGURE 3.1: AFM image of calcite surface in air before introducing
the solution.

Fresh growth solutions of supersaturation (equation 1.1) $SI = 0.30, 0.42, 0.52, 0.65$, ratio $Ca^{2+}/CO_3^{2-} = 0.34$, pH $= 9.00 \pm 0.02$ and ionic strength of 0.1 M were prepared each time by dissolving $CaCl_2$, $NaHCO_3$ and NaCl (all analytical grade, from Sigma Aldrich) in ultra pure water (Millipore, resistivity >18.2 $M\Omega$) and adjusting the volume, after which the pH was adjusted using a 0.1 MNaOH solution. For experiments in the presence of pentagylcine, after preparation of the pure growth solution with $SI = 0.52$, an aliquot was transferred to a new volumetric flask. 82 µM penta

glycine was transferred quantitatively to the flask and dissolved, and the volume was adjusted using the pure growth solution to obtain a growth solution with the same solution parameters as the pure solution and a known concentration of additive. I checked that the addition of the pentaglycine did not alter the pH of the solutions. Each experiment lasted 4 hours and the pH of the solution was monitored regularly during the experiment. I calculated the amounts of salts needed to obtain the desired solution composition and saturation indices with the Phreeqc software using the Minteq.v4 database. All the solutions concentrations were checked every hour by **I**nductively **C**oupled **P**lasma **M**ass **S**pectroscopy **ICP-MS** to assure the agreement between the exact considered solution concentration and the Phreeqc calculation.

Introduction of the growth solution always resulted in some contortion of the cantilever which led to poor quality. Therefore the system was allowed to relax for half an hour before the imaging could begin. The first step was always to locate a whole single growth pyramid (see figures 1.12 and 3.2). In general double dislocation spirals grow faster [120]. I measured growth on spirals growing from single dislocation. When I had found and example of stable spiral growth, the step velocities were measured for the all four sides (flanks) of the pyramid at certain applied forces. The range of applied force during this research was 0 to 750 nN.
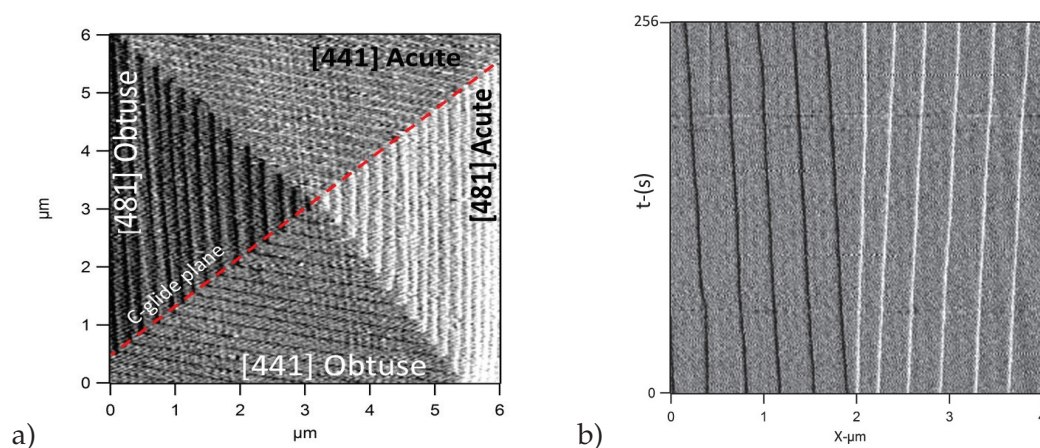

FIGURE 3.2: AFM deflection mode image showing a) A growth spiral formed on a freshly cleaved calcite surface in solution. The four line directions are shown. b) An example of growing spiral, collected with the Y scan disabled. This tip scans from bottom to top. As the steps move away from the apex of the pyramid the lines representing the edge of the steps slants outward.

Step velocities were measured by the same method that I described in the previous chapter (see section 2.1.2). To sum up, first I aligned the scan direction so two step edges (either $[441]_{acute}$ and $[441]_{obtuse}$ or $[481]_{acute}$ and $[481]_{obtuse}$) were parallel to the Y axis, then disabled the Y or *slow* scan (assuming instrument drift was negligible). Thereby the same linear area were scaned rapidly. This protocole resulted in image such as the one shown in figure 3.2. The step velocity was computed from the angle between the trace left by the step motion and the Y axis. Following every image the force was adjusted and imaging resumed. After the velocities of two parallel steps had been measured, I imaged the pyramid again (to document the morphology) and then rotated the scanning angle by 78°or 102°and measured the velocity of the other two directions. At least six images with Y-scan disabled were used to determine and measure the step velocities. Finally, the pyramid was imaged again.

During the experiments with pentaglycine I have repeated the same procedure with the regular growth solution. When I measured step velocities in coincidence with the rest of the experiments the solution with calcite growth was replaced by a solution with the same saturation index, pH and same ratio of Ca^{2+}/CO_3^{2-} but containing 82 μM pentaglycine. After the cantilever had been allowed to relax for another half an hour, the imaging could resume following the procedure just described.

3.1.2   Additive

The term amino acid might mean any molecule containing both an amino group and any type of acid group; however, the term is almost always used to refer to a carboxylic acid. The simplest acid is aminoacetic acid, called glycine. Although we commonly write amino acids with an intact carboxyl group and amino group, their actual structure is ionic and depends on the pH. The carboxyl group loses a proton, giving a carboxylate ion, and the amino group is protonated to an ammonium ion. This structure is called a dipolar ion or a zwitterion (German for "dipolar ion"). In an acidic solution, the group COO^- is protonated to a free COOH group, and the molecule has an overall positive charge. As the pH is raised further, the group NH_3^+ loses its proton and the molecule changes into NH_2 with an overall negative charge (figure 3.3).
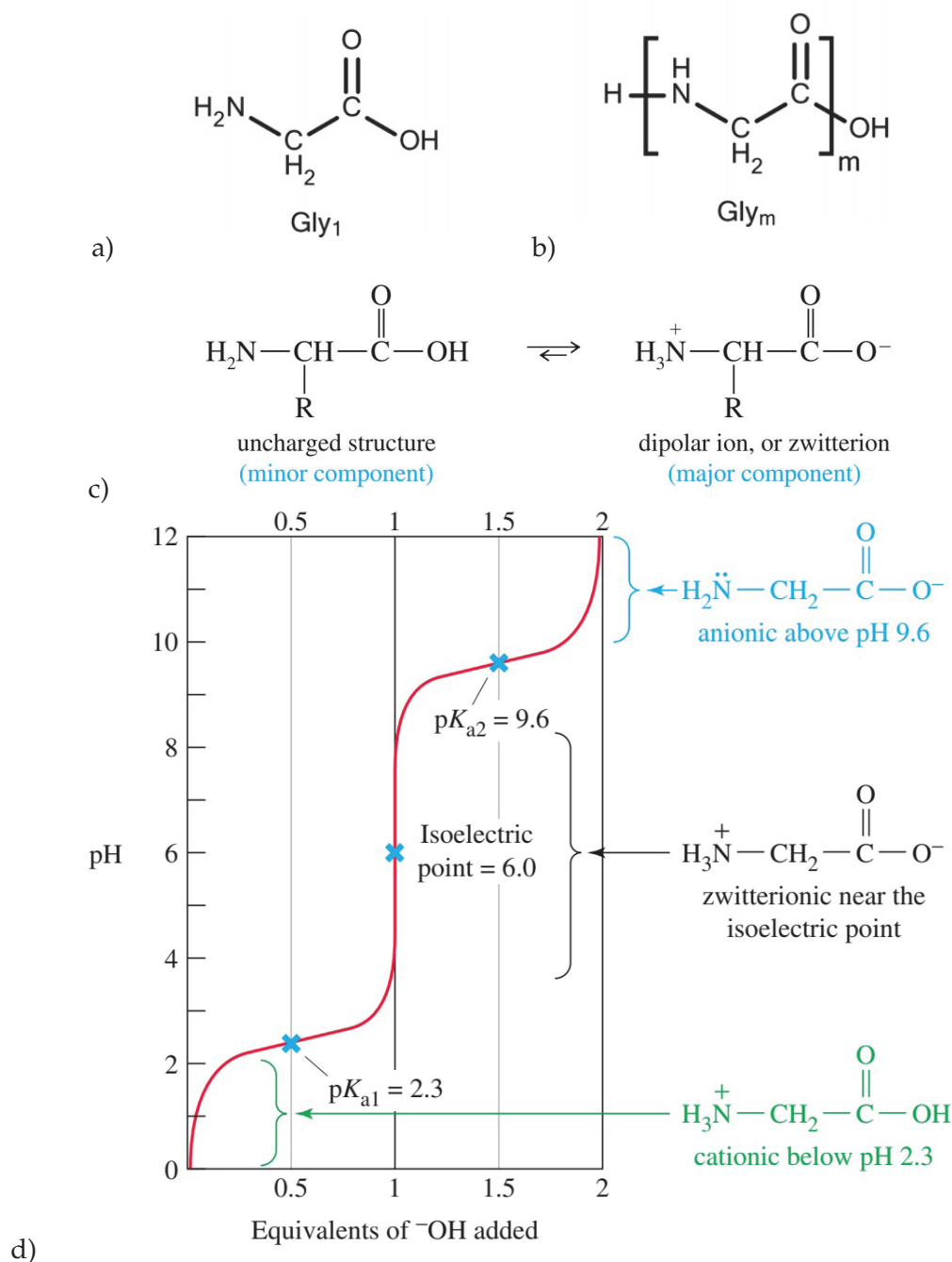
FIGURE 3.3: a) The structure of glycine, b) Gly_5 pentaglycine, c) dipolar nature of amino acids, d) a titration curve for glycine. The pH controls the charge on glycine: cationic below pH 2.3; zwitterionic between pH 2.3 and 9.6; and anionic above pH 9.6. The isoelectric pH is 6.0. This graph is adapted from [125].

I chose for this study pentaglycine because it is structurally simple and readily available. Thus it made possible to study the effects of pentaglycine on the dynamics of atomic steps on calcite surface at different applied force. The effect of pentaglycine on stress-free calcite growth was studied by Montanari and colleagues [86]. They prove that pentaglycine at low concentration slightly promotes calcite growth rate.

At the pH of the our experiments (9) carboxyl -COO$^-$ functional groups are deprotonated while the amino groups -NH$_3^+$ are protonated. So this molecule had

mostly a negative charge.

Pentaglycine (molecular weight 303.30 g/mol; aqueous solubility, at 37°C 1.3 mg/ml) was purchased from Sigma-Aldrich Chemical Company, and used without purification. Pentaglycine is neither hydrophilic not hydrophobic. Therefore hydrophilicity and hydrophobicity of other amino acids are expressed relatively to glycine.

3.1.3 Pyramid morphologies

When the calcite $\{10\bar{1}4\}$ face grows in supersaturation solution, there are two commons growth mechanism: 2D nucleation and precipitation at existing step edges and defects, which often results in spiral growth [120]. Growth spirals can originate from one or multiple dislocations and from defects. A more detailed description of the mechanisms of calcite growth is presented in the section about calcite growth in the introduction (see section 1.3.4). An example of a spiral growing from a single dislocation source in a solution without pentaglycine at $SI = 0.52$, $Ca^{2+}/CO_3^{2-} = 0.34$ and pH = 9 is shown in figure 3.2. The spiral forms a pyramid, with straight edges and sharp corners, similar to previous reports [118, 120]. All the observed pyramids in all saturated indices showed the same morphology. The morphology of spirals growing in solutions containing pentaglycine can be compared to the regularly shaped spirals grown in absence of pentaglycine.

The angle θ in a pyramid between two obtuse flanks in direction [441] or [481], and two acute flanks in direction [441] or [481], in a growing solution, is 149.8°, but this angle in a pyramid in a growing solution containing pentaglycin increases to 166°. This could be interpreted by the fact that in the absence of pentaglycine the two obtuse steps move faster, so the angle in this direction less than plane. The pyramids grown in the presence of pentaglycine, with wider angle between flanks, showed changes in the ratio of the obtuse and acute steps velocities.
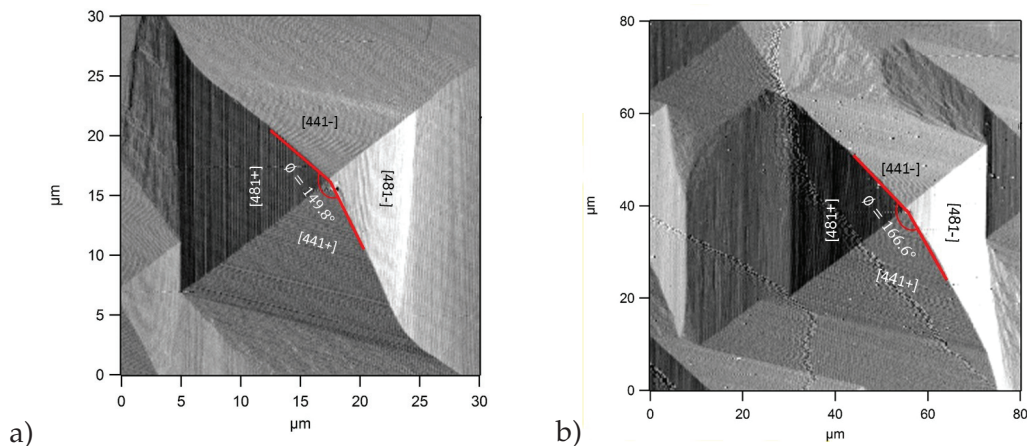
FIGURE 3.4: A single spiral growth illustrates the sensitivity of the geometry to the solution composition: a) The spiral growth in growing solution displayed paired flanks along the negative (acute) directions with larger areas than those along the positive (obtuse) direction; b) The same spiral growth in growing solution (180 minutes) with pentaglycine showing all flanks similar in size and slope.

3.1.4 Influence of stress on step velocities

I calculated the step velocities based on the method explained in section 2.1.2 for the four flanks. The sum of the steps $[441]_{obtuse}$ and $[481]_{obtuse}$ were displayed as obtuse and the sum of the steps $[441]_{acute}$ and $[481]_{acute}$ were displayed as acute steps. In both acute and obtuse steps the step velocities increased with increasing saturation index.

The step velocities for both acute and obtuse steps decrease when increasing the applied force until ≈ 180 nN. In the range of applied force between 180 to 200 nN it became apparent that the step velocities did not show any specific trend. The most obvious influence of the applied force was observed below 200 nN applied force. Above 200 nN there was a jump in the step velocities for both obtuse and acute step for all saturation indices. Beside the step velocity acceleration, the acute steps displayed higher step velocities than the obtuse ones, that was contradictory with their behavior for forces < 180 nN (figure 3.5).
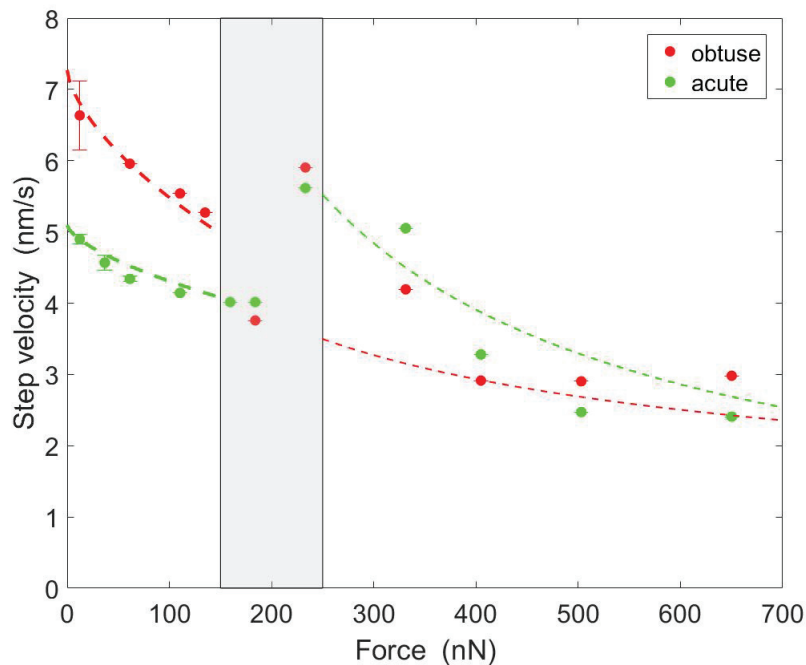

FIGURE 3.5: Evolution of step movement rates over varied applied force in growth solution SI= 0.52.
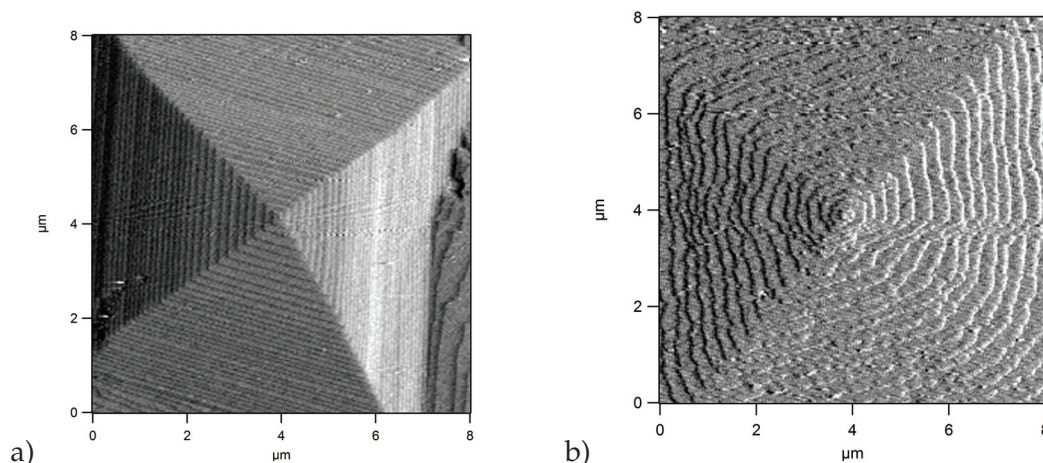
FIGURE 3.6: a) Morphology of the pyramid probed at 20 nN applied force. b) Deformed morphology of the pyramid at 140 nN applied force. The line where the tip has gone back and forth can still be seen in the middle of the image.

Overall, the changes in the step velocity behavior (obtuse and acute) with varied applied force can be classified in 2 applied force regimes (low force regime <180 nN and high force regime >200nN). This change in growth kinetics indicate that there are specific interactions between the force applied by tip and calcite.

The growth pyramid under the applied force has a healing ability, which means that after releasing the force it rebuilds the deformed steps. It returns to the vanished force morphology after releasing the force. In one experiment I proposed to probe several continuous Y scan-disabled and the tip stayed in the same X direction and moved forth and back in the line with the considered applied force. Then I released the force applied by the tip and I imaged the topography (X and Y image) of the pyramid with a high scan rate. I was able to record the deformed steps and pyramid under applied force before it self heals (figure 3.6).

Theoretical approach of the growth under stress

This reaction happens on the mineral surface by atomic attachments. Step advance proceeds preferentially through the attachment of the constituent ions, in this case, Ca^{2+} and CO_3^{2-} or HCO_3^-,to high energy surface sites along step edges, in kinks or corner sites:

$$Ca^{2+}(aq) + CO_3^{2-}(aq) \rightleftharpoons CaCO_3(s)$$
$$>CaCO_3^- + Ca^{2+} \rightleftharpoons >CaCO_3^+$$
$$>CaCO_3^+ + CO_3^{2-} \rightleftharpoons >CaCO_3^-$$
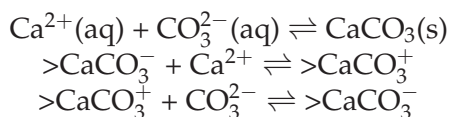
Where > denotes a surface site, as in surface complexation modeling [121, 98].

These reactions describe the reversible attachment of a growth unit Ca^{2+} or CO_3^{2-} and the transition from a Ca^{2+} surface site to a CO_3^{2-} surface site or vice versa, as the surface step grows or dissolves [108]. To attach to a kink site, an ion has to diffuse through the solution and over the surface and then dehydrate. The growth site must dehydrate before it can accommodate an additional cation or an anion. In the pH range of this study, HCO_3^- is the dominant carbonate specie (see figure 1.7).

The AFM tip applied a stress on the surface when it recorded the topography with a surface area of approximately 100 nm^2. To estimate this constraint, I considered the Hertzian type contact between the AFM tip and the crystal surface. The

model used for this study was the same model as used for gyspum dissolution (section 2.1.5). This was a study on growth and the solution is supersaturated. Considering this condition, I did a few adjustments on the model. The step velocities depend on the solid-liquid Gibbs free energy difference:

$$\Delta G = RT \ln \Omega + \delta U_e \tag{3.1}$$

with R the gas constant, T the temperature, Ω the solution supersaturation and δU_e the molar elastic energy of the solid (see equation 2.14). Finally the step velocity should follow this relation:

$$v = v_0 [\Omega \exp(-\frac{\alpha \sigma^2 \bar{V}}{2ERT} - 1)] \tag{3.2}$$

with v_0 the velocity without applying any force.

Calcite phase transition

For better understanding the mutation of step velocities by increasing the applied force I focused in this part to explain the possible structure of calcite in high pressure. The high pressure polymorphs of calcite are possible host structures of natural storage of C and CO_2 in the Earth's mantle. Pressures reached 13-23 GPa (upper mantle) and 23-135 GPa (lower mantle) (see figure 3.7) [129].
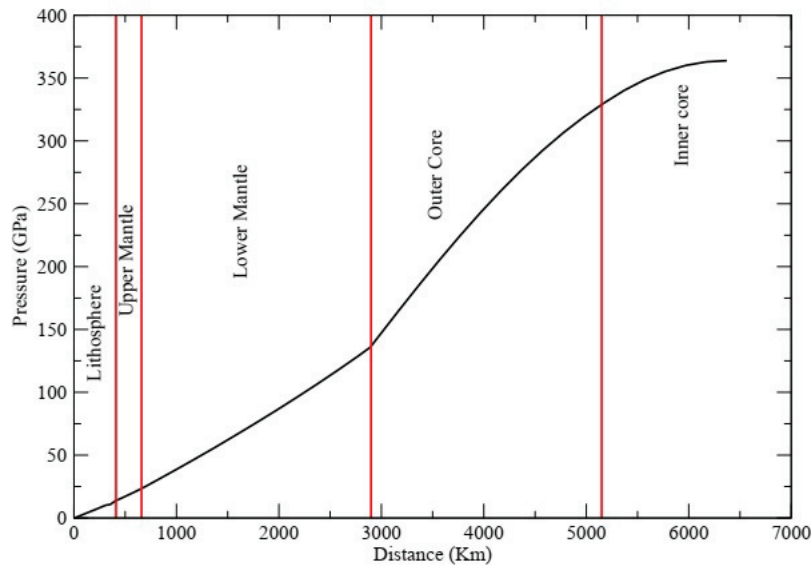

FIGURE 3.7: Profile of pressure versus distance from the surface of the earth. Figure adapted from [129].

In addition to pressure, temperature also significantly affects the stability of calcite. The effect of these two thermodynamic variables on $CaCO_3$ results in a rich pressure-temperature phase diagram containing 9 distinct solid phases: calcite I, II, III, IIIb, IV, V, VI, aragonite and vaterite. In fact, no other compound exhibits polymorphic variation as commonly and abundantly in nature as does $CaCO_3$ (see figure 3.8) [15]. At ambient temperature and by applying pressure, calcite I evolves from a highly symmetric structure ($R\bar{3}c$) to lower symmetric structures: calcite II

(monoclinic) with the space group of $P2_1/c$ [56], calcite III and calcite VI (both triclinic). There have been a number of investigations of this problem since 1939 [13]. The structure of the high pressure metastable phase, calcite-II, was determined using the single-crystal X-ray diffraction technique by Merrill and Bassett [83]. They suggested that the transition of calcite I to calcite II results from two kinds of displacement: 1) the rotation by an angle θ of 11°(see figure 3.9) in opposite directions of adjacent CO_3 groups along the c axis and 2) the small anti parallel displacement Δ of Ca^{2+} ions (see figure 3.9). These displacements reduce the lattice symmetry $R\bar{3}c$ to monoclinic.

As can be seen in figure 3.8, calcite I at ambient temperature and pressure $\approx$ 2 GPa transits to calcite-II (figure 3.9), and then calcite-III (figure 3.10), which can be an explanation for the behaviour observed in figure 3.5, where the step velocity changed their trend at an applied force around 200 nN. Indeed, the surface area of the contacting tip being $\sim$ 100 nm^2, 200 nN corresponds to a stress of $\sim$ 2 GPa. So the step rate jump around 200 nN can be interpreted as a phase transition from calcite I to calcite III (see figure 3.8). I also observed that the step velocity jumping at 200 nN is higher for acute steps (see figure 3.5).
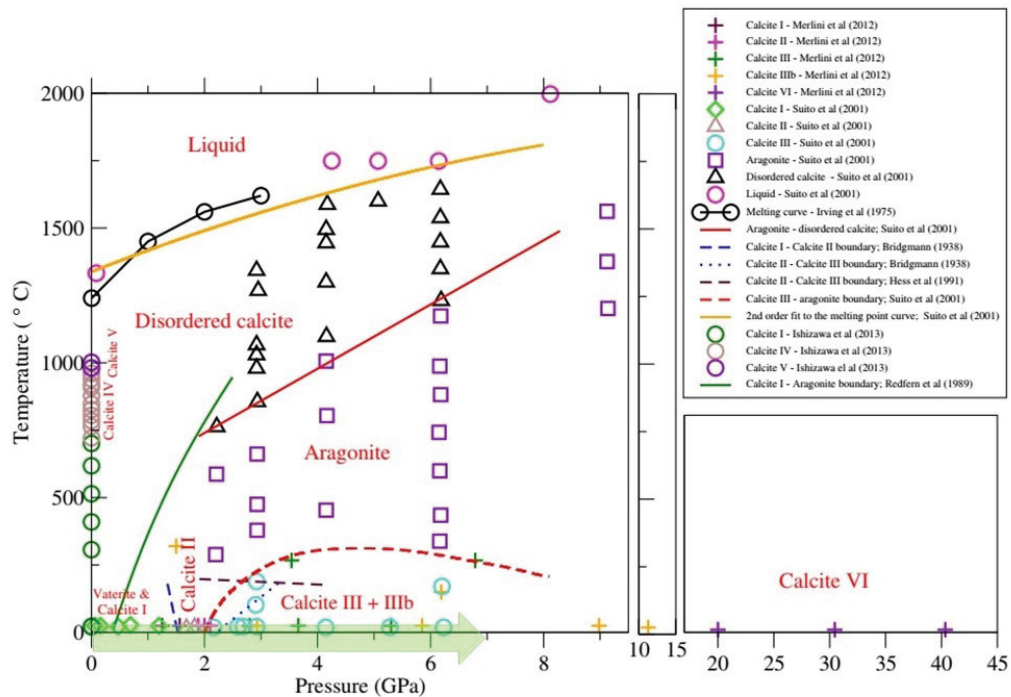

FIGURE 3.8: Experimental phase diagram of CaCO$_3$ gathering all the available information by David Carrasco de Busturia, Imperial College London. The light green arrow shows the applied pressure at ambient temperature in our work.

For the last 40 years calcite III has been extensively studied [23, 74], but the determination of its structure has generated considerable controversy. In 2012, Merlini et al. first characterized calcite III using single-crystal synchrotron X-ray diffraction [82]. At ambient temperature, they observed this phase above 2.5 GPa and up to 15 GPa, a pressure range that corresponds to that in the upper mantle (see figure 3.7).
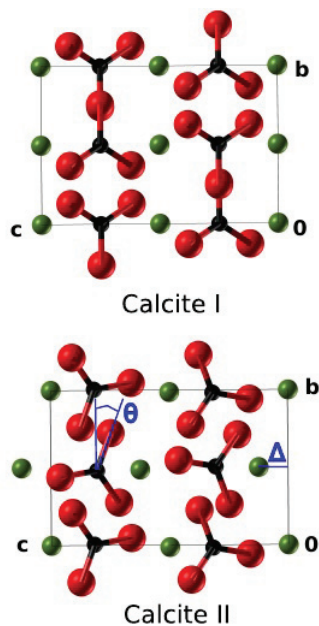
FIGURE 3.9: Structure of the calcite I transition to calcite II, result-
ing from two displacements. Figure adapted from David Carrasco de
Busturia, Imperial College London.

Merlini characterized Calcite III as triclinic (space group $P\bar{1}$). Its structure is iden-
tified by the presence of non-coplanar CO_3 groups see in figure 3.10.
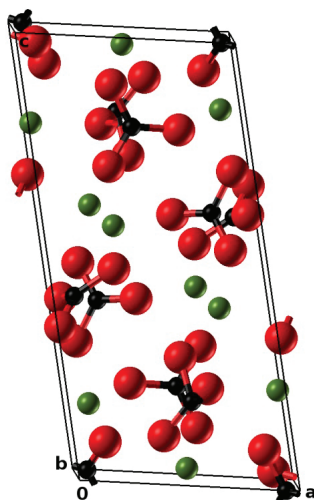
FIGURE 3.10: Unit cell of calcite III, with 10 formula units. Figure
adapted from David Carrasco de Busturia, Imperial College London

3.1.5 Effect of pentaglycine on step movement

I calculated the step movement rates, v, of acute and obtuse steps after addition
of 82 µM of pentaglycine. The velocities for obtuse and acute steps versus applied
force are shown in images 3.11 and 3.12. As displayed in figure 3.11, the obtuse step
velocity decreases slightly in the low force regime (< 200 nN), similar to without
pentaglycine. But unexpectedly, pentaglycine has led to the suppression of the jump
around 200 nN. The velocity keeps on decreasing without noticeable accident. Even

the slope of v seems less steep with pentaglycine, and v eventually tends to keep constant.

As presented in figure 3.12, the acute step velocity shows the same behaviour, with pentaglycine having cancelled, even more clearly, the jump around 200 nN, and a velocity almost constant for the highest forces. The amino acid has therefore visibly suppressed the phase transition calcite I-calcite III.
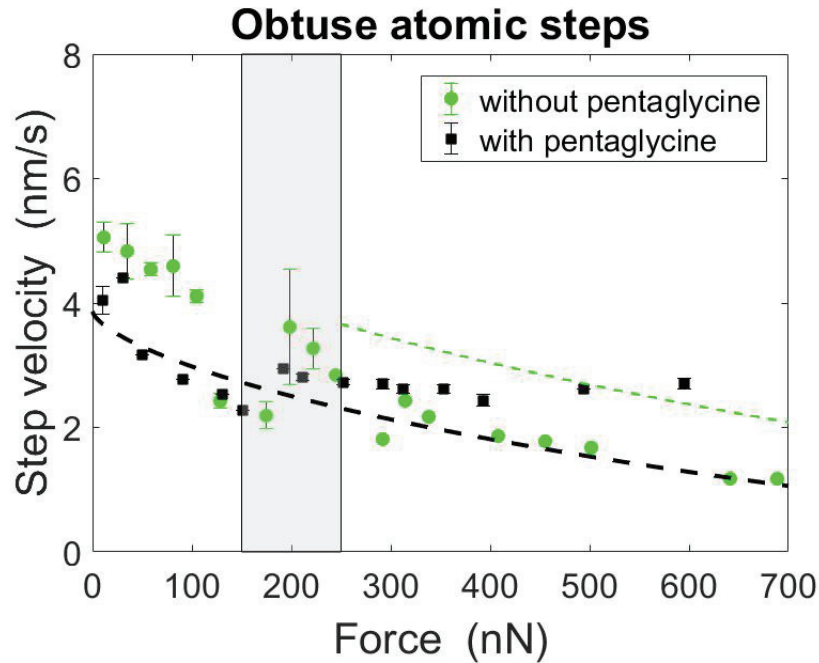

FIGURE 3.11: Obtuse step velocity as a function of applied force in presence and absence of pentaglycine.
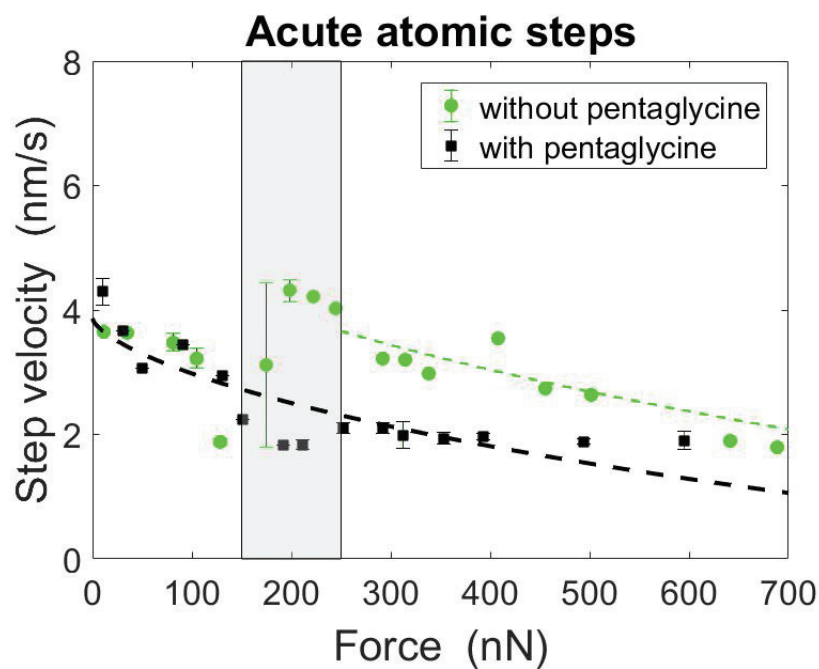
FIGURE 3.12: Acute step velocity as a function of applied force in presence and absence of pentaglycine.

3.2 Tuning biotic and abiotic calcite growth by stress

An article detailing these results, submitted for publication, is presented below.

Tuning biotic and abiotic calcite growth by stress

Bahareh Zareeipolgardani,[1] Agnès Piednoir,[1] and Jean Colombani[1, *]

[1]*Institut Lumière Matière; Université de Lyon; Université Claude Bernard Lyon 1;*
CNRS UMR 5306; Domaine scientifique de la Doua, F-69622 Villeurbanne, France

Identifying mineral growth mechanisms is fundamental to understand diagenesis, construction material hardening and biomeralization. This necessity is particularly true for calcium carbonate, widespread in these three fields. The transformation of loose grains into a cohesive solid requires the crystallites to grow eventually constrained by the surrounding grains. Whereas never measured, this confinement and the associated stress is expected to influence noticeably the growth, and the final properties of the material. We report here on atomic force microscopy measurements of atomic step velocity during calcite growth, with a varying stress applied by the tip to the surface. The stress has a double influence: it both slows down the growth, and modifies the material crystalline phase. Furthermore, the addition of a small quantity of oligopeptide in the growth solution is shown to have no significant influence on the kinetics, but to completely cancel the phase change under stress. Our results emphasize the previously unknown role of stress on growth mechanisms and identify a new possible role of organic molecules in tuning the morphology of biomineralized materials.

The ability to predict mineral nucleation and growth rate, and the understanding of the underlying mechanisms, have fostered recently an intense activity. Whereas new concepts have lately improved our comprehension, among which one can cite hydration layer disruption [1], polynuclear complex [2], amorphous precursors [3], or non-stoechiometric growth [4], and despite some successes of growth rate prediction [5, 6], the basic molecular events at the heart of growth are not firmly established yet [7]. Therefore we are still far from having a comprehensive view of the nucleation and growth processes. However, these phenomena involve crucial challenges in geological, biological and industrial contexts. We can cite the development of low energy consumption cements, the need of anthropogenic carbon dioxide sequestration, or the physical control on biomineralization as a promising new route for smart materials engineering [8].

Calcite is a major constituent of sedimentary rocks on the Earth surface, where it forms in inorganic or biogenic conditions [9]. Calcium carbonate growth from hydrated lime is also one of the oldest construction method of Man [10]. During the setting process of these natural or man-made materials, the condition for loose grains to transform into a cohesive material is that growing grains end up entering into contact, and progressively stick to each other. Thus stress develops between them and growth proceeds in constrained conditions, with potential dramatic consequences on the final properties of the material [11, 12]. Furthermore in burial conditions in the Earth Mantle, a lithostatic pressure of up to a few GPa adds to this stress [13]. As the actual contact surface area is generally much smaller than the apparent one, much higher stresses should build up. This fundamental aspect of calcite growth has so far not been addressed and the effect of stress remains unknown. Even though the consideration of the crucial importance of the confinement on calcite precipitation at the atomic scale has been demonstrated

accurately [14], all remains to be done concerning the way the stress resulting from this confinement influences the phenomenon.

Biotic calcite is grown by living organisms, using numerous and complex processes among which one can cite concentration and transport of constituting ions by vesicles [15], polymorph selection by incorporation of organics [16] or surface templating [17], or nanolayering by organo-mineral additives [18]. Organics used in these processes are in turn known to strongly modify the response to stress of their host biomaterials, in blocking dislocation migration [19] or modifying cleavage plane [16]. They are therefore expected to noticeably modify the response of the material to stress during growth.

The difficulty of studying stressed calcite lies in the fact that high applied stresses are likely to exceed the mechanical strength of the material. To circumvent this issue, we have used an original method, inspired by the configuration of real contact between grains, where the stress develops mainly at asperities. We have applied on a growing surface a well defined local force with an AFM tip, playing the role of an asperity, and parallely, used this tip to image the surface.

We have observed that the stress has a huge influence on the growth because it changes both its structure and its kinetics. Indeed on one hand it slows down significantly the growth rate and on the other hand it induces a phase transition. Furthermore, the addition of an amino acid at low concentration, widespread in biomineralized tissues, whereas having no significant effect on the growth rate, cancels this phase transition, showing how biomolecules are prone to tune the influence of stress on growth.

In all experiments, the ionic strength was fixed at 0.11 M with NaCl, the pH at 9.0 with NaOH (0.1 M), and the Ca/CO$_3$ activity ratio was held at 0.34. The saturation index SI $= \log(a(\text{Ca}^{2+})a(\text{CO}_3^{2-})/K_{sp})$, with a the activities and K_{sp} the solubility product of calcite,
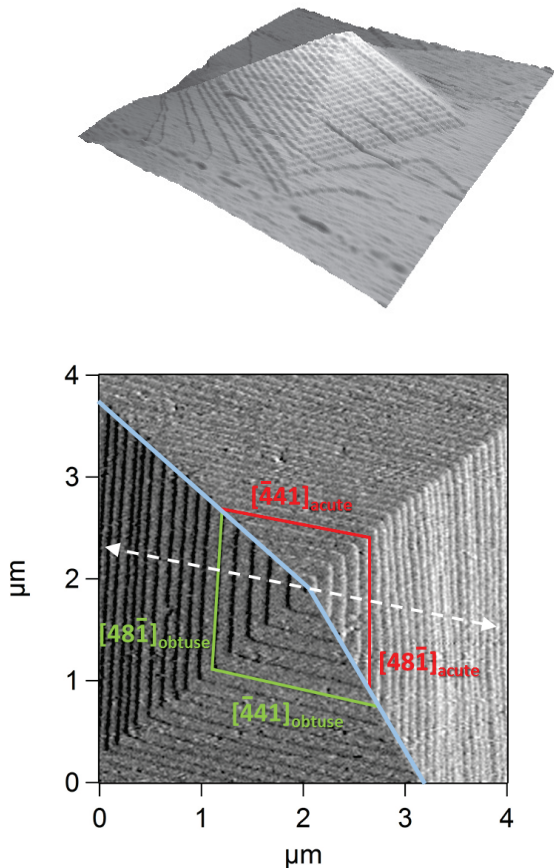
FIG. 1: Top: three dimensional AFM view of a grown spiral pyramid ~ 10 nm high on a calcite cleavage surface. The scanned zone is $10 \times 10 \ \mu m^2$ wide. Bottom: AFM deflection mode image of the top of the pyramid. The obtuse and acute steps are shown. The angle of the two lines sharing acute and obtuse steps, passing through the apex, is non-plane, due to nonequivalent velocities of the two steps. The white arrow shows the tip path during step velocity measurements.

was calculated using the speciation freeware Phreeqc [20] and controlled regularly by inductively coupled plasma mass spectrometry (ICP-MS). The supersaturation used for the chemical potential computation is defined as $\Omega = (a(\mathrm{Ca}^{2+})a(\mathrm{CO}_3^{2-})/K_{\mathrm{sp}})^{1/2}$.

Among amino acids, we have selected pentaglycine, because it is already known to contribute to biomineralization [21]. At pH 9.0, at which our experiments were performed, pentaglycine is zwitterionic, with 20% of its functional groups deprotonated.

The samples were made of Iceland spar from Chihuahua, Mexico, the purity of which was estimated as 99% of calcium content with inductively coupled plasma atomic emission spectroscopy (ICP-AES) and energy

dispersive X-ray spectroscopy (EDX)[57]. The calcite was cleaved in air by gently scratching a scalpel along the $(10\bar{1}4)$ cleavage plane to achieve a 1 to 2 mm thick calcite crystal with a fresh surface, which was cleaned of any dust by blowing pure nitrogen. The crystal was then mounted in a custom made flow cell.

In situ AFM imaging at $25\,^\circ$C was performed in contact mode (Digital MFP3D, Asylum Research, Oxford Instruments) during a continuous flow of supersaturated solution through a fluid cell at a constant 0.275 mL/min flow rate, ensuring a step growth velocity independent of the flow rate.

The step movement rates were measured by aligning the scan direction so that two facing steps, one acute and one obtuse (Fig. 1) were parallel to the Y scan direction and then disable this scan direction. Thereby a kymogram was obtained, with the step migration leaving a track in the (X, t) plane (t the time) and the velocity being the slope of the track [22, 23]. With this method the scanning AFM tip has a double role: it measures the step velocity and, to achieve this goal, it applies locally a given force to the crystal.

$\mathrm{Si}_3\mathrm{N}_4$ AFM tip cantilevers of low stiffness, with gold coating on detector side, were used to apply forces between 0 and 250 nN, and silicon tip with high stiffness were utilized to apply forces ranging from 0 to 800 nN to the scanned surface. The overlapping range was used for double-checking.

Spiral growth can originate from individual dislocation with Burgers vector being a multiple of the lattice parameter [24]. Thus we have observed double or triple spiral growth (see Fig. S1 and video 2 in Supplementary Information) but we have focused here only on the step velocity of single spiral growth.

We observe that the growth at the cleavage face $(10\bar{1}4)$ of calcite in a flowing supersaturated solution of saturation index ranging between 0.3 and 0.65 always proceeds through spiral growth, an hillock progressively forming from continuously nucleating and growing atomic steps (see Fig. 1 and video 1 in Supplementary Information). The starting point of the spirals is likely to be an outcropping screw dislocation [25]. This growth mechanism is characteristic of the range of low saturation indices we have investigated [24], higher indices inducing additionally island nucleation on flat terraces [26]. The spiral pyramids exhibit straight edges and sharp corners with rhombohedral cross section [27]. Each spreading layer is bounded by two obtuse, in the $[\bar{4}41]_{\mathrm{obtuse}}$ and $[48\bar{1}]_{\mathrm{obtuse}}$ crystallographic directions, and two acute, $[\bar{4}41]_{\mathrm{acute}}$ and $[48\bar{1}]_{\mathrm{acute}}$, steps edges (Fig. 1).

The two classes of steps are seen to migrate at different velocities (see Fig. 2 and 3), which induces a non-plane angle between facing edges of the pyramids (see Fig. 1). This discrepancy results from the geometric difference between the two classes of steps, leading in different rates of kink site nucleation at the step edge and
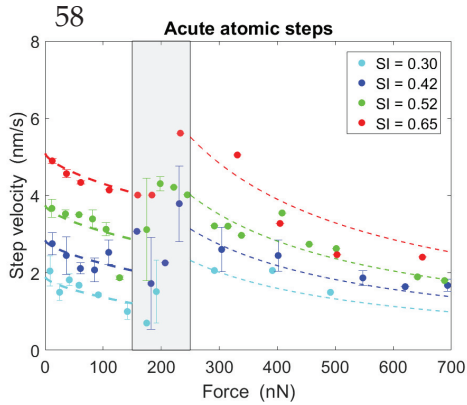
FIG. 2: Evolution of the acute step velocity as a function of the force applied by the scanning AFM tip on a calcite cleavage surface during growth in a solution of saturation index SI. The grey box marks the probable phase transition zone between calcite I and calcite III. The dashed curves are fits of the experimental data with Eq. 1.


FIG. 3: Evolution of the obtuse step velocity as a function of the force applied by the scanning AFM tip on a calcite cleavage surface during growth in a solution of saturation index SI. The grey box marks the probable phase transition zone between calcite I and calcite III. The dashed curves are fits of the experimental data with Eq. 1.

incorporation of ions at these kink sites during growth. Consequently, this discrepancy has been measured as being highly dependent on the chemical conditions, especially on the $[Ca^{2+}]/[CO_3^{2-}]$ ratio. Consistent with former studies, obtuse steps are seen to migrate faster in the chemical conditions of our solution [28–30].

As expected, step velocities increase when the saturation index raises, the driving force of growth being thus enhanced. But what had never been observed is that these velocities depend on the force the steps are submitted to as well (Fig. 2 and 3). Furthermore the step velocities display unexpectedly a non-monotonous evolution with the applied force, with an initial decay, followed by a kind of jump, and then a resumption of the decrease. So two distinct regimes appear, separated by an abrupt transition.

To evaluate the influence of organic molecules on biomineralization, we have tested the modification of growth under stress in presence of an oligopetide. The addition of 82 μM of pentaglycine in the solution is seen to provoke a radical change of the step velocity behavior. Indeed the jump around 200 nN disappears completely and the velocity exhibits now a smooth and continuous decrease up to 700 nN (Fig. 4).

As the steps move slower in the vicinity of the tip than elsewhere on the surface, the tip is expected to leave a trace of its passage. But the steps relax toward a straight shape as soon as the tip stops scanning back and forth along the line. Therefore this trace is difficult to observe. Nevertheless an example is shown in Fig. S2 in Supplementary Information.

For forces below $F \sim 200$ nN, the step velocity in all conditions exhibits a continuous and monotonic decrease (Fig. 2 and 3). We interpret this trend as a consequence of the change of Gibbs free energy of the mineral induced
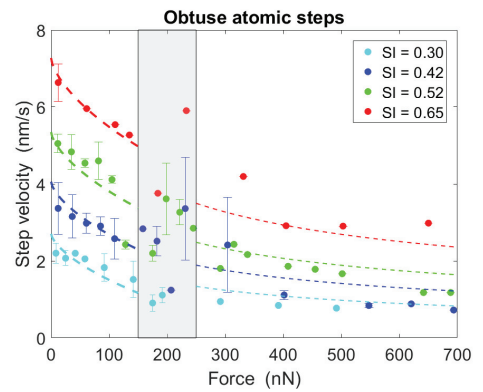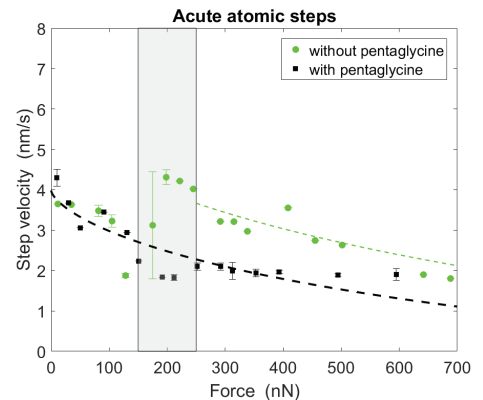

FIG. 4: Evolution of the acute step velocity as a function of the force applied by the AFM tip on a calcite cleavage surface during growth in a solution of saturation index SI = 0.55 with and without 82 μM of pentaglycine. The dashed curves are fits of the experimental data with Eq. 1.

by the elastic strain caused by the tip. Indeed, the step motion driving force is the chemical potential difference between the solid and liquid. The supersaturation of the solution induces an increase of the chemical potential of the liquid, that triggers the nucleation and growth. The elastic energy stored by the solid with the passage of the tip then enhances the chemical potential of the solid, which in turn reduces the disequilibrium, thus slowing down the growth. Very high forces could possibly totally hinder the growth, similarly to the dead zone seen in growth inhibition by impurities, where precipitation may be completely stopped even for high supersaturation [31]. This inhibiting effect of stress is reminiscent of the dissolution of crystals in supersaturated solutions, due to the strain induced by some adsorbed inhibitor [32]. This effect is opposite to the case of dissolution, where

the elastic energy amplifies the disequilibrium [23].

The velocity v dependence on the solid-liquid Gibbs free energy difference ΔG writes $v = v_0 (\exp(\Delta G/(RT)) - 1)$, where v_0 is the velocity at vanishing driving force, R the gas constant and T the temperature [27]. The driving force contains both the chemical and mechanical contributions: $\Delta G = RT \ln \Omega + \delta U_e$, where Ω is the solution supersaturation and δU_e the molar elastic energy of the solid [33]. This last quantity can be obtained via $\delta U_e = \sigma^2 \bar{V}/(2E)$, with $\bar{V}$ and E the molar volume and Young's modulus of calcite ($\bar{V} = 37 \times 10^{-5}\,\mathrm{m^3/mol}$ and $E = 86\,\mathrm{GPa}$) and σ the applied stress.

As the space between the pressing tip and the surface is inaccessible to the solute, growth should proceed at the periphery of the tip. So we approximate the tip-surface interaction by a Hertzian contact and take σ as the tensile stress at the contact line.

Consequently the step velocity should follow the following relationship:

$$v = v_0 \left(\Omega \exp(-\alpha \sigma^2 \bar{V}/(2ERT)) - 1 \right) \qquad (1)$$

with α a geometric factor linked to the range of the elastic field around the tip-surface contact. The experimental data are satisfactorily fitted by this thermodynamic law (see Fig. 2, 3 and 4).

An alternative explanation of the influence of the stress is to consider that this one does not reduce the attachment rate of the solute to the step, which Eq. 1 implicitly states, but increase the detachment rate, the balance of which determines the net growth rate [31]. Fig. S3 and S4 in Supplementary Information show a fit of the experimental data with the corresponding law. This one is very similar to the fit of Eq. 1 and it is not possible to discriminate between both processes.

No abrupt change is expected from this theory. The origin of the break around 200 nN is accordingly to be searched for elsewhere. Using again Hertzian mechanics, the corresponding maximal pressure experienced by the surface under the tip for this force value is ~ 2 GPa. Actually, this value is well-known to be the one where calcite exhibits a phase transition between the calcite I and calcite III polymorph, with a transitory calcite II phase [34]. So we ascribe the change of behaviour of the growing surface to a phase change from calcite I to calcite III triggered in the vicinity of the tip by the applied pressure [39]. This possible AFM-induced calcite phase transition had been evoked decades ago but never checked so far [35]. It originates in a rotation of the carbonate group in the crystalline cell. The determination of the bulk calcite III lattice is a challenging issue for years [13].

In the high force regime, the velocity decrease should again originate in the equilibrium displacement induced by the elastic energy provided by the tip pressure. But as the calcite III lattice, and a fortiori its mechanical properties, are still debated, we have fitted the experimental

data with the same functional law only as a guide to the eye (see Fig. 2 and 3).

The Bravais lattice of calcite III is different from the one of calcite I, and the moving steps likewise. Their crystallographic directions are unknown, but we observe that their mobility is completely modified, the ex-obtuse steps moving now slower than the ex-acute steps.

We recall that the two observed growing lattices of calcite are equilibrium phases, therefore once high forces are no more applied to the surface, calcite III transforms progressively into calcite I. A striking example of this spontaneous relaxation of the surface from its high pressure to its low pressure form is shown in videos 3 and 4 in Supplementary Information.

During dissolution, from a given threshold on, the application of a high force by the scanning AFM tip has been seen to induce a damaging of a gypsum or calcite surface, creating kink sites in the migrating steps [23, 36]. But the functional dependence of the step speed on the applied force was observed to be completely different from a pressure solution law, following instead a much faster Arrhenius increase. With this in mind, we have ruled out such a corrosive wear here because, in that case, (i) the $v(F)$ curve should not follow a pressure growth law like Eq. 1, and (ii) no abrupt jump in the $v(F)$ should be observed.

In the low force regime, no detectable change of step velocity by the pentaglycine addition is observed (Fig. 4). This absence of amino acid effect is in line with the weak modification of calcite growth rate by pentaglycine in bulk experiments in this concentration range [21], a common characteristic of peptides [37]. This absence of modification may derive from the fact that pentaglycine does not occlude within the growing calcite, or from the fact that the change of calcite rigidity due to its occlusion is negligible, as in the case of aspartate [38].

Even though the mechanisms of modification of calcite mechanical properties by incorporated amino acids has progressed lately [19], the interpretation of the way pentaglycine molecules mitigate the action of stress in the high force regime is delicate. We propose that the binding of pentaglycine to the surface carbonate groups [21] prevents their rotation and thus, despite its small concentration, impedes the structure change of the crystal.

We have shown that a stress imposed to a growing calcite crystal, an unavoidable step in the formation of a cohesive material, as much limestone as shells, has two visible effects: kinetically it slows down noticeably the mineral growth, and structurally it changes its crystalline lattice, these two feature having a broad potential impact on the final material properties. Furthermore, the presence of a prevalent amino acid in the solution, has no significant repercussion on the kinetics, but a huge influence on the structure, canceling the pressure-induced phase transition of calcite, thus selecting the growing polymorph. This process should depend on the nature

of amino acid[60] concentration, and mineral type, but adds to the collection of mechanisms by which organics tune biomineralization.

———————

* Electronic address: jean.colombani@univ-lyon1.fr

[1] S. L. Stipp and M. F. Hochella, Geochim. Cosmochim. Acta **55**, 1723 (1991).

[2] M. Andersson, S. Dobberschtz, K. Sand, D. Tobler, J. D. Yoreo, and S. Stipp, Angew. Chem. **128**, 1 (2016).

[3] A. E. S. Van Driessche, L. G. Benning, J. D. Rodriguez-Blanco, M. Ossorio, P. Bots, and J. M. García-Ruiz, Science **336**, 69 (2012).

[4] C. Perdikouri, C. V. Putnis, A. Kasioptas, and A. Putnis, Crystal Growth Des. **9**, 4344 (2009).

[5] J. N. Bracco, A. G. Stack, , and C. I. Steefel, Environ. Sci. Technol. **47**, 7555 (2013).

[6] M. Wothers, D. D. Tommaso, Z. Du, and N. de Leeuw, CrystEngComm **15**, 5506 (2013).

[7] M. de la Pierre, P. Raiteri, A. Stack, and J. Gale, Angew. Chem. Int. Ed. **56**, 8464 (2017).

[8] F. Bouville, E. Maire, S. Meille, B. V. de Moortèle, A. Stevenson, and S. Deville, Nature Mat. **13**, 508 (2014).

[9] K. Larsen, K. Bechgaard, and S. L. S. Stipp, Geochim. Cosmochim. Acta **74**, 2099 (2010).

[10] Vitruvius, *The ten books of architecture English - translation by M. H. Morgan* (Dover, New York, 1914).

[11] Y.-W. Wang, H. K. Christenson, and F. C. Meldrum, Adv. Funct. Mater. **23**, 5615 (2013).

[12] F. Kohler, L. Gagliardi, O. Pierre-Louis, and D. Dysthe, Phys. Rev. Lett. **121**, 096101 (2018).

[13] M. Merlini, M. Hanfland, and W. A. Crichton, Earth Planet. Sci. Lett. **333-334**, 265 (2012).

[14] Y. Diao and R. Espinoza-Marzal, Proc. Natl. Acad. Sci. USA **113**, 12047 (2016).

[15] S. Weiner and L. Addadi, Annu Rev. Mater. Res. **41**, 21 (2011).

[16] E. Weber and B. Pokroy, CrystEngComm **17**, 5873 (2015).

[17] C. Damle, A. Kumar, S. Sainkar, M. Bhagawat, and M. Sastry, Langmuir **18**, 6075 (2002).

[18] J. Ihli, J. Clark, N. Kanwal, Y. Kim, M. Holden, R. Harder, C. Tang, S. Ashbrook, I. Robinson, and F. Meldrum, Chem. Sci. (2019).

[19] Y.-Y. Kim, J. D. Carloni, B. Demarchi, D. Sparks, D. G. Reid, M. E. Kunitake, C. C. Tang, M. J. Duer, C. L. Freeman, B. Pokroy, et al., Nature Mat. **15**, 903 (2016).

[20] PHREEQC interactive, version 3.4.0-12927, a computer program for speciation, batch-reaction, one-dimensional transport and inverse geochemical calculations. U.S. Geological Survey, https://water.usgs.gov/software/.

[21] G. Montanari, L. Lakshtanov, D. Tobler, K. Dideriksen, K. N. Dalby, N. Bovet, and S. Stipp, Crystal Growth Des. **16**, 4813 (2016).

[22] C. Fan and H. Teng, Chem. Geol. **245**, 242 (2007).

[23] B. Zareeipolgardani, A. Piednoir, and J. Colombani, Journal of Physical Chemistry C **121**, 9325 (2017).

[24] H. H. Teng, , P. M. Dove, and J. J. De Yoreo, Geochim. Cosmochim. Acta **64**, 2255 (2000).

[25] J. Clark, J. Ihli, A. Schenk, Y. Kim, A. Kulak, J. Campbell, G. Nisbet, F. Meldrum, and I. Robinson, Nature Mater. **14**, 780 (2015).

[26] P. M. Dove and M. F. Hochella, Geochim. Cosmochim. Acta **57**, 705 (1993).

[27] H. H. Teng, P. M. Dove, C. A. Orme, and J. J. De Yoreo, Science **282**, 724 (1998).

[28] A. Stack and M. Grantham, Crystal Growth Des. **10**, 1409 (2010).

[29] M. Hong and H. H. Teng, Geochim. Cosmochim. Acta **141**, 228 (2014).

[30] K. K. Sand, D. J. Tobler, S. Dobberschütz, K. K. Larsen, E. Makovicky, M. P. Andersson, M. Wolthers, and S. L. S. Stipp, Crystal Growth Des. **16**, 3602 (2016).

[31] J. D. Yoreo, L. Zepeda-Ruiz, R. Friddle, S. Qiu, L. E. Wasylenki, A. Chernov, G. Gilmer, and P. Dove, Crystal Growth Des. **9**, 5135 (2009).

[32] J. Chung, I. Granja, M. Taylor, G. Mpourmpakis, J. Asplin, and J. Rimer, Nature **536**, 446 (2016).

[33] E. Pachon-Rodriguez, A. Piednoir, and J. Colombani, Phys. Rev. Lett. **107**, 146102 (2011).

[34] K. Suito, J. Namba, T. Horikawa, Y. Taniguchi, N. Sakurai, M. Kobayashi, A. Onodera, O. Shimomura, and T. Kikegawa, Am. Mineral. **86**, 997 (2001).

[35] S. Stipp, C. Eggleston, and B. Nielsen, Geochim. Cosmochim. Acta **58**, 3023 (1994).

[36] N. Park, M. Kim, S. Langford, and J. Dickinson, J. Applied Phys. **80**, 2680 (1996).

[37] S. Elhadj, J. J. De Yoreo, J. R. Hoyer, and P. M. Dove, Proc. Natl. Acad. Sci. USA **103**, 19237 (2006).

[38] A. Côté, R. Darkins, and D. Dufy, PCCP **17**, 20178 (2015).

[39] We would like to stress on the fact that the measurements between 150 and 250 nN are delicate, leading to unstable values. Therefore we do not claim that velocities in this range are representative of calcite II, the existence range of this polymorph being particularly tiny.

Chapter 4

Microscale influence of pH on calcite dissolution
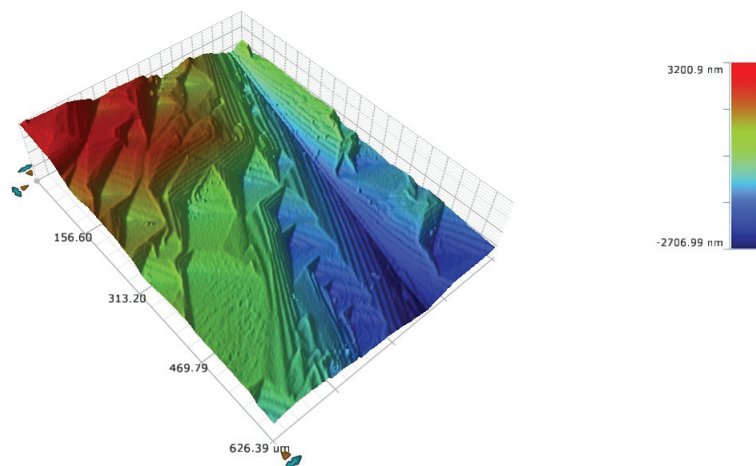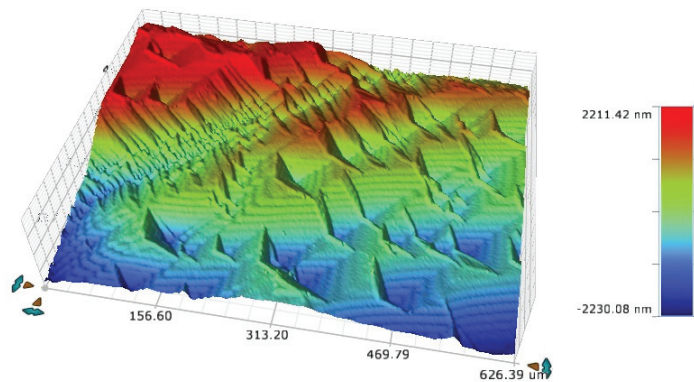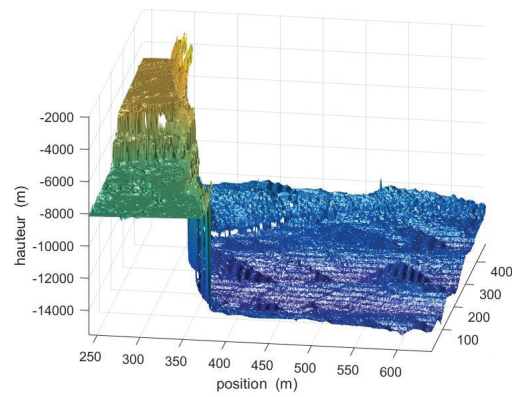
4.1 Preface

The reaction kinetics of minerals exerts fundamental constraints on their stability and fate in the natural systems and in their industrial applications. A comprehensive dissolution rate that integrates individual surface reactions into an overall rate is a long standing problem. Before the advent of surface microscopic techniques like atomic force microscopy (AFM) and vertical scanning interferometry (VSI), distinguishing potential sources of variation in dissolution rates was not conceivable [87].

The recently widespread use of these instruments has yielded a detailed understanding of the interaction of minerals with their ambient solution [105]. The surface microscopic techniques have greatly expanded the understanding of reaction kinetics for a diverse range of carbonates, silicates, and other important phases. These means measure the surface elevation and topography at microscopic scales. They are particularly attractive because they permit direct monitoring of localized changes at the surface, including the development and growth of etch pits. Consequently, such methods reveal the complexity of dissolution rates even for seemingly simple minerals, such as calcite [12]. However, despite the overall simplicity of calcite structure, these studies have also revealed complexity in step movement and morphology. This complexity indicates that the general morphology of the surface is a sensitive reflector, not only of its interactions with the solution, but with itself as well. Variations in morphology are tied to heterogeneities in rate. These phenomena have been termed intrinsic variations. The intrinsic variation is tied to crystallographic and microstructural factors. By AFM [52, 29, 69, 93] and VSI [73, 6, 37, 22, 12] we are able directly to observe the *in situ mineral surface*.

Early in situ AFM work determined the crystallographic control of the velocity of atomic scale steps in pure solutions. However AFM in situ does not provide details of the dynamics of surface features in minerals over large areas of interest, due to scanning range limitations, and cantilever constraints limit also the measurable depths. These limits make the study of variation in dissolution rates ambiguous. This ambiguity is originating from the probability of how local step velocities and spacing may be influenced by events or features outside the AFM immediate field of view.

VSI, with a significantly larger field of view in comparison with AFM, supplies rapid and accurate rate measurements, when acquisition of data is made in conjunction with a masked or coated surface portion, used as a reference surface. Although it is an indirect way, through the quantification of spatially resolved surface retreat or advance, it allows for quantitative analysis of heterogeneous topography evolution. The resulting data provide information about spatial distribution of material flux during reactions. An example of the relationship between the reaction rate and its distribution over the mineral surface is the dissolution stepwave model introduced by Lasaga & Luttge [65]. The authors illustrated the important role of screw dislocations that open first into etch pits and are subsequently responsible for the generation of most steps on the crystal surface. This mechanism ultimately controls the dissolution of the entire crystal surface through the generation of stepwaves. The heterogeneous distribution of reactive sites yields a correspondingly heterogeneous distribution of surface energy. Fischer et al. [37] concluded that the use of a single term, *mean* rate or rate *constant*, is unsubstantiated. Thus prediction of reactivity based on laboratory measurements are not directly applicable to natural settings without considering probabilistic approach. A probabilistic approach must be incorporated with both the variation of surface energy as a intrinsic variation, as well as constraints in this variation owing to the defects of the bulk material. The observed

intrinsic variability in crystalline materials is manifested as an inherent variability in dissolution rates from point to point across a given surface, which can be characterized statistically as a rate distribution or spectrum. The rate spectrum concept applies to identify both etch pits and atomic steps as the main contributors to the overall dissolution rate [32].

Luttge [72] put forward the assumption that the two different reaction mechanisms exist to dissolve a given crystal surface with two different rates ($rate(I)$ and $rate(II)$). At near-equilibrium conditions mechanism (I) operates alone and step motion is the leading. If the dissolution system deviates force of further from equilibrium, by increasing the undersaturation, the critical ΔG value (ΔG_{crit}, i.e., a critical undersaturation) will be reached. At this point etch pits can open spontaneously and the stepwave mechanism becomes active. The result is a significantly increased dissolution rate. After steady state is re-established the new dissolution rate will be given by the following equation:

$$Rate = rate(I) + rate(II) \tag{4.1}$$

The opening and creating of etch pits by screw dislocations serves as the "transition" between the two rate-controlling mechanisms. It must be considered that all measured intermediate rates are in fact non-steady-state rates. The result is an apparent transition between $rate(I)$ and the new rate that is the sum of $rate(I) + rate(II)$ because there is no purpose to assume that mechanism for $rate(I)$ shuts down when pits are opening up. This view of the dissolution process has constituted a major step forward, because it permits to understand why the rate depends on the sample history. Indeed, depending on whether etch pits have been opened or not during a previous phase of the sample history, the dissolution rate may appear different for the same saturation index.

4.2   Aim of the study

In this part of my thesis I choose to study calcite due to its widespread presence in the geological setting and industrial application. The calcite properties and importance have been explained in the first chapter (see section 1.3).

Calcium carbonate is a major constituent of deep-sea sediments, and its dissolution and burial are important parts of the global carbon cycle. The distribution of calcite in deep sea sediments is controlled by the kinetics of dissolution competing with the rate of burial. The ultimate sink for anthropogenic CO_2 is thought to be the uptake into the oceans and neutralization by growth of biogenic calcite. [107]. One of the consequences of massive CO_2 uptake in the ocean is ocean acidification, therefore absorbed anthropogenic CO_2 is lowering ocean surface water pH. Anthropogenic ocean acidification perturbs the oceanic $CaCO_3$ cycle, impeding biogenic calcification and promoting its dissolution. Consequently ocean acidification would have huge environmental impact.

The overall goal of this research is to try to investigate the calcite surface dissolution at far from equilibrium condition at varied in a wide pH range. I have focused to understand which predominant mechanism controls surface dissolution at different pH. The relative abundance of negatively and positively charged surface sites depends on the relative concentration of H^+ and OH^- in solution. These ions behave as potential determining ions for the surface. Consequently, the net surface charge depends on the solution pH [76].

One of the objective of this study is to track calcite crystal surface morphology over several time intervals in a broad pH range to investigate the possibility that rate spectra may have an intrinsic time dependence. Time-dependent rate spectra, even at constant pH, would be expected if the density of kink sites were to change with time and opening the screw dislocations were time-dependent. This could happen if the density and type of crystalline defects were to vary with depth beneath the initial surface. If a significant time-dependence of the height digging were to be observed, it would mean that detailed characterization of the dissolution of a given material requires three considerations: one of these points is related to the surface, one of them is related to the height and one specifies the time. Furthermore, time-dependent rates would imply that the average dissolution rate has no intrinsic value and changes with sampling time.

Several studies have investigated processes governing biomineralization by examining calcite growth and dissolution in the presence of proteins, amino acids, and other organic compounds [70, 51]. Previous studies suggested that the geometry and chemistry of functional groups that characterize the charged amino acids have highly specialized interactions with specific surface site types [77]. My observation (chapter 3) suggests that pentaglycine, as an amino acid, influences the free calcite growth and changes the calcite growth behaviour in presence of external pressure. These observations supported the idea that the new forms of calcite are stabilized by the molecular recognition of amino acid functional groups by specific surface sites. Regarding these observations, for the final aim of this study, I propose that the dissolution studies offer as an alternative means of determining the crystal forms that develop during biomineralizing processes and a more direct means of identifying those surface sites involved. I choose glycine as a zwitterionic amino acid that shows different charges at different pH (see section 3.1.2) to study in detail the "recognition" of amino acid by the surface.

4.3 Material and methods

At the beginning of each experiment, a calcite rod of section measuring roughly 1.5×1 cm^2 (Iceland spar, Mexico, purchased from Treasure Mountain mining) was cleaved in air by gently scratching a scalpel along the $\{10\bar{1}4\}$ cleavage plane to achieve a 1 to 2 mm high calcite crystal with a fresh surface. Inductively coupled plasma optical emission spectroscopy (ICP-OES) of an acid-digested crystal and SEM-EDX indicated <0.1% magnesium by mass and detected no significant concentration of any other common impurity in calcite. Details are presented in appendix A.2. Measurements of absolute dissolution rate require the availability of a reference plane that does not change in elevation during the experiment. This was accomplished by physical vapor deposition of 5 nm of chromium onto a portion of the surface. Chromium was used because it was observed to provide better adhesion to the calcite then the surface coated by 50 nm of gold.

The reactant solution used here was ultra pure water (Millipore, resistivity >18.2 MΩ) and, for adjusting pH, 0.1 M NaOH and 0.1 M HCl were utilized. The solutions used here were identical in composition, with a saturation index equal to zero. The investigated pH are 3, 4, 5, 6, 7, 8, 9 and 10. After preparation, this solution was sparged with N$_2$ in order to attain equilibrium with respect to atmospheric pCO$_2$ and a stable pH. Constant sparging was sufficient to agitate the solution over the course of the experiment and produced a pH stable over 5 h. Solution pH was monitored regularly. In solution with presence of glycine, first 0.1 M of glycine was

transferred to 1 a liter flask, then the volume was adjusted by adding ultra pure water (Millipore, resistivity >18.2 MΩ), subsequently its pH was adjusted by 0.1 NaOH or 0.1 M HCl to the desired pH. Glycine did not change the pH. This solution contained essentially no calcium and was highly under-saturated with respect to calcite, so the saturation index was considered as 0. The input solution temperature was maintained at 22°C.

The sample was mounted in the fluid cell and the solution introduced to the cell open surface. The solution was flown to the cell by a peristaltic pump at a volumetric flow rate of $\approx$ 0.6 liter per hour. The sample was reacted 4 hours at a certain pH and the surface evaluations were done every hour. For surface analyzing the vertical scanning interferometry (VSI, from Bruker) with a 10$\times$ objective was used. The field of view was detected by VSI before introducing the solution. In every hour interval the sample was taken out from solution and dried by filtered laboratory air. Then by mechanical tools it was fixed on VSI to collect topographic data. Consequently measurements are obtained over the same field of view and the resulting sequence can be used to evaluate the overall morphological changes in surface topography. In addition, I subtracted various maps to produce a corresponding difference map, showing the spatial distribution of dissolution flux. The dissolution rate R computed by the methodology presented here refers to the surface normal dissolution rate, defined as:

$$R = \frac{1}{V_m}\frac{\Delta h}{\Delta t} = \frac{v_s}{V_m} \tag{4.2}$$

with:

- V_m is the molar volume, which for calcite is 3.693×10^{-5} m^3 mol^{-1}.

- v_s is the surface normal velocity, which refers to the change in height over time $\frac{\Delta h}{\Delta t}$.

The surface normal dissolution rates are computed in each experiment independently on different portions of the calcite surface. The gold masked region, which provided a constant reference height, was not included in any detected view.

4.4   Results and discussion

4.4.1   Evolution of surface topography and dissolution rate maps

The dissolution maps after 1 and 4 hours for pH 3 and 4 are shown in figure 4.1. Different surface morphologies were observed. These differences expressed different mechanisms of dissolution at pH 3 and 4. Different calcite crystal dissolution morphologies were explained in chapter 1.3.3.

At pH 3 in the first hour of reaction the surface height retreat was $\approx$ 1µm. The surface shows several deep etch pits and mega steps. This surface after 4 hours retreated of $\approx$ 35 µm and the surface shows mostly mega steps.

At pH 4 in the first hour of reaction the surface height retreat was $\approx$ 400 nm and shallow etch pits, terraces and steps were observed. After 4 hours of reaction the surface height retreated of $\approx$ 8 µm. The surface shows deep etch pits, few terraces and mega steps.

a)

b)

c)

d)

e)

f)

g)

h)
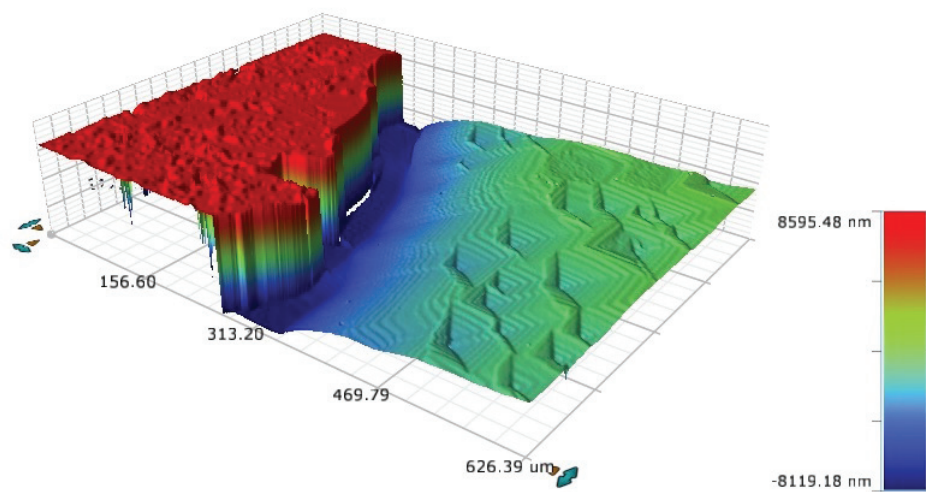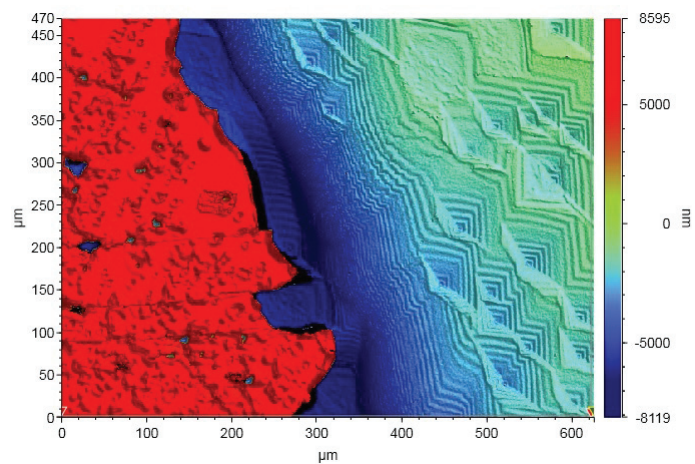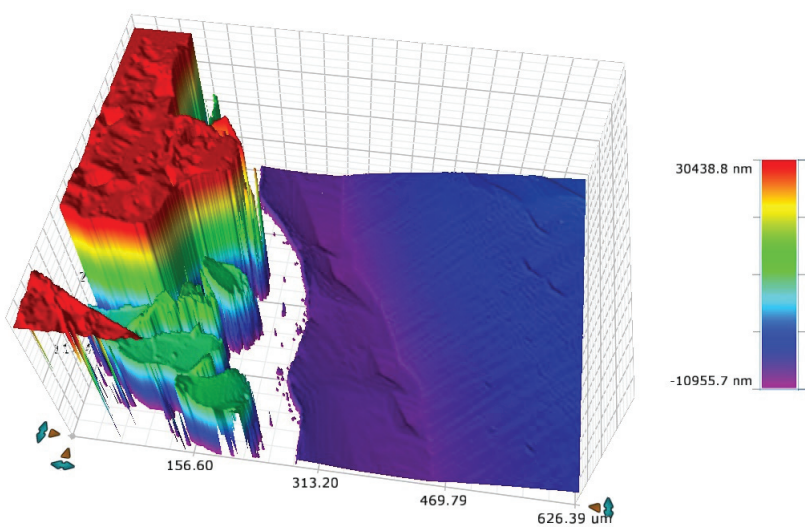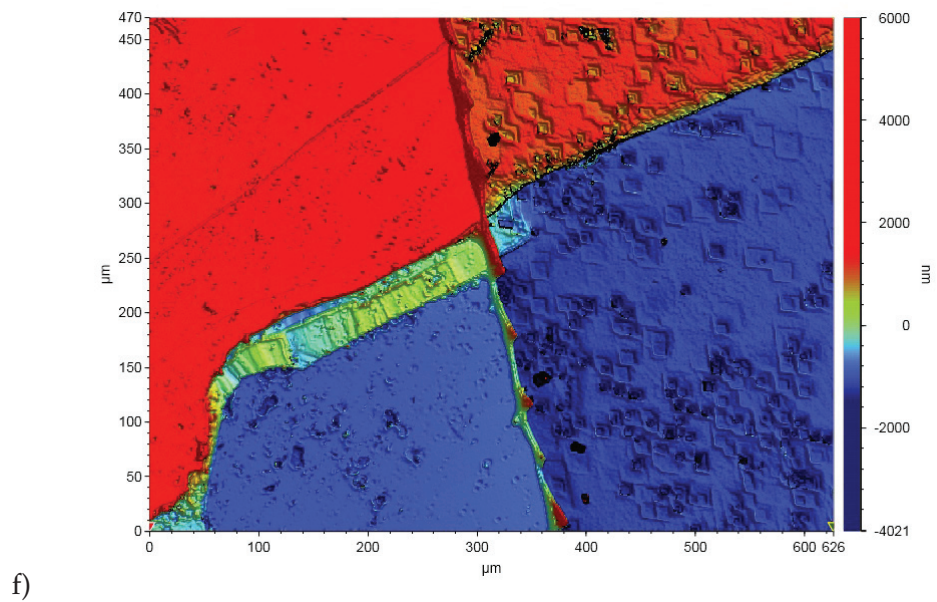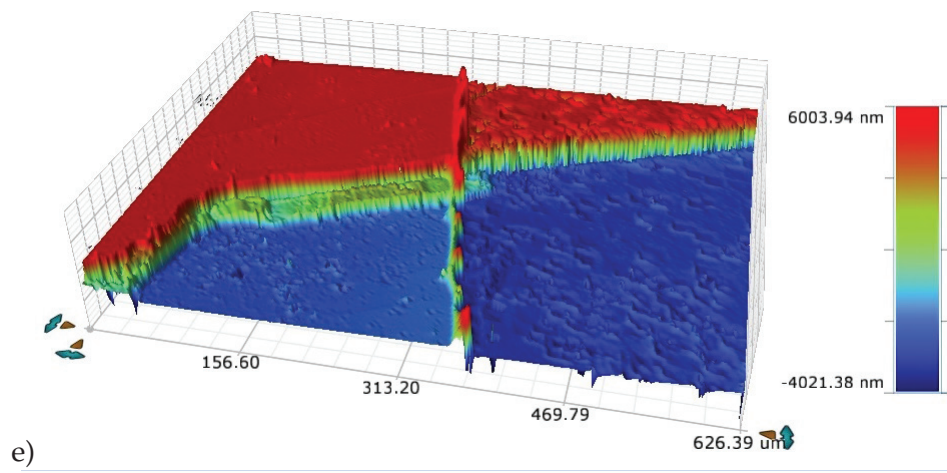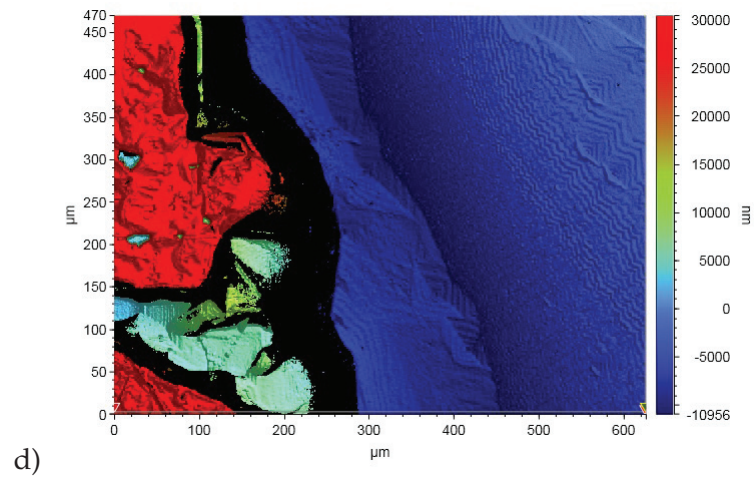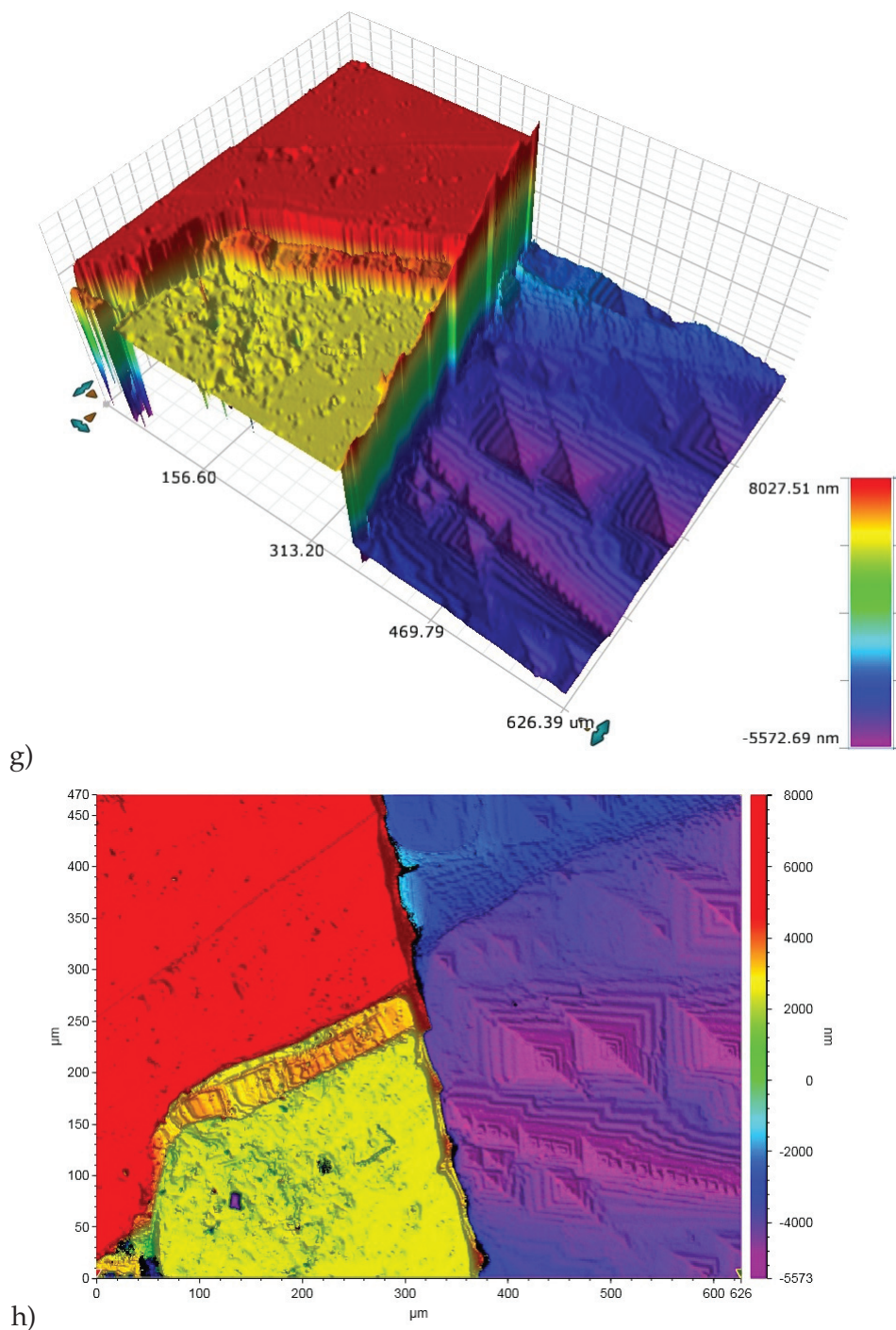
FIGURE 4.1: Variability in surface morphology after dissolution at pH 3 and pH 4. Morphological features include: a) Three-dimensional VSI view of the calcite crystal surface after 1 hour of reaction at pH 3. b) VSI image of the calcite crystal surface after 1 hour of reaction at pH 3. c) Three-dimensional VSI view of the calcite crystal surface after 4 hours of reaction at pH3. d) VSI image of the calcite crystal surface after 4 hours of reaction at pH 3. e) Three-dimensional VSI view of the calcite crystal surface after 1 hour of reaction at pH4. f) VSI image of the calcite crystal surface after 1 hour of reaction at pH 4. g) Three-dimensional VSI view of the calcite crystal surface after 4 hours of reaction at pH4. h) VSI image of the calcite crystal surface after 4 hours of reaction at pH 4. Red colour is masked area.

The dissolution maps after 1 and 4 hours for pH 6 and 10 are shown in figure 4.2. At pH 6 in the first hour of reaction the surface height retreat was $\approx$ 100 nm. After 4 hours of reaction the surface height retreated of $\approx$ 600 nm. The surface shows deep etch pits, terraces and steps. At pH 10 in the first hour of reaction the surface height retreat was $\approx$ 100 nm and opening of etch pits, terraces and steps were observed. After 4 hours of reaction the surface height retreated of $\approx$ 600 nm. The surface shows shallow etch pits, terraces and steps.

a)

b)

c)

d)

e)

f)
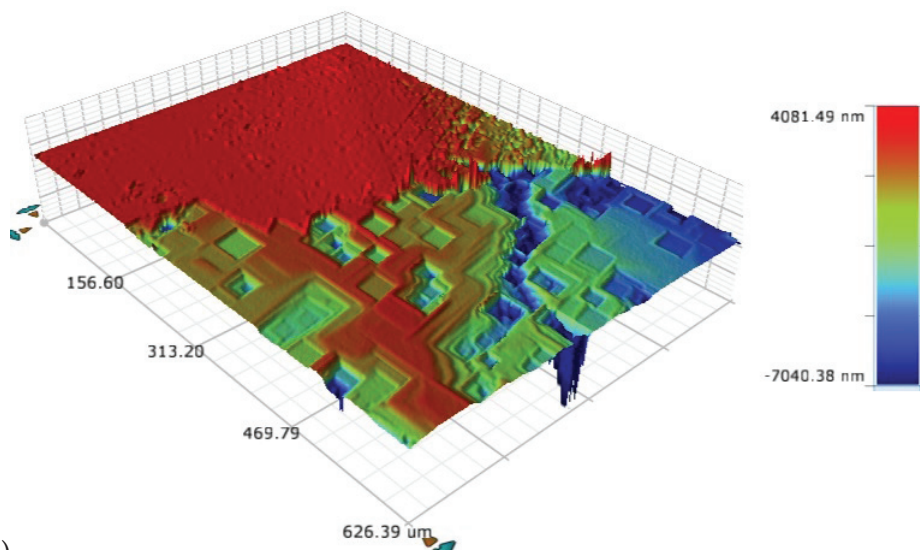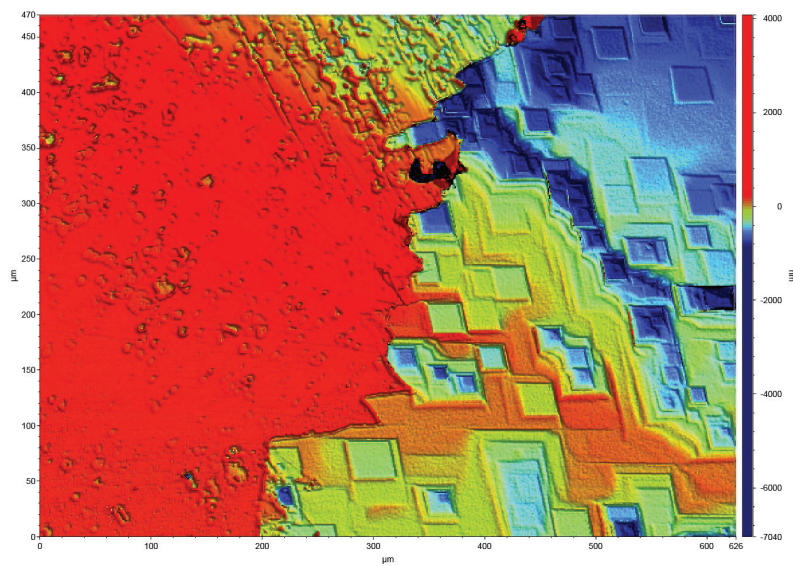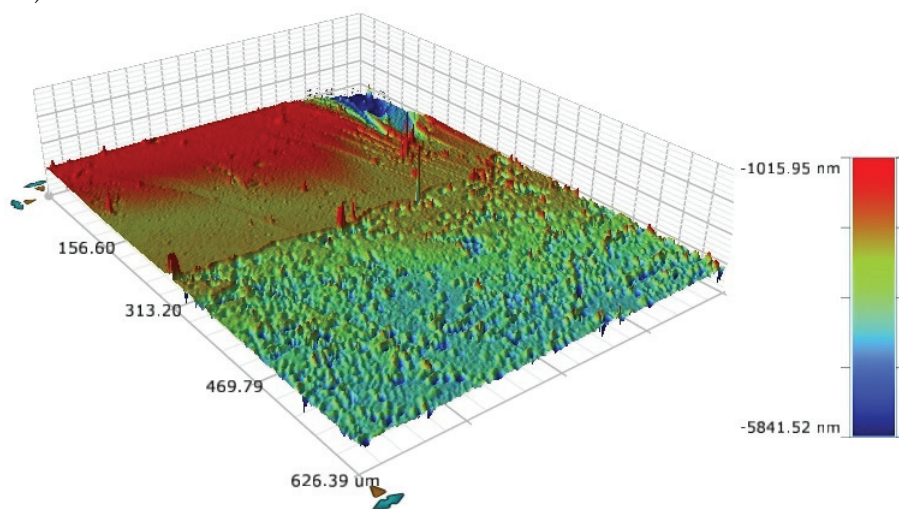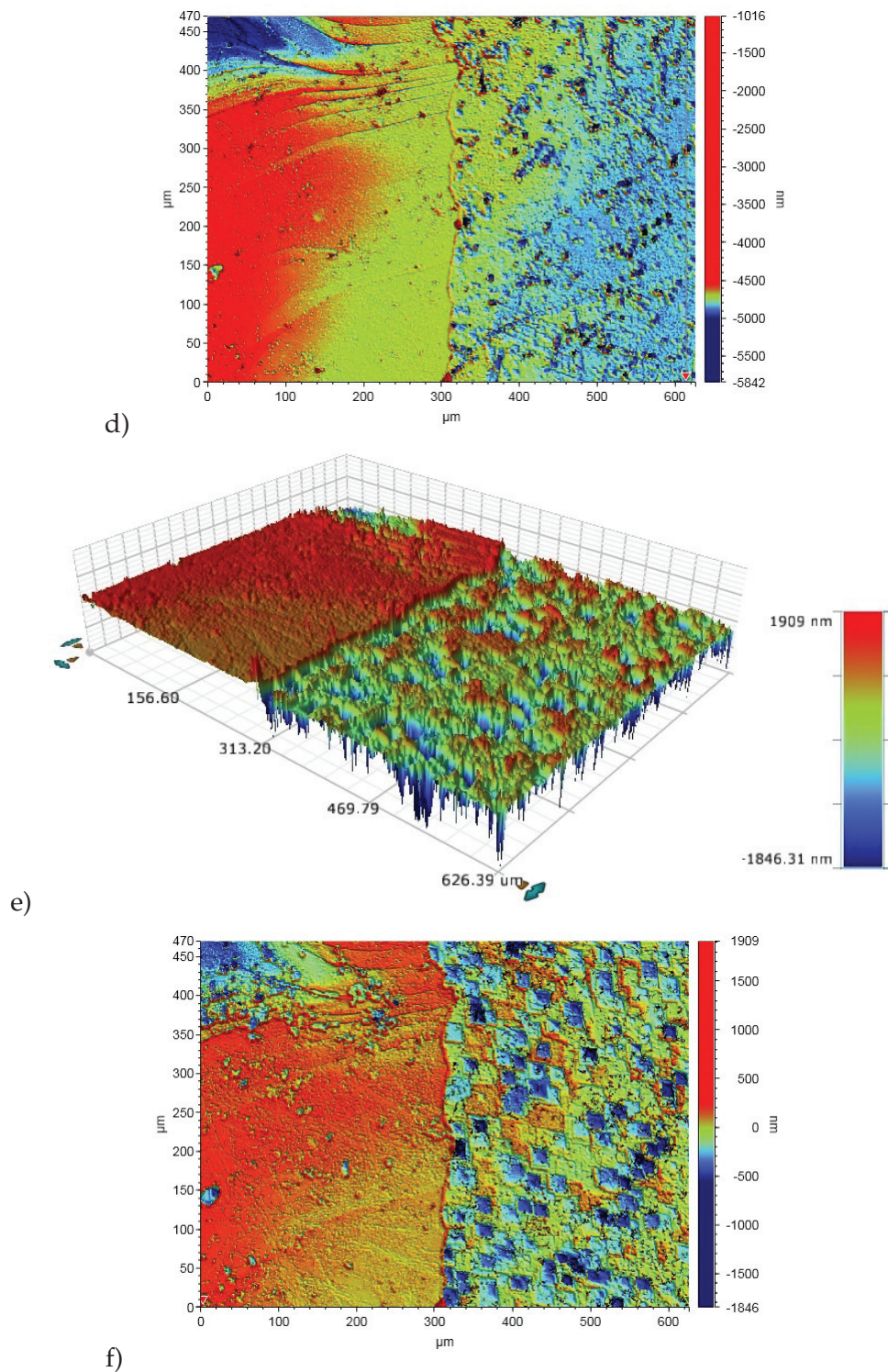
FIGURE 4.2: Variability in surface morphology after dissolution at pH 6 and pH 10. Morphological features include: a) Three-dimensional VSI view of the calcite crystal surface after 4 hours of reaction at pH6. b) VSI image of the calcite crystal surface after 4 hours of reaction at pH 6. c)Three-dimensional VSI view of the calcite crystal surface after 1 hour of reaction at pH10. d) VSI image of the calcite crystal surface after 1 hour of reaction at pH 10. e) Three-dimensional VSI view of the calcite crystal surface after 4 hours of reaction at pH 10. f) VSI image of the calcite crystal surface after 4 hours of reaction at pH 10. Red colour is masked area.

4.4.2 Height retreat over time and rate spectra

For the calculation of the dissolution rate for every pH, first the rate of changing of the average surface height was computed for every pH. Plots of average surface height versus time for different pH (3, 4, 6 and 10) show different trends. Linear and non linear trends were observed, depending on the pH (see figure 4.3). The frequency distribution of rates measured at different pH (3, 4, 6 and 10) are shown in figure 4.3.

The average surface height versus time for pH 3 displayed a linear trend. The peak rate value for the frequency distribution of rates measured at pH is $3 \approx 5.8 \times 10^{-5}$ mol m^{-2} s^{-2}.

The average surface height versus time for pH 4 displayed a non-linear trend. The retreating surface height accelerated after 2 hours. The dug depth for the first 2 hours was 1µm, then it increased to 7µm for the last 2 hours. The peak rate values for the frequency distribution of rates measured at pH 4 is $\approx 1.2 \times 10^{-5}$ mol m^{-2} s^{-2}.

The average surface height versus time for pH 6 showed a linear digging trend and ≈ 600 nm digging over 4 hours. The peak rate value for the frequency distribution of rates measured at pH 6 is $\approx 1.1 \times 10^{-6}$ mol m^{-2} s^{-2}.

The average surface height versus time for pH 10 displayed a linear trend and ≈ 600 nm digging over 4 hours. The peak rate value for the frequency distribution of rates measured at pH 10 is $\approx 1 \times 10^{-6}$ mol m^{-2} s^{-2}.

a)

b)

c)

d)
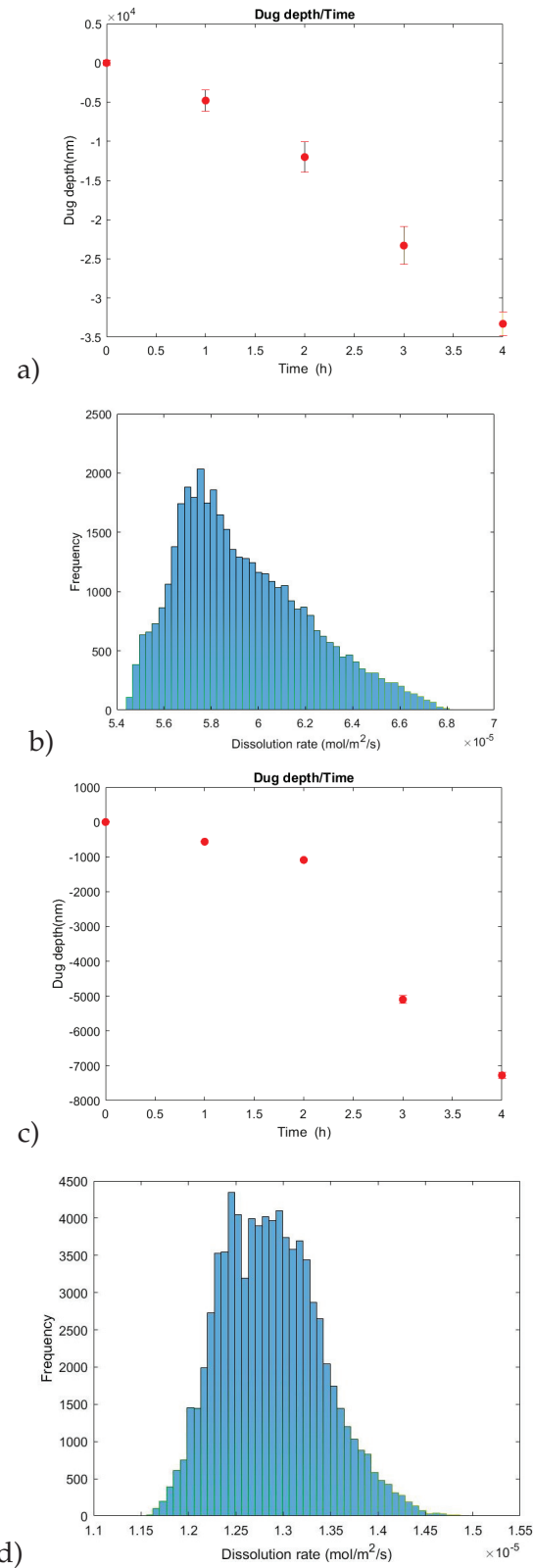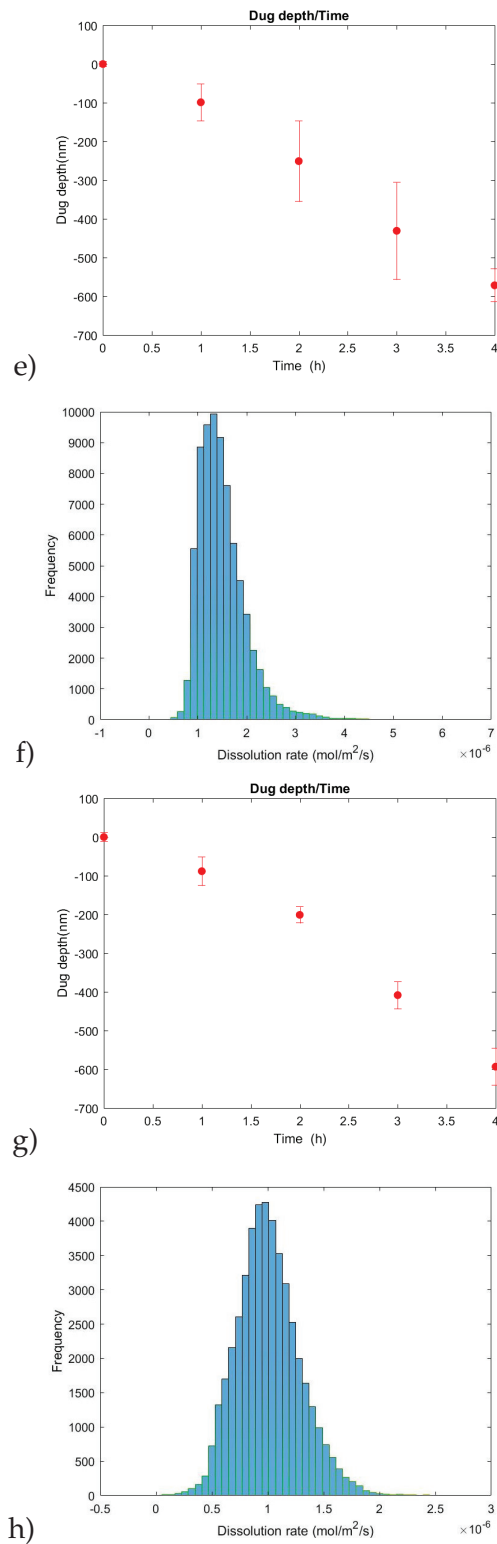
FIGURE 4.3: Average surface height over time for unmasked surfaces and surface normal dissolution rate spectra at different pH. a) Average surface height for pH 3. b) Surface normal dissolution rate spectrum for pH 3. c) Average surface height for pH 4. d) Surface normal dissolution rate spectrum for pH 4. e) Average surface height for pH 6. f) Surface normal dissolution rate spectrum for pH 6. g) Average surface height for pH 10. h) Surface normal dissolution rate spectrum for pH 10.

These observed nonlinearity and linearity of digging height evolution proves that the surface normal velocity is not constant at different depths. It changes abruptly over 1 μm dug depth. If the dissolution during the first hour is fast enough to dig more than 1 μm —case of pH 3— this acceleration is not observable because it occurs before the first measurement. If the dissolution for 4 hours is not enough to dig 1 μm, this increasing is not observable. Consequently in both cases the surface height versus time showed a linear trend.

Thanks to the VSI height measurements, the dissolution rate can be computed in each pixel of the image of a given area on the surface. From these local dissolution rates, a histogram of the distribution of the rates can be constructed, providing a statistical sampling of the behaviour of this portion of the surface. The analysis of this histogram provides information about the frequency of given contributors to the reaction for given conditions. The shape of the function (single peak versus several discrete peaks) is relevant to analyze surface energy range and distribution. Secondly the peak heights provide information about the frequency of distinct energetic sites [38].
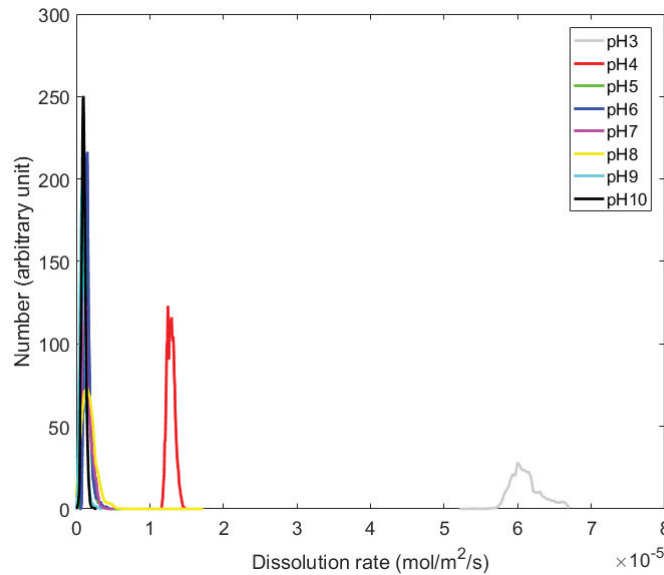

FIGURE 4.4: Surface normal dissolution rate spectra at different pH

The frequency distribution of rates measured at different pH are presented in figures 4.3 and 4.4. Three overall calculated rate ranges for different pH were observed. For the pH range of 5, 6, 7, 8, 9 and 10 the dissolution rate is less than 1.3×10^{-6} mol m^{-2} s^{-2}, for pH 4, it is $\approx 1.2 \times 10^{-5}$ mol m^{-2} s^{-2} and for pH 3, it is larger than 5.8×10^{-6} mol m^{-2} s^{-2}. The lowest rates corresponded to the opening and creating of etch pits (*rateI* in equation 4.1), and characterize the neutral and alkaline regimes. The highest rates correspond to the retreat from highly reactive sites like deep etch pits and mega steps movement (*RateI* + *RateII* in equation 4.1), and characterize the acidic regime.

Negative dissolution rates, i.e., net growth, in our experiment was not observed. This phenomenon was reported in other dissolution studies [12].
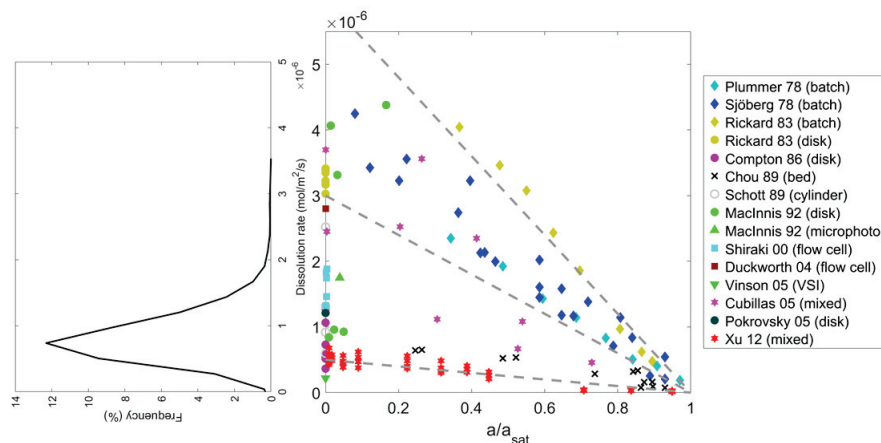
FIGURE 4.5: Dissolution rates reported in the literature for the calcite
surface compared to
this research.

In figure 4.5, the reported data for calcite dissolution measured in different ways like batch, rotating disk, VSI . . . in comparison of this research were plotted. The peak of dissolution this work is similar to the same condition (freshly cleaved calcite) as in the works reported in the literature. This lower amount of dissolution in freshly cleaved calcite is due to lower energy surface and less surface defects in comparison to polished surface and small grains.
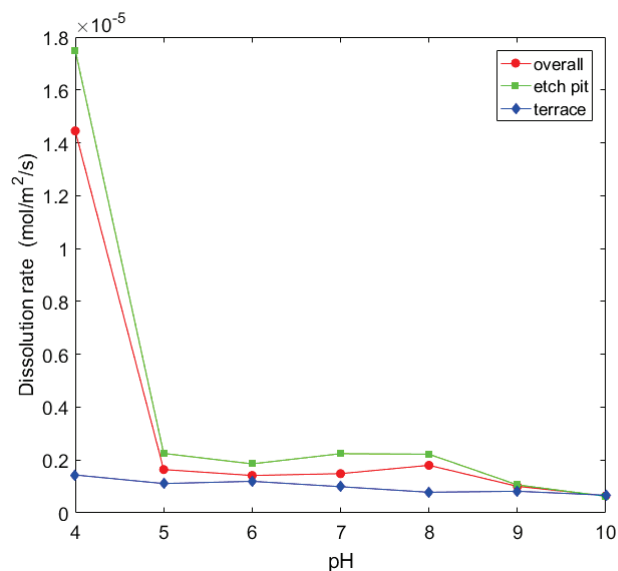
FIGURE 4.6: Average dissolution rate, for the overall surface, for etch
pits, and for terraces, at different pH.

Evolution of surface topography presented in the section 4.4.1 showed different surface morphologies depending on time and pH. In sum the propagating mega steps were the dominant morphology changes for pH 3,growing deep etch pits and terraces were major morphology changes for pH 4 and for pH 5, 6, 7, 8, 9 and 10

etch similarly etch pits and terraces were observed. Three dissolution rates were then calculated for every pH and plotted: a dissolution rates concerning etch pit,one corresponding to terraces and a third one for the overall dissolution (see figure 4.6). At pH 4 the overall dissolution rate is mainly controlled by etch pit motion and terrace movement showed a minor role on the dissolution. On the contrary the etch pit dissolution rate shows an equal dissolution rate as terrace dissolution rate for all other pH. This clearly shows that a major change of reaction is occuring at the surface when the dominant attacking specie switch from H_2O to H^+.

4.4.3   Effect of glycine on dissolution rates and surface morphology

To better understand the dissolution of the calcite and also bio-mineralisation, glycine as additive was used in this study. Glycine is a widespread amino acid and it is zwitterionic. Glycine properties were explained in chapter 3 (section 3.1.2). The reacted calcite surface in presence of glycine showed shallow etch pits and terraces.
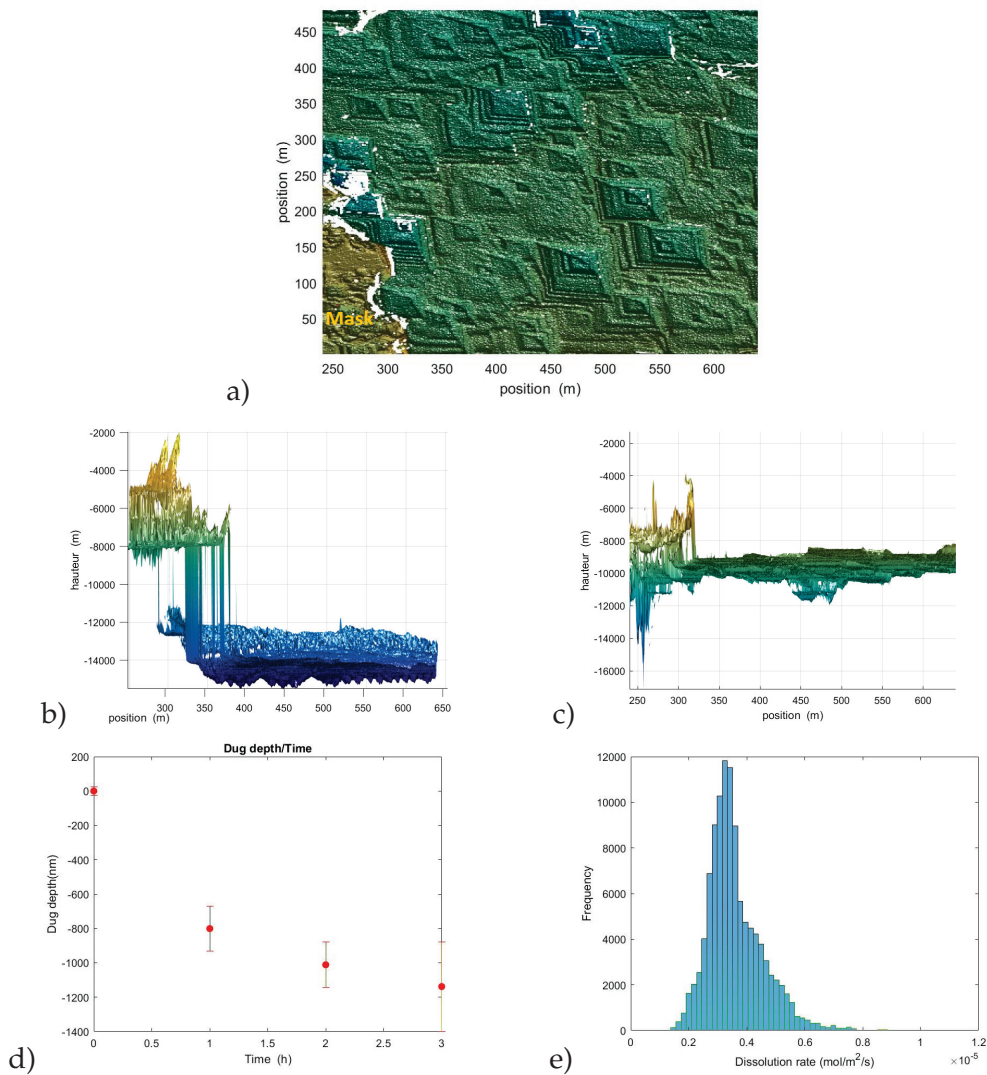
FIGURE 4.7: a) Surface morphology after dissolution at pH 4 and 0.1 M glycine. b) Three-dimensional view of the calcite crystal surface imaged in absence of glycine at pH 4. c) Three-dimensional view of the calcite crystal surface imaged in presence of glycine at pH 4. c) Average surface height for pH 4 and 0.1 M glycine. d) Surface normal dissolution rate spectra for pH 4 and 0.1 M glycine.

The average surface height versus time showed a non linear trend. In the first hour of dissolution, the surface height retreated of ≈ 700 nm, then the dissolution rate decreased dramatically. The last 3 hours the surface was dug of only ≈ 300 nm (see figure 4.7). The peak rate value for the frequency distribution of rates measured at pH was $6 \approx 1.8 \times 10^{-6}$ mol m^{-2} s^{-2}.
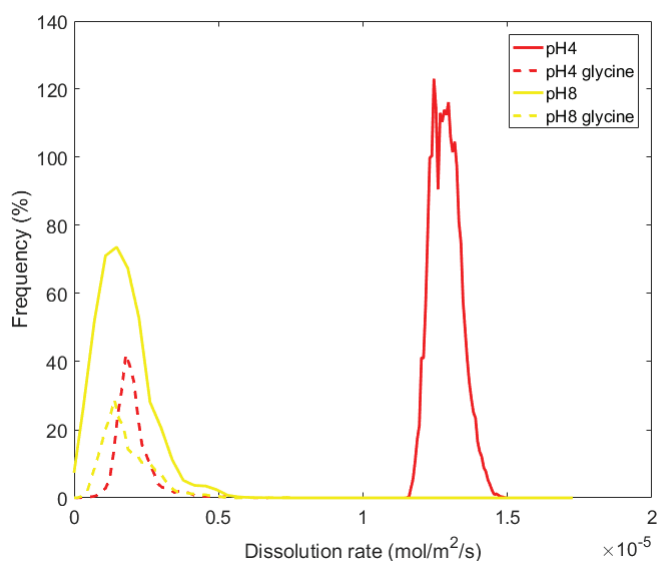
FIGURE 4.8: Surface normal dissolution rate spectra at pH 4 and 8 in
absence and presence of 0.1 M glycine.

The surface normal dissolution rate in presence of glycine at pH 4 is one order
of magnitude lower than without glycine. So at pH 4 the glycine hindered the dis-
solution rate significantly (see figure 4.8). On the contrary the dissolution at pH 8
with glycine showed the same dissolution rate as dissolution rate without glycine
(see figure 4.8). This varying influence of glycine between acidic and alkaline condi-
tions should be linked to the change of atomic mechanism of dissolution when the
attacking specie switches from H^+ to H_2O. Apparently, glycine acts exclusively on
the mechanism driving the acidic dissolution, but shows a negligible influence on
the mechanism at play during the alkaline dissolution. The origin of this difference
of behaviour should be searched in the noticeable modification of the surface charge
of calcite with pH [76].

Chapter 5

Conclusions and perspectives
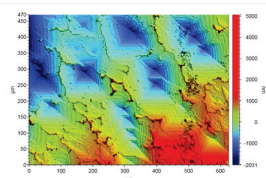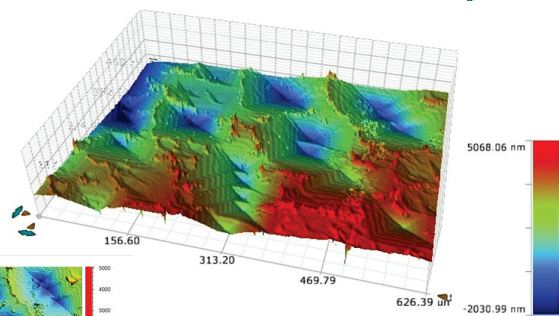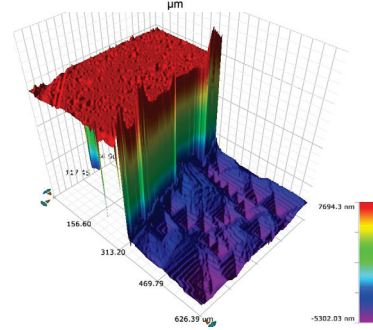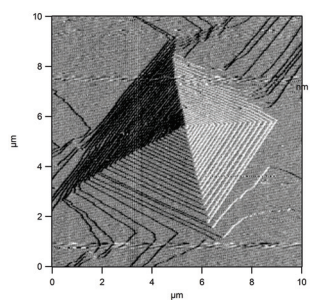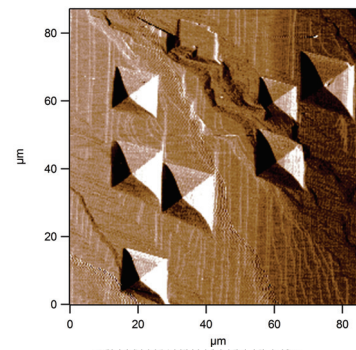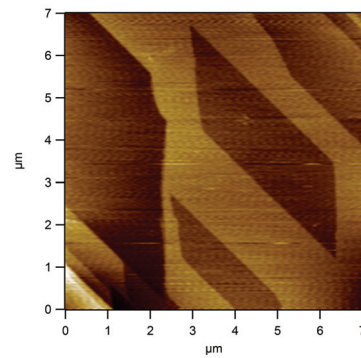
Any modern attempts to quantify complex natural systems require accurate rate laws for the mineral surface reactions including dissolution and growth [28, 73]. But these Mineral-fluid reactions depend on a variety of parameters. These parameters include the mineral structure, the surface defects, the reactive surface area, adsorbed ligands, pH, temperature, pressure, and ΔG of the mineral reaction. The majority of the kinetic data that can be used to determine the relation between the parameters listed above and the mineral reaction rate result from bulk fluid experiments [17]. On the simulation side, molecular simulations, like kinetic Monte Carlo, shed light on the possible mechanisms of material release from solid to liquid at the atomic scale [60]. Ab-initio methods have been used to analyze the relation between the bonding energetics of surface and solution atomic and molecular species and the rate constants, activation energies, and mechanisms of the mineral-fluid reactions [73]. An essential element needed in addition to the bulk experimental and the numerical methods is the direct observation of the dynamics of mineral surfaces in contact with fluids. Since two decays technological invention such as AFM and VSI have allowed researchers to focus on and quantify the relevant reaction processes at the crystal surface over a wide range of scale.

This thesis is an integrated study of calcite and gypsum reaction —dissolution and growth— conducted over multiple spatial and temporal-scales. It aims at being a step forward in establishing crossed-links between atomic and macro-scale.

By using AFM a microscopic dissolution rate can be inferred from the dynamics of molecular events, among which the atomic step migration are the dominant ones. Unfortunately, both hardly ever agree, even qualitatively. In the worst cases, orders of magnitude separate the two. Besides a general theory linking the kinetics at the two scales is still lacking. Therefore in the first part of thesis I addressed the gypsum dissolution with the objective to bridge these two scales. I used AFM not only to probe the dissolution of gypsum but also to apply a force while scanning the surface. I observed that the force applied by the AFM tip on the surface increased the solubility of the mineral and the rate of dissolution. With this in mind, working with a low non-disturbing applied force, I identified the the driving molecular mechanism of dissolution, namely the migration of rough steps, which has often been neglected in former studies. I was able to measure the rough step velocity and finally deduced a macroscopic dissolution rate from this atomic scale observation, in agreement with the bulk measurements. This result showed that a careful analysis of the topographic changes during the dissolution of a mineral may permit to deduce a reliable macroscopic dissolution rate.

In the second part of the thesis, I studied calcite, the most widespread crystalline form of calcium carbonate, because it is ubiquitous both in nature and in the industry. In particular the knowledge of its mechanisms of growth, both biogenic and inorganic, are of foremost importance, in the modelling of the carbon cycle, in the simulation of oil reservoirs, or in the design of better cements. One parameter, often present during calcite growth, has not been considered in most studies. When calcite grains grow from nuclei, they eventually enter into contact, and stresses develop at their interfaces, particularly if the material grows inside a mold (cement), or in geological setting and rock diagenesis. To address this issue, I used an atomic force microscope (AFM), both to apply a local stress on a growing calcite surface, and to image it. I found that the stress has a double influence: it slows down significantly the growth and more important it induces a change of the type of growing phase from calcite I to calcite II, as a transition phase, and finally to calcite III. I observed that calcite has an ability to recover and heal itself from the damages created by a high applied force. Calcite biomineralization proceeds in presence of organic

materials, among which amino acids are widespread. Therefore I investigated the influence of pentaglycine on the growth kinetics. This amino acid showed the striking ability to cancel or postpone the phase transition induced by the applied force and seemingly made the calcite harder.

In the third part of this work I worked in the larger than nm scale to study the dissolution mechanism of the calcite at different pH by VSI. The obtained results showed that the dissolution mechanisms changed with the pH. In fact, by using dissolution rate spectra, I observed that different mechanisms control dissolution at different pH. For pH 3 dissolution is mainly controlled by the motion of mega steps. The spreading of deep etch pits triggered the dissolution at pH 4. For the pH 5, 6, 7, 8, 9 and 10 the dissolution proceeded by a combination of shallow etch pits, step migration and terrace retreat. Respectively I observed a higher dissolution rate for pH 3 than pH 4 and pH 5, 6, 7, 8, 9 and 10. The dissolution rate is a combination of two dissolution rates (*rateI* and *rateII*). Dissolution *rateI* characterizes the weathering of the very surface of the mineral, the part of it influenced by the preparation of the sample. It is non-stationary regime and it is not representative of bulk defects but the defects induced by the surface creation. Dissolution *rateII* is stationary and it is driven by bulk defects. I used glycine as an additive to investigate the effect of a simple amino acid, widely present in living organisms, on dissolution. This additive was seen to hinder dissolution at pH 4 but had no effect at higher pH.

Among future works, one will be to estimate the feasibility of deducing macroscopic dissolution rates from the atomic dissolution rate for the calcite. This topic has already attracted considerable interest but final conclusions have not been reached yet, concerning the predictability of calcite dissolution rates.

Other supplementary works will be using different amino acids, monosacharid and carboxylic acids, which present small parts of more complex polymeric chains, on the growth of calcite at load of different forces to study their influence on calcite phase changing, and growth rate. To get closer to a realistic inter-grain contact, the study of growth in presence of multiple contacts constitutes the next step. This type of configuration could be experimentally modelled in the lab in applying a nano-patterned surface on the growing face. The simplicity of the chosen geometry would help in interpreting the way contacts at asperities interact, via the solid and liquid, and drive the growth.

Appendix A

Calcite crystal impurities

A.1   Calcite purity test ICP-MS

| Elements	concentration ppb
Mg	1010.00
Mn	227.39
Fe	1.97
Al	4.51
Na	2.03
V	1.04
Cr	0.15
Co	0.56
Ni	0.25
Cu	0.14
Zn	0.22
Ba	0.43
Sr	197.62
Y	4.33

TABLE A.1: Calcite: Impurity measurements by inductively coupled plasma atomic emission spectroscopy (ICP-AES).

A.2 Calcite purity test SEM-EDX

SEM – EDX analysis of calcite
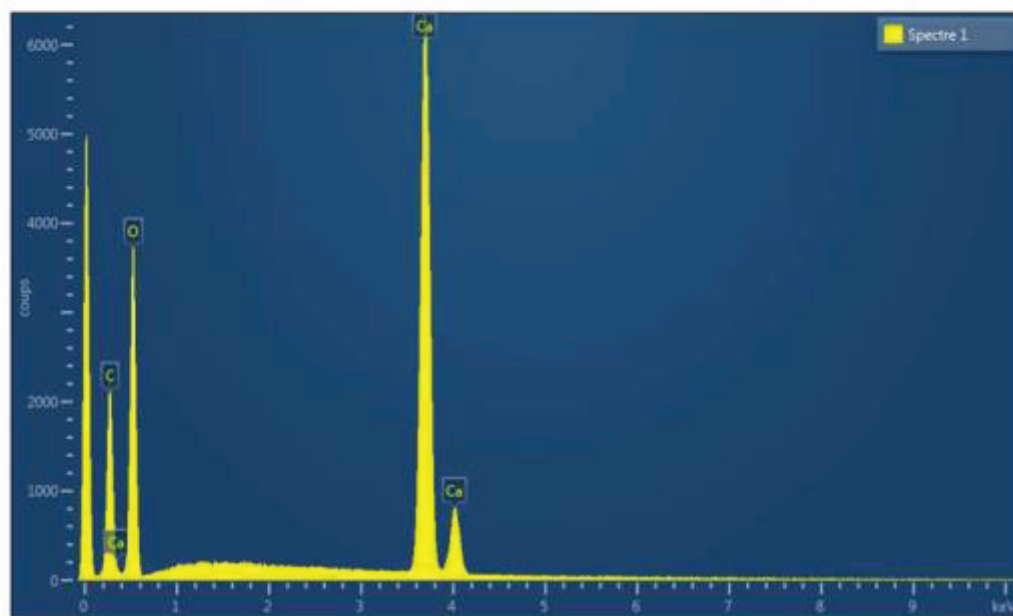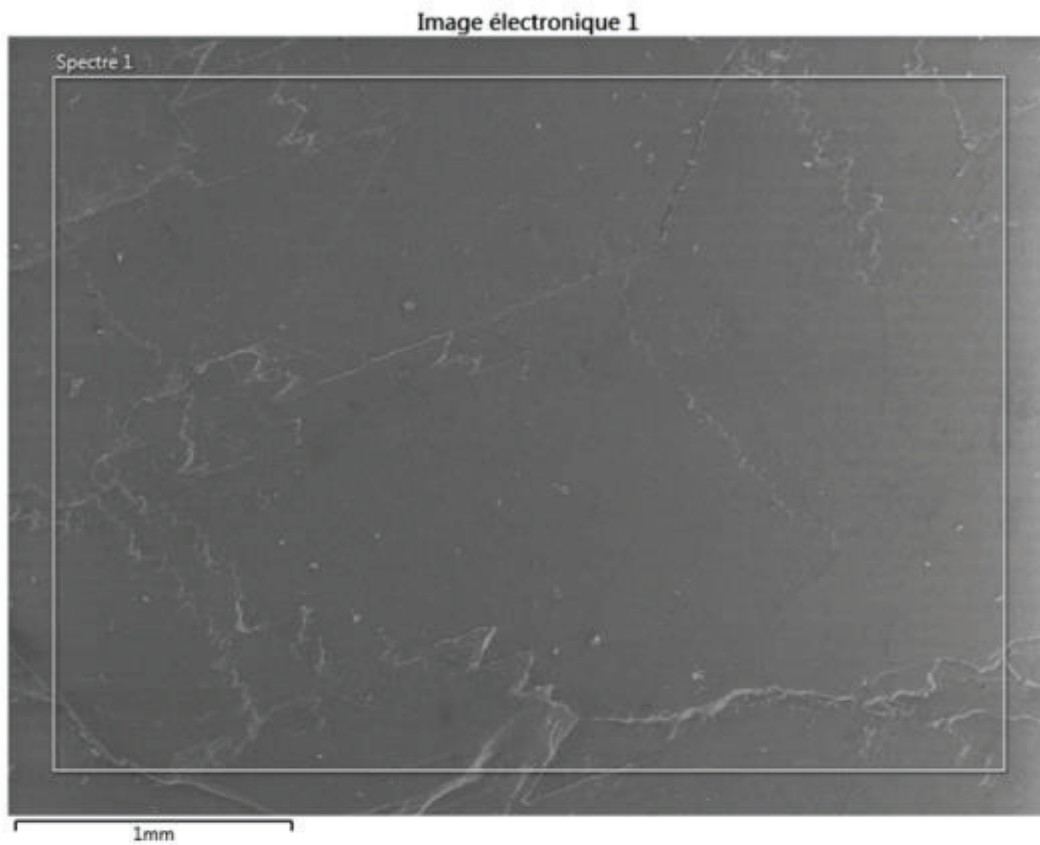
SEM-EDX analysis of calcite surface

SEM – EDX analysis of calcite
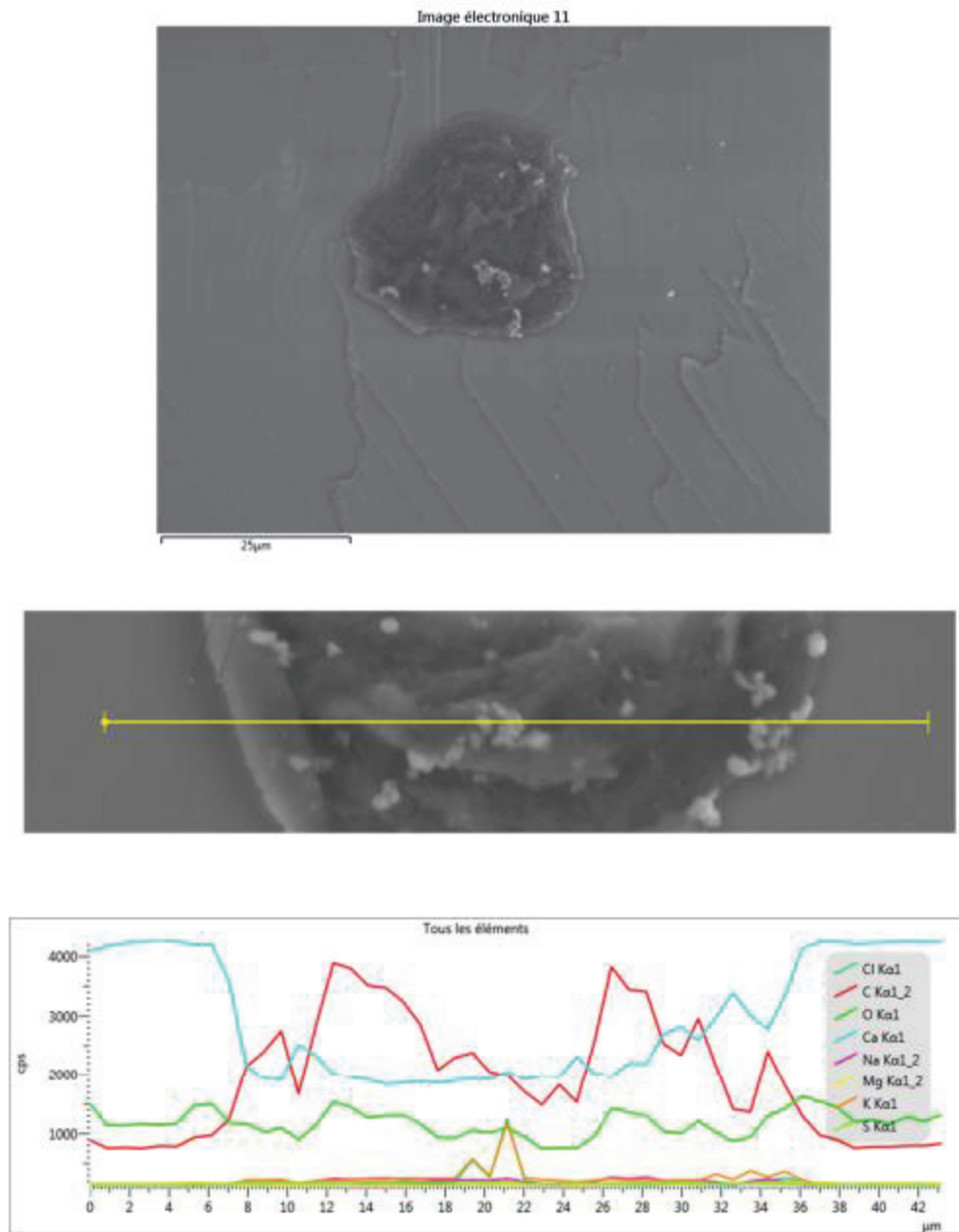
SEM-EDX analysis of salt inclusion on calcite surface

Reference

[1] L. Addadi and S. Weiner. "Interactions between acidic proteins and crystals: stereochemical requirements in biomineralization." In: *Proceedings of the National Academy of Sciences* 82.12 (1985), pp. 4110–4114. ISSN: 0027-8424. DOI: 10.1073/pnas.82.12.4110. URL: http://www.pnas.org/cgi/doi/10.1073/pnas.82.12.4110.

[2] Norma Alcantar, Jacob Israelachvili, and Jim Boles. "Forces and ionic transport between mica surfaces: Implications for pressure solution". In: *Geochimica et Cosmochimica Acta* 67.7 (2003), pp. 1289–1304. ISSN: 00167037. DOI: 10.1016/S0016-7037(02)01270-X.

[3] Denis Allemand et al. "Biomineralisation in reef-building corals: From molecular mechanisms to environmental control". In: *Comptes Rendus - Palevol* 3.6-7 SPEC.ISS. (2004), pp. 453–467. ISSN: 16310683. DOI: 10.1016/j.crpv.2004.07.011.

[4] Martin Andersson et al. "A Microkinetic Model of Calcite Step Growth". In: *Angewandte Chemie (International ed. in English)* 55 (Aug. 2016). DOI: 10.1002/anie.201604357.

[5] David Arcos et al. "Long-term geochemical evolution of the near field repository: Insights from reactive transport modelling and experimental evidences". In: *Journal of Contaminant Hydrology* 102.3-4 (2008), pp. 196–209. ISSN: 01697722. DOI: 10.1016/j.jconhyd.2008.09.021.

[6] Rolf S Arvidson et al. "Variation in calcite dissolution rates: A fundamental problem?" In: *Geochimica et Cosmochimica Acta* 67.9 (2003), pp. 1623–1634. ISSN: 00167037. DOI: 10.1016/S0016-7037(02)01177-8.

[7] J.M. Astilleros et al. "The effect of barium on calcite 1014 surfaces during growth". In: *Geochimica et Cosmochimica Acta* 64.17 (2000), pp. 2965 –2972. ISSN: 0016-7037.

[8] Christensen R.J. Hansma P.K. Stucky G.D. Belcher A. M Wu X.H and Morse D.E. "Control of Crystal Phase Switching and Orientation by Soluble Mollusc-Shell Proteins". In: *Nature* (1996).

[9] R.A. Berner. "The role of magnesium in the crystal growth of calcite and aragonite from sea water". In: *Geochimica et Cosmochimica Acta* 39.4 (1975), pp. 489 –504. ISSN: 0016-7037.

[10] Quate C.F. Binning G. and Geber Ch. "Atomic Force Microscope". In: *Physical Review Letters* 56 (1986), pp. 930–933.

[11] Dirk Bosbach and Michael F. Hochella. "Gypsum growth in the presence of growth inhibitors: a scanning force microscopy study". In: *Chemical Geology* 132.1 (1996). Chemical And Biological Control On Mineral Growth And Dissolution Kinetics, American Chemical Society Meeting, pp. 227 –236. ISSN: 0009-2541. DOI: https://doi.org/10.1016/S0009-2541(96)00059-9.

[12] Alexander S. Brand, Pan Feng, and Jeffrey W. Bullard. "Calcite dissolution rate spectra measured by in situ digital holographic microscopy". In: *Geochimica et Cosmochimica Acta* 213 (2017), pp. 317–329. ISSN: 00167037. DOI: 10.1016/j.gca.2017.07.001. URL: http://dx.doi.org/10.1016/j.gca.2017.07.001.

[13] P. W. Bridgman. "The high pressure behavior of miscellaneous minerals". In: *American Journal of Science* 237 (1939).

[14] A. Burgos-Cara et al. "Hydration effects on gypsum dissolution revealed by in situ nanoscale atomic force microscopy observations". In: *Geochimica et Cosmochimica Acta* 179 (2016), pp. 110–122. ISSN: 00167037. DOI: 10.1016/j.gca.2016.02.008.

[15] W. D. Carlson. "The polymorphs of CaCO3 and the aragonite-calcite transformation". In: *SAE Technical Papers* (1983), pp. 191–225. ISSN: 0402-1215.

[16] Jian kang Chen and Min qiang Jiang. "Long-term evolution of delayed ettringite and gypsum in Portland cement mortars under sulfate erosion". In: *Construction and Building Materials* 23.2 (2009), pp. 812–816. ISSN: 09500618. DOI: 10.1016/j.conbuildmat.2008.03.002.

[17] Lei Chou and Roland Wollast. "Study of the Weathering of Albite at Room Temperature and Pressure with a Fluidized Bed Reactor". In: *Geochimica et Cosmochimica Acta* 48 (Nov. 1984), pp. 2205–2217. DOI: 10.1016/0016-7037(84)90217-5.

[18] Jean Colombani. "Measurement of the pure dissolution rate constant of a mineral in water". In: *Geochimica et Cosmochimica Acta* 72 (2008), pp. 5634–5640. DOI: 10.1016/j.gca.2008.09.007. URL: https://hal.archives-ouvertes.fr/hal-00432693.

[19] S. F. Cox and M. S. Paterson. "Experimental dissolution-precipitation creep in quartz aggregates at high temperatures". In: *Geophysical Research Letters* 18.8 (), pp. 1401–1404. DOI: 10.1029/91GL01802.

[20] Delphine Croizé, François Renard, and Jean Pierre Gratier. "Compaction and Porosity Reduction in Carbonates: A Review of Observations, Theory, and Experiments". In: *Advances in Geophysics* 54 (2013), pp. 181–238. ISSN: 00652687. DOI: 10.1016/B978-0-12-380940-7.00003-2.

[21] Delphine Croizé et al. "Experimental calcite dissolution under stress: Evolution of grain contact microstructure during pressure solution creep". In: *Journal of Geophysical Research* 115 (Sept. 2010), p. 09207. DOI: 10.1029/2010JB000869. URL: https://hal-insu.archives-ouvertes.fr/insu-00549096.

[22] Damien Daval et al. "Linking nm-scale measurements of the anisotropy of silicate surface reactivity to macroscopic dissolution rate laws: New insights based on diopside". In: *Geochimica et Cosmochimica Acta* 107 (2013), pp. 121–134. ISSN: 00167037. DOI: 10.1016/j.gca.2012.12.045.

[23] Kevin J. Davis, Patricia M. Dove, and James J. De Yoreo. "The Role of Mg2+ as an Impurity in Calcite Growth". In: *Science* 290.5494 (2000), pp. 1134–1137. ISSN: 0036-8075. DOI: 10.1126/science.290.5494.1134.

[24] Bas Den Brok, Mohsine Zahid, and Cees W. Passchier. "Pressure solution compaction of sodium chlorate and implications for pressure solution in NaCl". In: *Tectonophysics* 307.3-4 (1999), pp. 297–312. DOI: 10.1016/S0040-1951(99)00103-1.

[25]   Julie Desarnaud, Daniel Bonn, and Shahidzadeh Noushine. "Measurement of the Pressure induced by salt crystallization in confinement". In: *Scientific Reports* 6 (Jan. 2016). DOI: `10.1038/srep30856`.

[26]   Yijue Diao and Rosa M. Espinosa-Marzal. "Molecular insight into the nanoconfined calcite–solution interface". In: *Proceedings of the National Academy of Sciences* 113.43 (2016), pp. 12047–12052. ISSN: 0027-8424. DOI: `10.1073/pnas.1605920113`. eprint: `https://www.pnas.org/content/113/43/12047.full.pdf`. URL: `https://www.pnas.org/content/113/43/12047`.

[27]   Wenming Dong et al. "Influence of calcite and dissolved calcium on uranium(VI) sorption to a Hanford subsurface sediment". In: *Environmental Science and Technology* 39.20 (2005), pp. 7949–7955. ISSN: 0013936X. DOI: `10.1021/es0505088`.

[28]   Patricia M Dove and Stephen F Elston. "Dissolution kinetics of quartz in sodium chloride solutions: Analysis of existing data and a rate model for 25°C". In: *Geochimica et Cosmochimica Acta* 56.12 (1992), pp. 4147 –4156. ISSN: 0016-7037. DOI: `https://doi.org/10.1016/0016-7037(92)90257-J`. URL: `http://www.sciencedirect.com/science/article/pii/001670379290257J`.

[29]   Patricia M. Dove and Forest M. Platt. "Compatible real-time rates of mineral dissolution by Atomic Force Microscopy (AFM)". In: *Chemical Geology* 127.4 (1996), pp. 331 –338. ISSN: 0009-2541. DOI: `https://doi.org/10.1016/0009-2541(95)00127-1`. URL: `http://www.sciencedirect.com/science/article/pii/0009254195001271`.

[30]   D.W. Durney. "SOLUTION-TRANSFER, AN IMPORTANT GEOLOGICAL DEFORMATION MECHANISM". In: *Nature* 238 (1972), pp. 37–38. ISSN: 0028-0836. DOI: `10.1038/239137a0`.

[31]   S. Elhadj et al. "Peptide controls on calcite mineralization: Polyaspartate chain length affects growth kinetics and acts as a stereochemical switch on morphology". In: *Crystal Growth and Design* 6.1 (2006), pp. 197–201. ISSN: 15287483. DOI: `10.1021/cg050288+`.

[32]   Simon Emmanuel and Yael Levenson. "Limestone weathering rates accelerated by micron-scale grain detachment". In: *Geology* 42 (June 2014). DOI: `10.1130/G35815.1`.

[33]   Chunfang Fan and H. Henry Teng. "Surface behavior of gypsum during dissolution". In: *Chemical Geology* 245.3-4 (2007), pp. 242–253. ISSN: 00092541. DOI: `10.1016/j.chemgeo.2007.08.007`.

[34]   L Fernández-Diaz, J M Astilleros, and C M Pina. "The morphology of calcite crystals grown in a porous medium doped with divalent cations". In: *Chemical geology* 225.3 (2006), pp. 314–321. ISSN: 1868-4394.

[35]   E. Finot et al. "Reactivity of gypsum faces according to the relative humidity by scanning force microscopy". In: *Surface Science* 384.1-3 (1997), pp. 201–217. ISSN: 00396028. DOI: `10.1016/S0039-6028(97)00220-3`.

[36]   Eric Finot et al. "Correlation between surface forces and surface reactivity in the setting of plaster by atomic force microscopy". In: *Applied Surface Science* 161.3-4 (2000), pp. 316–322. ISSN: 01694332. DOI: `10.1016/S0169-4332(00)00030-1`.

[37]   Cornelius Fischer, Rolf S. Arvidson, and Andreas Lüttge. "How predictable are dissolution rates of crystalline material?" In: *Geochimica et Cosmochimica Acta* 98 (2012), pp. 177–185. ISSN: 00167037. DOI: 10.1016/j.gca.2012.09.011.

[38]   Cornelius Fischer and Andreas Luttge. "Beyond the conventional understanding of water–rock reactivity". In: *Earth and Planetary Science Letters* 457 (2017), pp. 100 –105. ISSN: 0012-821X. DOI: https://doi.org/10.1016/j.epsl.2016.10.019. URL: http://www.sciencedirect.com/science/article/pii/S0012821X16305763.

[39]   Cornelius Fischer and Andreas Luttge. "Pulsating dissolution of crystalline matter". In: 115.5 (2018). DOI: 10.1073/pnas.1711254115.

[40]   G. Fu et al. "Acceleration of Calcite Kinetics by Abalone Nacre Proteins". In: *Advanced Materials* 17.22 (2005), pp. 2678–2683. DOI: 10.1002/adma.200500633.

[41]   Luca Gagliardi and Olivier Pierre-Louis. "Thin film modeling of crystal dissolution and growth in confinement". In: *Phys. Rev. E* 97 (1 2018), p. 012802. DOI: 10.1103/PhysRevE.97.012802. URL: https://link.aps.org/doi/10.1103/PhysRevE.97.012802.

[42]   Ellis Gartner. "Industrially interesting approaches to "low-CO2" cements". In: *Cement and Concrete Research* 34.9 (2004), pp. 1489–1498. ISSN: 00088846. DOI: 10.1016/j.cemconres.2004.01.021.

[43]   P. U. P. A. Gilbert. "The Organic-Mineral Interface in Biominerals". In: *Reviews in Mineralogy and Geochemistry* 59.1 (2005), pp. 157–185. ISSN: 1529-6466. DOI: 10.2138/rmg.2005.59.7.

[44]   Jean-pierre Gratier et al. "earth ' s upper crust The role of pressure solution creep in the ductility of the Earth ' s upper crust". In: (2013). DOI: 10.1016/B978-0-12-380940-7.00002-0..

[45]   PE Gratz, AJ ; Hillner. "STEP DYNAMICS DURING GROWTH AND DISSOLUTION - AFM STUDIES ON MINERALS". In: *Geochimica et Cosmochimica Acta* 57 (1993), pp. 491–495.

[46]   Astrid Gutjahr, Heinz Dabringhaus, and Rolf Lacmann. "Studies of the growth and dissolution kinetics of the CaCO3 polymorphs calcite and aragonite II. The influence of divalent cation additives on the growth and dissolution rates". In: *Journal of Crystal Growth* 158.3 (1996), pp. 310 –315. ISSN: 0022-0248. DOI: https://doi.org/10.1016/0022-0248(95)00447-5.

[47]   Christopher Hall and David C. Cullen. "Scanning Force Microscopy of Gypsum Dissolution and Crystal Growth". In: *AIChE Journal* 42.1 (1996), pp. 232–238. ISSN: 00011541. DOI: 10.1002/aic.690420119.

[48]   John W Harbaugh. "Carbonate Oil Reservoir Rocks". In: *Algae* (1967), pp. 349–398. DOI: 10.1016/S0070-4571(08)71115-4.

[49]   T. Hassenkam et al. "Tracking single coccolith dissolution with picogram resolution and implications for CO2 sequestration and ocean acidification". In: *Proceedings of the National Academy of Sciences* 108.21 (2011), pp. 8571–8576. ISSN: 0027-8424. DOI: 10.1073/pnas.1009447108.

[50]   Frank Heberling et al. "Reactivity of the calcite-water-interface, from molecular scale processes to geochemical engineering". In: *Applied Geochemistry* 45 (2014), pp. 158–190. ISSN: 18729134. DOI: 10.1016/j.apgeochem.2014.03.006.

[51] H HENRY TENG and PATRICIA M. DOVE. "Surface site-specific interactions of aspartate with calcite during dissolution: Implications for biomineralization". In: *American Mineralogist* 82 (Sept. 1997). DOI: 10.2138/am-1997-9-1005.

[52] P E Hillner et al. "AFM images of dissolution and growth on a calcite crystal". In: *Ultramicroscopy* 42-44.PART 2 (1992), pp. 1387–1393. ISSN: 03043991. DOI: 10.1016/0304-3991(92)90454-R.

[53] Mina Hong and H. Henry Teng. "Implications of solution chemistry effects: Direction-specific restraints on the step kinetics of calcite growth". In: *Geochimica et Cosmochimica Acta* 141 (2014), pp. 228–239. ISSN: 00167037. DOI: 10.1016/j.gca.2014.06.023. URL: http://dx.doi.org/10.1016/j.gca.2014.06.023.

[54] Alexander A. Jeschke, Katrin Vosbeck, and Wolfgang Dreybrodt. "Surface controlled dissolution rates of gypsum in aqueous insolutions exhibit nonlinear dissolution kinetics". In: *Geochimica et Cosmochimica Acta* 65.1 (2001), pp. 27–34. ISSN: 00167037. DOI: 10.1016/S0016-7037(00)00510-X.

[55] Guntram Jordan and Wener Rammensee. "Dissolution rates of calcite (1014) obtained by scanning force microscopy: Microtopography-based dissolution kinetics on surfaces with anisotropic step velocities". In: 62.6 (1998), pp. 941–947.

[56] Jun Kawano et al. "Molecular dynamics simulation of the phase transition between calcite and CaCO3-II". In: *Journal of Physics Condensed Matter* 21.27 (2009). ISSN: 09538984. DOI: 10.1088/0953-8984/21/27/275403.

[57] Alexander. Klimchouk. "Chapter 1.2 THE DISSOLUTION AND CONVERSION OF GYPSUM AND ANHYDRITE Alexander Klimchouk". In: *International Journal of Speleology* 25 (1996), pp. 3–4. ISSN: 0392-6672. DOI: 10.5038/1827-806X.25.3.2.

[58] Daniel Koehn, Dag Kristian Dysthe, and Bjørn Jamtveit. "Transient dissolution patterns on stressed crystal surfaces". In: *Geochimica et Cosmochimica Acta* 68.16 (2004), pp. 3317–3325. ISSN: 00167037. DOI: 10.1016/j.gca.2004.02.004.

[59] Roland Kuechler, Klaus Noack, and Torsten Zorn. "Investigation of gypsum dissolution under saturated and unsaturated water conditions". In: *Ecological Modelling* 176.1-2 (2004), pp. 1–14. ISSN: 03043800. DOI: 10.1016/j.ecolmodel.2003.10.025.

[60] I. Kurganskaya and A. Lüttge. "Kinetic Monte Carlo approach to study carbonate dissolution". In: *J. Phys. Chem. C* 120 (2016), pp. 6482–6492.

[61] Susan L. Stipp and Michael Hochella. "Structure and bonding environments at the calcite surface as observed with X-ray Photoelectron Spectroscopy (XPS) and low energy electron diffraction (LEED)". In: *Geochimica et Cosmochimica Acta* 55 (June 1991), pp. 1723–1736. DOI: 10.1016/0016-7037(91)90142-R.

[62] Leonid Lakshtanov, Nicolas Bovet, and S.L.S. Stipp. "Inhibition of calcite growth by alginate". In: *Geochimica et Cosmochimica Acta* 75 (July 2011), pp. 3945–3955. DOI: 10.1016/j.gca.2011.04.014.

[63] Antonio C. Lasaga and Andreas Lüttge. "A model for crystal dissolution". In: *European Journal of Mineralogy* 15.4 (2003), pp. 603–615. ISSN: 09351221. DOI: 10.1127/0935-1221/2003/0015-0603.

[64] Antonio C Lasaga and Andreas Luttge. "Variation of Crystal Dissolution Rate Based on a Dissolution Stepwave Model". In: 200.1998 (2000).

[65] Antonio C. Lasaga and Andreas Luttge. "Variation of Crystal Dissolution Rate Based on a Dissolution Stepwave Model". In: *Science* 291.5512 (2001), pp. 2400–2404. ISSN: 0036-8075. DOI: 10 . 1126 / science . 1058173. eprint: http : / / science . sciencemag . org / content / 291 / 5512 / 2400 . full . pdf. URL: http://science.sciencemag.org/content/291/5512/2400.

[66] C. Le Guern et al. "Arsenic trapping by iron oxyhydroxides and carbonates at hydrothermal spring outlets". In: *Applied Geochemistry* 18.9 (2003), pp. 1313–1323. ISSN: 08832927. DOI: 10.1016/S0883-2927(03)00053-2.

[67] Lei Li et al. "Growth of Calcite in Confinement". In: *Crystals* 7 (Dec. 2017). DOI: 10.3390/cryst7120361.

[68] Y Liang et al. "Interplay between step velocity and morphology during the dissolution of CaCO3 surface". In: *Journal of Vacuum Science and Technology A* 14.3 (1996), pp. 1368–1375. ISSN: 07342101. DOI: 10.1116/1.579956.

[69] Yong Liang et al. "Dissolution kinetics at the calcite-water interface". In: 60.23 (1996), pp. 4883–4887.

[70] HA Lowenstam. "Minerals formed by organisms". In: *Science* 211.4487 (1981), pp. 1126–1131. ISSN: 0036-8075. DOI: 10 . 1126 / science . 7008198. eprint: http : / / science . sciencemag . org / content / 211 / 4487 / 1126 . full . pdf. URL: http://science.sciencemag.org/content/211/4487/1126.

[71] A Lttge, U Winkler, and A.C Lasaga. "Interferometric study of the dolomite dissolution: a new conceptual model for mineral dissolution". In: *Geochimica et Cosmochimica Acta* 67.6 (2003), pp. 1099 –1116. ISSN: 0016-7037. DOI: https : //doi.org/10.1016/S0016-7037(02)00914-6.

[72] Andreas Luttge. "Crystal Dissolution Kinetics and Gibbs Free Energy". In: *Journal of Electron Spectroscopy and Related Phenomena* 150 (Feb. 2006), pp. 248–259. DOI: 10.1016/j.elspec.2005.06.007.

[73] Andreas Luttge and Edward Bolton. "An interferometric study of the dissolution kinetics of anorthite: The role of reactive surface area". In: November 2014 (1999). DOI: 10.2475/ajs.299.7-9.652.

[74] C M. Holl et al. "Compression of witherite to 8 GPa and the crystal structure of BaCO3II". In: *Physics and Chemistry of Minerals* 27 (2000), pp. 467–473. DOI: 10.1007/s002690000087.

[75] I N Macinnis and S L Brantley. "{the} {Role} {of} {Dislocations} {and} {Surface}-{Morphology} {in} {Calcite} {Dissolution}". In: *Geochimica Et Cosmochimica Acta* 56.3 (1992), pp. 1113–1126. ISSN: 0016-7037.

[76] Dawoud Al Mahrouqi, Jan Vinogradov, and Matthew D. Jackson. "Zeta potential of artificial and natural calcite in aqueous solution". In: *Advances in Colloid and Interface Science* 240 (2017), pp. 60 –76. ISSN: 0001-8686. DOI: https : //doi.org/10.1016/j.cis.2016.12.006. URL: http://www.sciencedirect. com/science/article/pii/S0001868616302007.

[77] Stephen Mann. "Mann, S. Molecular recognition in biomineralization. Nature 332, 119-124". In: *Nature* 332 (Mar. 1988), pp. 119–124. DOI: 10 . 1038 / 332119a0.

[78] Paolo Martins. "Caractérisation mécanique des matériaux pour les micro / nanosystèmes Procédés applicables aux épaisseurs submicroniques". In: *These* (2009), p. 228.

[79] Vinson MD and Andreas Luttge. "Multiple length-scale kinetics: An integrated study of calcite dissolution rates and strontium inhibition". In: *American Journal of Science* 305 (Feb. 2005), pp. 119–146. DOI: 10.2475/ajs.305.2.119.

[80] Siese Meer and Christopher J. Spiers. "Uniaxial compaction creep of wet gypsum aggregates". In: *Journal of Geophysical Research: Solid Earth* 102.B1 (1997), pp. 875–891. DOI: 10.1029/96JB02481.

[81] Fiona C. Meldrum and Helmut Cölfen. "Controlling mineral morphologies and structures in biological and synthetic systems". In: *Chemical Reviews* 108.11 (2008), pp. 4332–4432. ISSN: 00092665. DOI: 10.1021/cr8002856.

[82] M. Merlini, M. Hanfland, and W. A. Crichton. "CaCO3-III and CaCO3-VI, high-pressure polymorphs of calcite: Possible host structures for carbon in the Earth's mantle". In: *Earth and Planetary Science Letters* 333-334 (2012), pp. 265–271. ISSN: 0012821X. DOI: 10.1016/j.epsl.2012.04.036. URL: http://dx.doi.org/10.1016/j.epsl.2012.04.036.

[83] L. Merrill and W. A. Bassett. "The crystal structure of CaCO ₃ (II), a high-pressure metastable phase of calcium carbonate". In: *Acta Crystallographica Section B Structural Crystallography and Crystal Chemistry* 31.2 (1975), pp. 343–349. ISSN: 0567-7408. DOI: 10.1107/S0567740875002774.

[84] E Meyer. "Atomic Force Microscope". In: *Progress in Surface Science* 41.9 (1992), pp. 3–49.

[85] George HNancollas Michael M Reddy. "The crystallization of calcium carbonate: I. Isotopic exchange and kinetics". In: 36.2 (1971), pp. 166–172.

[86] G. Montanari et al. "Effect of Aspartic Acid and Glycine on Calcite Growth". In: *Crystal Growth and Design* 16.9 (2016), pp. 4813–4821. ISSN: 15287505. DOI: 10.1021/acs.cgd.5b01635.

[87] J W Morse. "The dissolution kinetics of major sedimentray carbonate minerals". In: *Earth-Science Reviews* 58 (2002), pp. 51–84. DOI: http://dx.doi.org/10.1016/S0012-8252(01)00083-6.

[88] L. Neveux et al. "Experimental simulation of chemomechanical processes during deep burial diagenesis of carbonate rocks". In: *Journal of Geophysical Research: Solid Earth* 119.2 (2014), pp. 984–1007. DOI: 10.1002/2013JB010516. URL: https://agupubs.onlinelibrary.wiley.com/doi/abs/10.1002/2013JB010516.

[89] Ö Nilsson and J Sternbeck. "A mechanistic model for calcite crystal growth using surface speciation". In: *Geochimica et Cosmochimica Acta* 63.2 (1999), pp. 217 –225. ISSN: 0016-7037.

[90] Branka Njegic-Dzakula et al. "Calcite Crystal Growth Kinetics in the Presence of Charged Synthetic Polypeptides". In: *Crystal Growth & Design* 9.5 (2009), pp. 2425–2434. DOI: 10.1021/cg801338b. URL: https://doi.org/10.1021/cg801338b.

[91] Christine Orme et al. "Formation of chiral morphologies through selective binding of amino acids to calcite surface steps". In: *Nature* 411 (July 2001), pp. 775–9. DOI: 10.1038/35081034.

[92] Wierzbicki A. Mcbride M.T Grantham M. Teng H.H. Dove P.M. Orme C.A. Noy A. and DeYoreo J.J. "Formation of chiral morphologies through selective binding of amino acids to calcite surface steps". In: *Nature* (2001), pp. 775–779.

[93] Edgar Alejandro Pachon-Rodriguez, Agnès Piednoir, and Jean Colombani. "Pressure solution at the molecular scale". In: *Physical Review Letters* 107.14 (2011), pp. 30–33. ISSN: 00319007. DOI: 10.1103/PhysRevLett.107.146102.

[94] Edgar Alejandro Pachon-Rodriguez et al. "Pressure solution as origin of the humid creep of a mineral material". In: *Phys. Rev. E* 84 (6 2011), p. 066121. DOI: 10.1103/PhysRevE.84.066121. URL: https://link.aps.org/doi/10.1103/PhysRevE.84.066121.

[95] Nam-Seok Park et al. "Tribological Enhancement of CaCO3 Dissolution during Scanning Force Microscopy". In: *Langmuir* 12.19 (1996), pp. 4599–4604. DOI: 10.1021/la950904b. URL: https://doi.org/10.1021/la950904b.

[96] Nam-Seok Park et al. "Atomic layer wear of single-crystal calcite in aqueous solution using scanning force microscopy". In: *Journal of Applied Physics* 80.5 (1996), pp. 2680–2686. ISSN: 0021-8979. DOI: 10.1063/1.363185. URL: http://aip.scitation.org/doi/10.1063/1.363185.

[97] L.Niel Plummer and Eurybiades Busenberg. "The solubilities of calcite, aragonite and vaterite in CO2-H2O solutions between 0 and 90℃, and an evaluation of the aqueous model for the system CaCO3-CO2-H2O". In: *Geochimica et Cosmochimica Acta* 46.6 (1982), pp. 1011 –1040. ISSN: 0016-7037. DOI: https://doi.org/10.1016/0016-7037(82)90056-4.

[98] O. S. Pokrovsky and J. Schott. "Surface Chemistry and Dissolution Kinetics of Divalent Metal Carbonates". In: *Environmental Science & Technology* 36.3 (2002). PMID: 11871558, pp. 426–432. DOI: 10.1021/es010925u. URL: https://doi.org/10.1021/es010925u,.

[99] Michael A. Raines and Thomas A. Dewers. "Mixed transport/reaction control of gypsum dissolution kinetics in aqueous solutions and initiation of gypsum karst". In: *Chemical Geology* 140.1-2 (1997), pp. 29–48. ISSN: 00092541. DOI: 10.1016/S0009-2541(97)00018-1.

[100] Rishi Raj. "Creep in polycrystalline aggregates by matter transport through a liquid phase". In: *Journal of Geophysical Research: Solid Earth* 87.B6 (), pp. 4731–4739. DOI: 10.1029/JB087iB06p04731. URL: https://agupubs.onlinelibrary.wiley.com/doi/abs/10.1029/JB087iB06p04731.

[101] Krishnam U.G. Raju and Gordon Atkinson. "The Thermodynamics of "Scale" Mineral Solubilities. 3. Calcium Sulfate in Aqueous NaCl". In: *Journal of Chemical and Engineering Data* 35.3 (1990), pp. 361–367. ISSN: 15205134. DOI: 10.1021/je00061a038.

[102] S. J. B. Reed. *Electron microprobe analysis and scanning electron microscopy in geology.* University of Cambridge, 2005.

[103] F. Renard et al. "An integrated model for transitional pressure solution in sandstones". In: *Tectono physics* 312.2 (1999), pp. 97 –115. ISSN: 0040-1951. DOI: https://doi.org/10.1016/S0040-1951(99)00202-4.

[104] E Ruiz-Agudo et al. "The role of background electrolytes on the kinetics and mechanism of calcite dissolution". In: *Geochimica et Cosmochimica Acta* 74.4 (2010), pp. 1256–1267. ISSN: 00167037. DOI: 10.1016/j.gca.2009.11.004. URL: http://dx.doi.org/10.1016/j.gca.2009.11.004.

[105] Encarnación Ruiz-Agudo et al. "An atomic force microscopy study of calcite dissolution in saline solutions: The role of magnesium ions". In: *Geochimica et Cosmochimica Acta* 73 (June 2009), pp. 3201–3217. DOI: 10.1016/j.gca.2009.03.016.

[106] Paola Rumolo et al. "Heavy metals in benthic foraminifera from the highly polluted sediments of the Naples harbour (Southern Tyrrhenian Sea, Italy)". In: *Science of the Total Environment* 407.21 (2009), pp. 5795–5802. ISSN: 00489697. DOI: 10.1016/j.scitotenv.2009.06.050. URL: http://dx.doi.org/10.1016/j.scitotenv.2009.06.050.

[107] Wallace S. Broecker and Taro Takahashi. "The relationship between lysocline depth and in situ carbonate ion concentration. Deep-Sea Res 25F(1): 65-95". In: *Deep Sea Res* 25 (Jan. 1978), pp. 65–95.

[108] K K Sand et al. "Calcite Growth Kinetics: Dependence on Saturation Index, Ca2+:CO32-Activity Ratio, and Surface Atomic Structure". In: *Crystal Growth and Design* 16.7 (2016), pp. 3602–3612. ISSN: 15287505. DOI: 10.1021/acs.cgd.5b01792.

[109] K. K. Sand et al. "Controlling biomineralisation with cations". In: *Nanoscale* 9 (35 2017), pp. 12925–12933. DOI: 10.1039/C7NR02424J. URL: http://dx.doi.org/10.1039/C7NR02424J.

[110] George W Scherer. "Crystallization in". In: *October* 29.August 1998 (1986), pp. 1986–1986.

[111] Siese de Meer Christopher J. Spiers. *On Mechanisms and Kinetics of Creep by Intergranular Pressure Solution*. Springer, Dordrecht, 1999. DOI: https://doi.org/10.1007/978-94-015-9179-9_16.

[112] H.Catherine W. Skinner. "A review of apatites, iron and manganese minerals and their roles as indicators of biological activity in black shales". In: *Precambrian Research* 61.3 (1993). Metalliferous Black Shales and Related Ore Deposits, pp. 209 –229. ISSN: 0301-9268. DOI: https://doi.org/10.1016/0301-9268(93)90114-H. URL: http://www.sciencedirect.com/science/article/pii/030192689390114H.

[113] Carl I. Steefel and Peter C. Lichtner. "Diffusion and reaction in rock matrix bordering a hyperalkaline fluid-filled fracture". In: *Geochimica et Cosmochimica Acta* 58.17 (1994), pp. 3595–3612. ISSN: 00167037. DOI: 10.1016/0016-7037(94)90152-X.

[114] S L S Stipp, C M Eggleston, and Nielsen B.S. "Calcite surface structure observed at microtopographic and molecular scales with atomic force microscopy (AFM)*". In: 58.0 (1994).

[115] S.L.S Stipp. "Toward a conceptual model of the calcite surface: hydration, hydrolysis, and surface potential". In: *Geochimica et Cosmochimica Acta* 63.19 (1999), pp. 3121 –3131. ISSN: 0016-7037. DOI: https://doi.org/10.1016/S0016-7037(99)00239-2. URL: http://www.sciencedirect.com/science/article/pii/S0016703799002392.

[116] Colin Summerhayes. *Deep Water – The Gulf Oil Disaster and the Future of Offshore Drilling*. Vol. 30. 2. 2011, pp. 113–115. ISBN: 9780160873713. DOI: 10.3723/ut.30.113. arXiv: arXiv:1011.1669v3.

[117]   H. Henry Teng and Patricia M. Dove. "Surface site-specific interactions of aspartate with calcite during dissolution: Implications for biomineralization". In: *American Mineralogist* 82.9-10 (1997), pp. 878–887. ISSN: 0003004X. DOI: 10.2138/am-1997-9-1005.

[118]   H. Henry Teng et al. "Thermodynamics of calcite growth: Baseline for understanding biomineral formation". In: *Science* 282.5389 (1998), pp. 724–727. ISSN: 00368075. DOI: 10.1126/science.282.5389.724.

[119]   H.H Teng. "AFM measurement of step kinetics for the growth and dissolution of crystallites". In: *Spectroscopy* (2005).

[120]   H.H. Teng, P.M. Dove, and J.J. De Toreo. "Kinmetics of calcite growth: surface processes and relationships to macroscopic laws". In: *Gca* 64.13 (2000), pp. 2255–2266.

[121]   P Vancappellen et al. "A surface complexation model of the carbonate mineral-aqueous solution interface". In: *Geochimica Et Cosmochimica Acta* 57.15 (1993), pp. 3505–3518. ISSN: 0016-7037.

[122]   Michael D. Vinson and Andreas Luttge. "Multiple length-scale kinetics: An integrated study of calcite dissolution rates and strontium inhibition". In: *American Journal of Science* 305.2 (2005), pp. 119–146. ISSN: 00029599. DOI: 10.2475/ajs.305.2.119.

[123]   Manfred Von Ardenne. "Das Elektronen-Rastermikroskop. Theoretische Grundlagen." In: *Zeitschrift für Physik* Vol. 109 (1938).

[124]   Owen W. Duckworth and Scot Martin. "Dissolution rates and pit morphologies of rhombohedral carbonate minerals". In: *American Mineralogist* 89 (Apr. 2004). DOI: 10.2138/am-2004-0410.

[125]   L. G. Wade. *Organic chemistry*. Pearson Prentice Hall in Upper Saddle River, N.J ., 2010, Pearson Pre. ISBN: 9780321592316.

[126]   Deron A. Walters et al. "Modification of calcite crystal growth by abalone shell proteins: An atomic force microscope study". In: *Biophysical Journal* 72.3 (1997), pp. 1425–1433. ISSN: 00063495. DOI: 10.1016/S0006-3495(97)78789-7.

[127]   Laura E. Wasylenki et al. "Nanoscale effects of strontium on calcite growth: An in situ AFM study in the absence of vital effects". In: *Geochimica et Cosmochimica Acta* 69.12 (2005), pp. 3017–3027. ISSN: 00167037. DOI: 10.1016/j.gca.2004.12.019.

[128]   Ulrike G.K. Wegst et al. "Bioinspired structural materials". In: *Nature Materials* 14.1 (2015), pp. 23–36. ISSN: 14764660. DOI: 10.1038/nmat4089.

[129]   Hans-Rudolf Wenk and Andrei Bulakh. *Minerals: Their Constitution and Origin*. Cambridge University Press, 2004. DOI: 10.1017/CBO9780511811296.

[130]   M Wolthers and S L S Stipp. "Calcite Growth Kinetics: Dependence on Saturation Index, Ca 2+ :CO 32 Activity Ratio, and Surface Atomic Structure". In: *Crystal Growth and Design* 16.7 (2016), pp. 3602–3612. DOI: 10.1021/acs.cgd.5b01792.

[131]   Mariëtte Wolthers. "How minerals dissolve". In: *Science* 349.6254 (2015), pp. 1288–1288. ISSN: 0036-8075. DOI: 10.1126/science.aad0852. eprint: http://science.sciencemag.org/content/349/6254/1288.full.pdf. URL: http://science.sciencemag.org/content/349/6254/1288.

[132] Mariëtte Wolthers et al. "Calcite growth kinetics: Modeling the effect of solution stoichiometry". In: *Geochimica et Cosmochimica Acta* 77 (2012), pp. 121 –134. ISSN: 0016-7037. DOI: https://doi.org/10.1016/j.gca.2011.11.003. URL: http://www.sciencedirect.com/science/article/pii/S0016703711006466.

[133] Bahareh Zareeipolgardani, Agnès Piednoir, and Jean Colombani. "Gypsum Dissolution Rate from Atomic Step Kinetics". In: *Journal of Physical Chemistry C* 121.17 (2017), pp. 9325–9330. ISSN: 19327455. DOI: 10.1021/acs.jpcc.7b00612.

[134] X. ZHANG, C. J. SPIERS, and C. J. PEACH. "Effects of pore fluid flow and chemistry on compaction creep of calcite by pressure solution at 150°C". In: *Geofluids* 11.1 (Feb. 2011), pp. 108–122. ISSN: 1468-8123. DOI: 10.1111/j.1468-8123.2010.00323.x. URL: https://doi.org/10.1111/j.1468-8123.2010.00323.x.

[135] Zuoping Zheng, Tetsu Tokunaga, and Jiamin Wan. "Influence of Calcium Carbonate on U(VI) Sorption to Soils". In: *Environmental Science & Technology* 37.24 (2003), pp. 5603–5608.